Environmental Science Nano

ROYAL SOCIETY OF CHEMISTRY

CRITICAL REVIEW

View Article Online
View Journal | View Issue

Cite this: *Environ. Sci.: Nano*, 2025, 12, 4796

Emerging 2D MXene-conjugated nanoarchitectures for nanozymes: current advances and future frontiers in biochemical sensing technologies

Ramar Rajamanikandan, [ab] Kandasamy Sasikumar [ab] and Heongkyu Ju *[ab]

Received 1st August 2025,
Accepted 30th September 2025

DOI: 10.1039/d5en00710k

rsc.li/es-nano

Nanozymes, nanostructured materials with exceptional catalytic performance, are recognized for their unique benefits over natural enzymes, including notably low fabrication costs and high chemical stability. Emerging as a captivating frontier in nanozyme research, MXene-based composite material nanozymes (MXzymes) have sparked intense research interest owing to their unique compositions and structural features, which can be engineered to unlock their enzyme-mimicking catalytic prowess. This approach opens groundbreaking opportunities for detecting biologically significant, food-related, and environmentally crucial analytes. This review highlights the innovative fabrication methods of MXzymes, focusing on their diverse nanozyme activity types reported thus far, including peroxidase-like and oxidase-like functionalities, while unveiling the underlying catalytic mechanisms in detail. In addition, recent pioneering breakthroughs in MXzymes are comprehensively reviewed, including catalytic signal amplification by MXzymes, which can function as cutting-edge sensing platforms, as evidenced by colorimetric, smartphone-based, chemiluminescent, electrochemical, and surface-enhanced Raman scattering-based analyses. Finally, the promising potential applications of MXzymes and fundamental challenges associated with their scalability, stability, and biocompatibility for MXzyme-based chemical/biomedical sensors are addressed.

Environmental significance

Antibiotics, heavy metals, pesticides, organic contaminants, food contaminants, and amino acids each impact the environment. Antibiotics from agriculture and healthcare promote resistance and disrupt microbes. Heavy metals like Pb and Hg are poisonous, tenacious, and bioaccumulate. Pesticides harm non-target species and contaminate soil and water. Organic pollutants such as OPs and dioxins are toxic, carcinogenic, and degrade slowly. Food contaminants, including pesticide residues and plasticizers, enter ecosystems *via* waste. While amino acids are non-toxic, excess runoff can cause eutrophication. Together, these substances threaten biodiversity, disrupt ecosystems, and highlight the need for strict monitoring and regulation to protect health and the environment. This review article collects the sensitive detection of these substances *via* MXene-conjugated nanomaterial-based nanozyme sensors.

1. Introduction

Natural enzymes, bio-macromolecules with extreme effectiveness and specificity for enzymatic reactions, play an essential role in biological functions.[1] However, their applications have been hampered by poor stability, high production cost, and labor-intensive purification. As alternatives, artificial nanozymes were designed to overcome these limitations in recent decades.[1,2] Many efforts focused on finding molecules to synthesize them, including cyclodextrins,[3] fullerenes,[4] polymers,[5] porphyrins,[6] dendrimers,[7] biomolecules,[8] and metal complexes.[9]

The past few years have seen explosive growth in enzyme-like catalytic nanomaterials (nanozymes) since the discovery in 2007 that peroxidase (POD)-like catalytic features, resembling natural POD-like horseradish peroxidase (HRP), existed in magnetic nanoparticles (NPs).[10] A nanozyme, a nano-sized material (1–100 nm) with enzyme-mimicking catalytic abilities, combines features of chemical and biological catalysts,[1,2] thus expanding their uses.[10] Hundreds of nanomaterials mimicking enzyme operations have been reported for the eco-friendly industry, healthcare, and typical catalysis.[11–15] Nanozymes offer advantages over natural enzymes: inexpensive and simple fabrication, chemical stability, and customizable design.[1,2,13] As nanozyme catalysis

[a] *Department of Physics and Semiconductor Science, Gachon University, Seongnam-si, Republic of Korea. E-mail: batu@gachon.ac.kr*
[b] *Gachon Bionano Research Institute, Gachon University, Seongnam-si, 13120, Republic of Korea*

produces amplified signals for quantitative determination and allows flexible activity adjustment, nanozymes have lent themselves to chemo-bio sensing.[14,15] With developments in bio-/nano-catalysis, nano(bio) technology, machine learning, and computational design, various 2D material-based nanozymes have emerged using transition metal dichalcogenide nanosheets,[16] graphene,[17] metal–organic frameworks (MOFs),[13] and MXenes[18] owing to their surface area, conductivity, and active sites.

Since their discovery in 2011, MXenes, a family of two-dimensional transition-metal carbides, nitrides, and carbonitrides, have gained interest due to their physical and chemical characteristics (including electrical conductivity, thermal conductivity, and configurable interlayer spacing).[19] The term "MXene" enables this 2D material to be distinguished from graphene, encompassing both the MAX phase and derived MXenes from the MAX phase.[20,21] The chemical formula of MAX phases is $M_{n+1}AX_n$, where "M" denotes a transition metal, n = 1, 2, or 3, "A" is mainly a grouping of III–IV elements, and "X" refers to C and/or N (Fig. 1a). Chemical etching of the MAX phases' A-layers is the primary method exploited for fabricating MXenes (Fig. 1b).[21] Thus, the attained MXenes have a 2D stacked arrangement with a formulation of $M_{n+1}X_nT_x$, where M represents metals (Mo, Nb, Ti, Ta, V, Hf, Cr, or Sc), X signifies N or C, and "T_x" denotes exterior functional groups (–F, –O, and –OH) generated through synthetic etching.[21,22] With extensive study on optical, mechanical, thermal, and magnetic characteristics, MXenes have drawn interest from various sectors, demonstrating promise in analytical sciences, particularly in optical and electrochemical sensors.[22,23] Owing to their unique physicochemical properties, Zhou L. *et al.* developed chitosan-2D Ti_3C_2 nanocomposites as an effective enzyme immobilization support for constructing high-performance biosensors.[21] Similarly, Yu Chen *et al.* reported a Fenton-reaction-based nano-catalytic system on 2D Ti_3C_2 nanosheets, employing photothermal conversion nanoprobes to enhance cancer cell ablation efficiency.[12] These works have inspired many subsequent studies on MXzyme-based catalysis. Beyond sensing, MXenes have been applied in catalysis, energy storage, photodetectors,

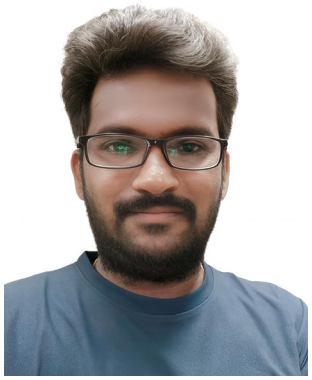

Ramar Rajamanikandan

Dr. Ramar Rajamanikandan completed his doctoral degree from Bharathiar University, Coimbatore, Tamil Nadu, India. Currently, he is working as a Research assistant professor in the Department of Physics and Semiconductor Sciences at Gachon University, Gyeonggi-do, Republic of Korea. Currently, he is working on MXene-based nano materials for sensing technologies. His research interest is mainly in colorimetric and fluorometric optical biochemical sensors using metal nanomaterials and quantum dots.

Kandasamy Sasikumar

Dr. Kandasamy Sasikumar is a Research Assistant Professor in the Department of Physics and Semiconductor Sciences, Gachon University, Gyeonggi-do, Republic of Korea. He received his PhD from Bharathiar University, Coimbatore, Tamil Nadu, India. His research interests include photocatalysts, carbon dots, and nanomaterials for energy and environmental applications.

Heongkyu Ju

Prof. Heongkyu Ju is currently a professor at the Department of Physics and Semiconductor Science, Gachon University, South Korea. He received his D. Phil. degree in the Department of Condensed Matter Physics from the University of Oxford, UK, and worked as a postdoctoral researcher at Eindhoven University of Technology, Netherlands, and NTT Basic Research Laboratories, Japan, before joining the faculty at the Department of Physics, Gachon University, South Korea. He has so far authored more than hundred ten peer-reviewed international journal papers published over the last 22 years. The central interests of his research involve surface plasmon-based nanophotonics, hot carrier dynamics, and plasmon–quantum dot coupling, with applications in ultrasensitive biosensing, hazardous chemical detection, environmental monitoring, advanced photodetection, solar energy harvesting, photocatalysis, and surface-enhanced spectroscopy.

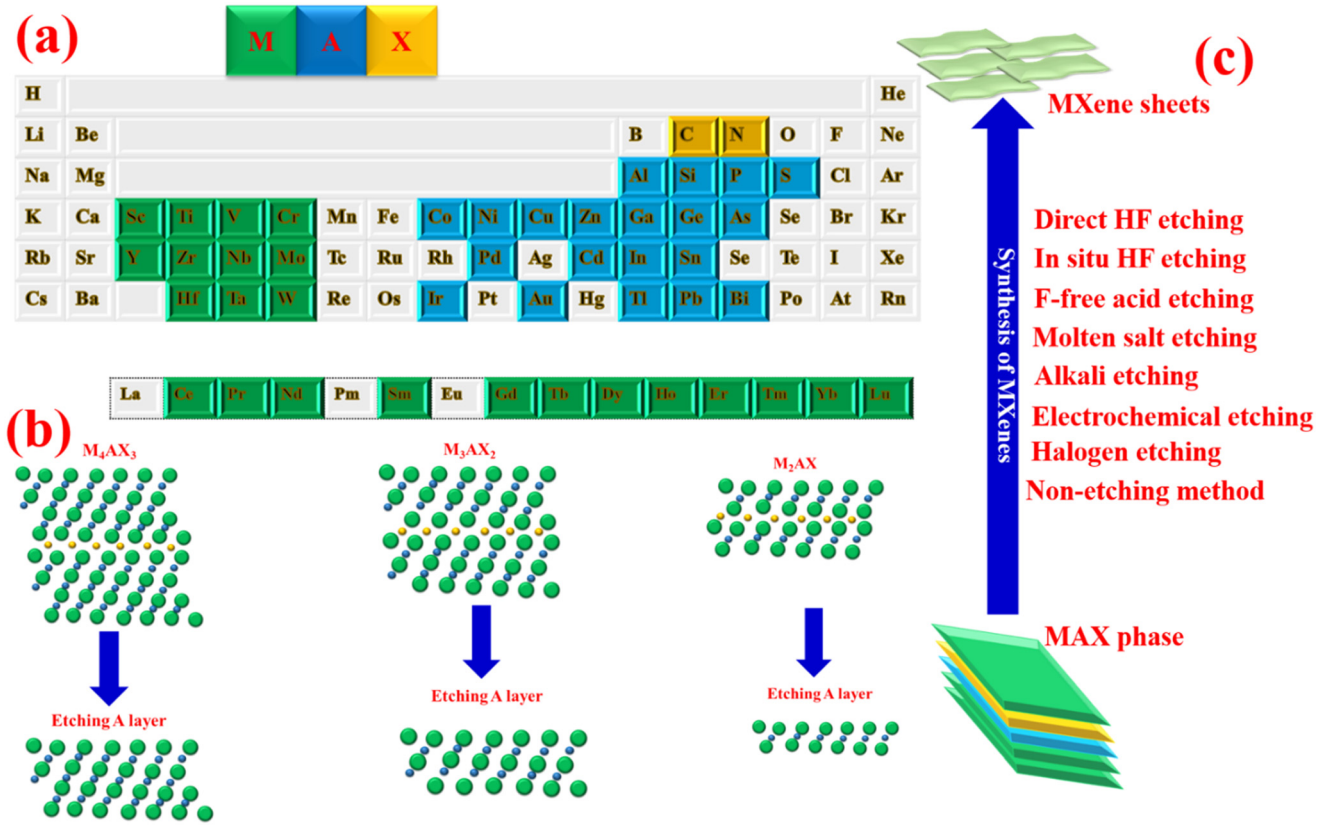

Fig. 1 Chemical constituents of MXenes. (a) The elements involved in MXene preparation are denoted, with M, A, and X constituents marked in three different colors. (b and c) Schematic illustration of the MXenes' synthetic processes by removing the A layer and different synthetic ways for MAX phase materials to MXene synthesis.

environmental remediation, nanozymes, and drug delivery.[24–27]

MXenes' functions make them suitable supports for nanozyme-based catalytic reactions.[18,21] Their physicochemical features enhance the chemical stability of supported NPs and catalytic efficiency.[28] The 2D MXene Ti_3C_2 nanosheet-based nanozyme has unique properties: (i) water dispersibility and functionalization capability because of hydrophilic surface groups such as –OH and –O, (ii) charge-carrier transport and redox reactivity from exposed terminal Ti's valence states and metallic conductivity, (iii) eco-friendly biocompatibility, and (iv) Ti_3C_2 NSs exhibit inherent POD-like action.[29] Due to these special characteristics, 2D MXenes are preferred over other nanozymes, including graphene, MOFs, and transition metal dichalcogenide nanosheets, in MXzyme sensors.[13,14,16,17]

Many reviews on MXene-based nanocomposites cover their fabrication, characteristics, and applications in energy conversion,[30,31] environmental monitoring,[32] photodetectors,[33] electrochemical sensors,[25] information technology,[34] *etc.*[35] However, few papers have addressed the biomedical potential of MXzymes; future investigations should focus on thorough studies and evaluations for their great potential in biomedicine, covering therapeutic applications.[36,37] While a review of MXzyme sensors for food contaminants was recently published,[38] a comprehensive review of MXzyme sensors for detecting potent analytes remains unreported.

This review summarizes recent advancements in MXene nanocomposites with enzyme-like features for chemo-biosensors of biological and toxic analytes (Scheme 1). Initially, we provide an overview of MXenes' fabrication and functionalization techniques. Next, we discuss the types of nanozyme properties and catalytic mechanisms of MXenes. Subsequently, we examine the benefits of nanozyme-based sensors in various strategies, *i.e.*, conventional colorimetry, smartphone-assisted colorimetry, fluorescence, chemiluminescence, electrochemiluminescence, and surface-enhanced Raman scattering (SERS). We explore nanozyme-mediated reactions and their application in analyte detection. Lastly, we discuss the trailblazing sensing strategies in this discipline, address technical limitations, and emphasize their significance in advanced sensors and diagnostics. We believe that this timely review with perspectives will advance our understanding of nanozyme characteristics and the development of novel nanomaterials with enzyme-mimicking activities.

2. MXene synthesis

The M–X bond in MAX phases shows metallic, covalent, and ionic characteristics. In contrast, the M–A bond is

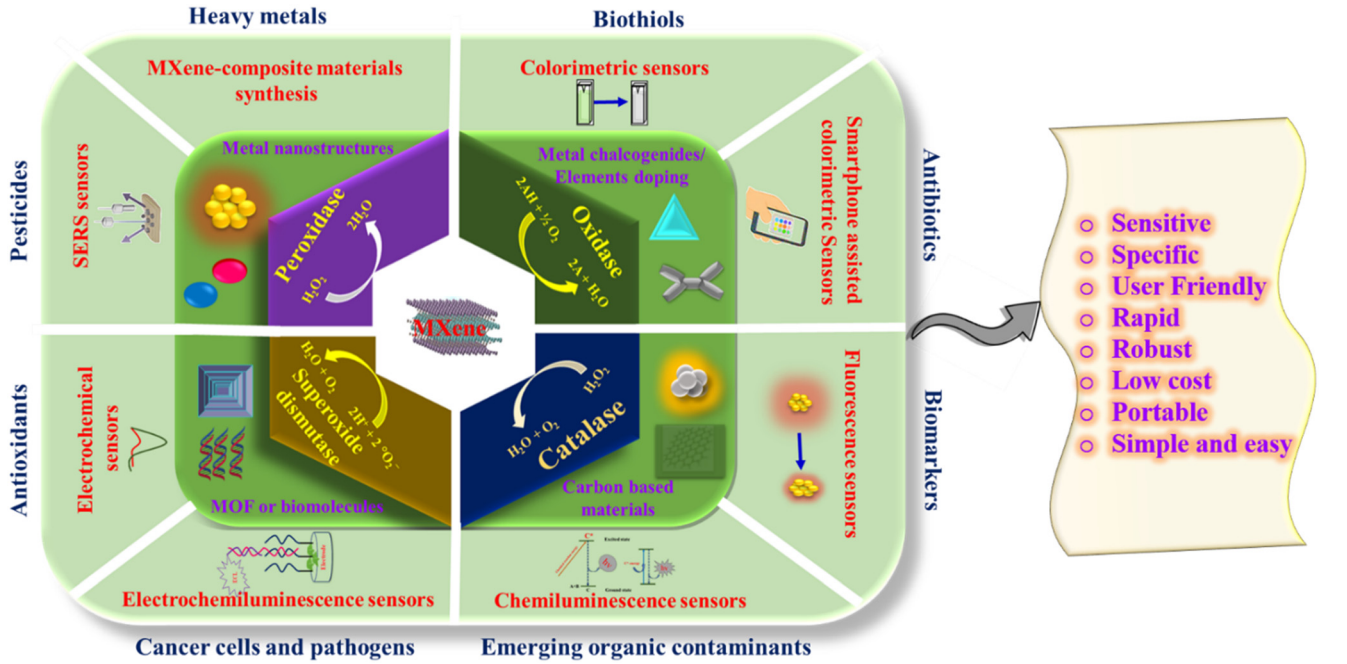

Scheme 1 Schematic illustration of MXzyme sensors for highly potent analytes with their advantages.

metallic and more chemically reactive, allowing it to break easily.[39] Because of weaker M–A bonds compared to M–X bonds, the A layers can be selectively etched from MAX phase materials. Synthetic protocols from MAX phase materials to MXene (Fig. 1c) are described as follows.

2.1. Direct hydrofluoric acid etching

Notably, 2D MXenes were first exfoliated from MAX precursors using 50% hydrofluoric acid (HF) by Naguib *et al.* in 2011.[40] The Al layer was selectively detached from the Ti_3AlC_2 MAX phase at room temperature within 2 h reaction time. The prepared accordion-like MXenes ($Ti_3C_2T_x$) possessed termination groups (–F, –OH, and –O) and defects at the surface, as shown in Fig. 2a. The etching mechanism can be described by the following reactions.

$$Ti_3AlC_2 + 3HF = AlF_3 + 1.5H_2 + Ti_3C_2 \quad (1)$$

$$Ti_3C_2 + 2H_2O = Ti_3C_2(OH)_2 + H_2 \quad (2)$$

$$Ti_3C_2 + 2HF = Ti_3C_2F_2 + H_2 \quad (3)$$

According to eqn (1), the A element in the MAX phase reacts with fluoride ions from HF, initiating the removal of the M–X layer as described in reaction (2). The surface transition metal then actively interacts with water molecules or fluoride ions to develop an exfoliated graphite-like structure, *i.e.*, MXene, terminated with –O, –OH, or –F groups (eqn (2) and (3)). This etching process was subsequently extended to many more MAX phases with diverse chemical compositions to produce MXenes by selectively removing Al or Si layers.[41–44] In this context, Ti_3AlC_2 is used as a representative example to illustrate the general principle of direct HF etching, since it is the most extensively studied MAX phase for MXene synthesis. Different transition metals (*e.g.*, Ti, Nb, V) provide unique electronic structures and redox properties, which influence catalytic activity. Furthermore, the interaction between the etching environment and the specific MAX phase affects the termination ratio, further customizing the catalytic properties.[39,41] Therefore, although the etching principle remains consistent, the nanozyme activity of MXenes is not universal and is significantly affected by the choice of MAX precursor and the surface chemistry introduced during HF etching.

HF etching is common owing to its simplicity, versatility, and high yield, but concerns about safety and environmental impact persist because of its extreme toxicity and corrosiveness.[45] The aggressive etching conditions can introduce defects, compromising the structural integrity and quality of the resulting MXene. Therefore, controlling HF concentration, reaction time, and temperature for each MAX phase composition is crucial to ensure successful transformation into MXene. HF etching typically produces multilayered MXene with an accordion-like structure, where adjacent MXene layers are connected by a combination of van der Waals forces and hydrogen bonding.[46] Consequently, an extra delamination step is necessary to exfoliate these multilayered MXene structures into individual 2D nanosheets.

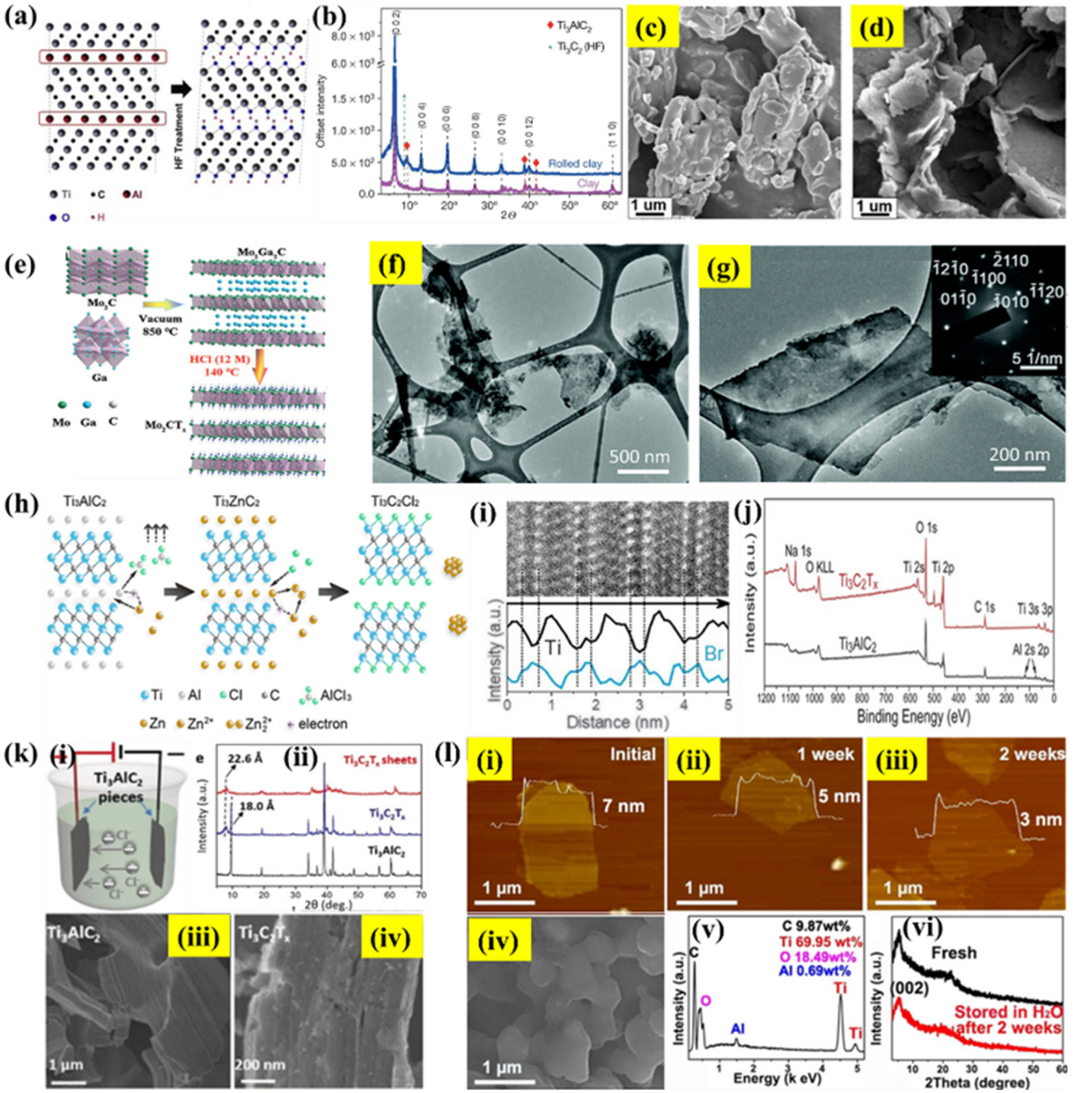

Fig. 2 (a) Illustration of the exfoliation process for Ti_3AlC_2, highlighting the replacement of Al atoms by –OH groups after HF treatment [reproduced from ref. 40, with permission from John Wiley and Sons, copyright 2011]. (b) XRD patterns of samples etched using a LiF + HCl solution. The pink trace represents multilayer $Ti_3C_2T_x$, exhibiting a sharp and intense (0002) peak along with higher-order (000*l*) reflections corresponding to a *c*-lattice parameter of 28 Å and well-ordered stacking in the *c* direction [reproduced from ref. 47 with permission from Springer Nature, copyright 2014]. (c and d) SEM images of Ti_3AlC_2 and hydrothermally synthesized h-Ti_3C_2 (16 h reaction time) [reproduced from ref. 56 with permission from Elsevier, copyright 2018]. (e) Schematic of the HCl-assisted hydrothermal etching mechanism for fluoride-free Mo_2CT_x [reproduced from ref. 58 with permission from John Wiley and Sons, copyright 2021]. TEM photograph of (f) several delaminated flakes and (g) a single $Ti_4N_3T_x$ flake (inset: the corresponding SAED pattern, confirming the hexagonal basal plane symmetry) [reproduced from ref. 59 with permission from the Royal Society of Chemistry, copyright 2016]. (h) Replacement reaction between the MAX phase and late transition-metal halides [reproduced from ref. 61 with permission from the American Chemical Society, copyright 2019]. (i) EDX analysis (line scan) of $Ti_3C_2Br_2$ MXene [reproduced from ref. 62 with permission from the American Association for the Advancement of Science, copyright 2020]. (j) XPS full scan spectrum of the pristine Ti_3AlC_2 and the final $Ti_3C_2T_x$ [reproduced from ref. 65 with permission from John Wiley and Sons, copyright 2018]. Anodic etching of bulk Ti_3AlC_2 in a binary aqueous electrolyte: (k(i–iv)), the electrochemical cell setup, XRD patterns of Ti_3AlC_2, $Ti_3C_2T_x$, and $Ti_3C_2T_x$ MXenes, SEM images of Ti_3AlC_2 and $Ti_3C_2T_x$ [reproduced from ref. 67 with permission from John Wiley and Sons, copyright 2018]. (l(i–vi)) Stability of MXene: AFM images of MXenes after exposure to water, SEM image, and XRD patterns of fresh and ageing MXene flakes [reproduced from ref. 68 with permission from John Wiley and Sons, copyright 2021].

2.2. *In situ* HF etching

To ensure safety and minimize environmental impact, an alternative etching method was developed in 2014 by Ghidiu *et al.* This approach uses a LiF + HCl mixture to form HF *in situ*, enabling the selective etching of Al layers from the Ti_3AlC_2 MAX phase to synthesize $Ti_3C_2T_x$ MXene.[47] The LiF + HCl etchant is milder than HF, producing MXene flakes with larger lateral dimensions and fewer defects. Etching with metal halides results in intercalation between cations (such as Li^+) and water molecules, leading to larger lattice parameters in MXene crystals. Fig. 2b shows the XRD patterns of multilayered $Ti_3C_2T_x$, with sharp (000*l*) peaks (pink trace). The lattice parameter was $c \approx 27$–28 Å greater compared to the value ($c \approx 20$ Å) obtained for HF-produced $Ti_3C_2T_x$. This increment was due to the intercalation of water molecules and metal cations between hydrophilic and negatively charged MXene sheets. The sample, after rolling into a thick film (~40 μm), preserved the same *c*-direction peaks, but the major (110) peak was not seen, indicating reduced order in non-basal directions.

This method has been extended to various fluoride salts, including NaF, KF, CaF_2, CsF, FeF_3, NH_4F, $NaHF_2$, and KHF_2.[47–50] Replacing HCl with milder acids like H_2SO_4 yields similar etching behavior. $Ti_3C_2T_x$ synthesized using ammonium bifluoride (NH_4HF_2) etchant had intercalations of NH_3 and NH^{4+} species, and its *c*-lattice parameter (~25 Å) was 25% larger than that of HF-derived $Ti_3C_2T_x$ films.[51] The optimal ratio (12 : 9 M) of LiF + HCl used in the minimally intensive layer delamination (MILD) method eliminated the need for additional delamination steps required in direct HF etching. Manual shaking was sufficient to delaminate MXene into single large flakes.[52] This one-pot process combines HF synthesis, etching, and intercalation into a single step. *In situ* HF etching offers advantages over direct HF etching, including larger lateral dimensions, lower defect concentration, improved stability, and increased interlayer spacing, due to intercalation of metal cations like K^+, Na^+, and NH^{4+} between MXene layers.[53] While enabling milder exfoliation, this method is time-consuming and limited to specific MAX phase precursors for carbide and carbonitride MXenes. The etching process can be difficult to control, leading to over-etching and structural degradation. MXenes produced *via in situ* HF etching have surface terminations (–OH, –F, –O) dependent on etching conditions, often resulting in non-uniform surface chemistry.

2D MXenes can be synthesized using hydrothermal etching.[54,55] Peng *et al.* produced Ti_3C_2 and Nb_2C through hydrothermal etching using $NaBF_4$ and HCl at 180 °C. Under reaction conditions, $NaBF_4$ reacts with HCl to create HF *in situ*, which acts as the fluorine source for etching the parent MAX phase. As shown in Fig. 2c and d, the Ti_3AlC_2 precursor appears as a solid structure, but after 16 h of hydrothermal treatment, it transforms into a layered *h*-Ti_3C_2 structure, indicating broken Ti–Al bonds between layers. Compared to conventional HF-based etching, the hydrothermal approach provides more efficient Al layer removal and increases interlayer spacing in 2D Mxenes.[56] Enhancing experimental safety and producing 2D MXene nanosheets with greater –O and –OH termination ratios and fewer defects are the two main benefits of the *in situ* HF etching method. Nevertheless, throughout the preparation process, cations (Li^+, Na^+, K^+, *etc.*) will intercalate into MXenes' interlayers and are difficult to remove from MXenes, potentially impairing the final MXenes' hydrophilicity, catalytic activity, and electronic conductivity.[39,41,44] Thus, it will affect the nanozyme sensors.

2.3. Fluorine-free acid etching

Fluorine-free etching has emerged as a safer synthesis approach that avoids the use of hazardous HF. Novel fluorine-free techniques are being developed. Researchers introduced thermal-assisted electrochemical etching using diluted HCl to prepare V_2CT_x, Cr_2CT_x, and Ti_2CT_x MXenes.[39,57] A controllable HCl-assisted hydrothermal etching method has been reported for Mo_2Ga_2C, using 12 M HCl (40%) at 140 °C.[58] The schematic process is shown in Fig. 2e. The as-prepared Mo_2CT_x had high purity with only –Cl and –O surface terminations and showed a layered structure with slightly increased interlayer spacing. During etching, concentrated HCl could inhibit oxidation, while lower temperature or diluted HCl would decrease efficiency and product quality.

2.4. Molten salt etching

Aqueous etching methods are effective for most Al-based MAX phases at low temperatures, yielding hydrophilic MXenes, but are unsuitable for nitride-based MAX phases. To address this, a molten fluoride salt method was used by mixing Ti_4AlN_3 MAX with a fluoride salt mixture (1 : 1 ratio). The salt mixture contained KF (59 wt%), LiF (29 wt%), and NaF (12 wt%) corresponding to the ternary eutectic composition. Etching was performed at 550 °C for 30 min under an argon atmosphere, producing $Ti_4N_3T_x$ MXene. The product was delaminated using tetrabutylammonium hydroxide (TBAOH) to produce multilayer- and monolayer-flakes of $Ti_4N_3T_x$ (T = –F, –O, or –OH).[59] During etching, Al layers were selectively removed while Ti–N bonds were preserved, maintaining the layered hexagonal Ti_4N_3 structure. Fig. 2f and g show TEM photographs of $Ti_4N_3T_x$ flakes. The SAED of these flakes (inset in Fig. 1(g)) viewed normal to the basal (002) plane confirms their single crystalline nature and hexagonal symmetry ($P6_3/mmc$) retention from the parent MAX phase. The calculated lattice parameter ($a \sim 2.9$ Å) matches that of the original MAX precursor, indicating that the in-plane structure remains unchanged after Al removal.[60] Owing to ion intercalation during molten salt treatment and water molecules between layers after delamination, the out-of-plane lattice parameter (*c*) increases from 23 Å to ~28 Å. This increase is smaller than that observed in previously reported MXenes, like HF-etched $Nb_4C_3T_x$ (*c*-lattice parameter ~31 Å), likely because of lower water content between

$Ti_4N_3T_x$ layers. This molten salt etching is preferred for MXenes with high formation energies and can be extended to other MAX phases for preparing MXenes.

The nonaqueous molten salt method uses Lewis acidic salts as etchants to synthesize MXenes without fluoride. In this method, MAX phase precursors are modified at high temperatures using transition metal halides in their molten state, which act as strong electron acceptors. M. Li demonstrated etching of the Ti_3AlC_2 MAX phase in a molten salt mixture of $ZnCl_2$/NaCl/KCl under N_2 atmosphere.[61] Zn^{2+} cations react with Al atoms in the MAX phase, converting weakly bonded Al atoms into Al^{3+}. The reduced Zn atoms intercalate between Ti_3C_2 layers and occupy Al sites, creating Ti_3ZnC_2, as shown in Fig. 2h. Excessive $ZnCl_2$ etches the interlayer Zn atoms in the Ti_3ZnC_2 MAX phase, producing MXenes. The reaction outcome depends on the molar ratio of Al-MAX phase to $ZnCl_2$. Because this approach is both nonaqueous and fluoride-free, the surface of the resulting $ZnCl_2$-etched MXene is often terminated with –Cl groups instead of the typical –O, –OH, and –F groups. This approach extends to other MAX precursors like Ti_2AlC, Ti_2AlN, and V_2AlC, resulting in MXenes with tunable surface terminations. Using Cl/Br molten salts yields MXenes with –Cl/–Br groups, shown by the EDX line scan in Fig. 2i, revealing –Br terminations on the $Ti_3C_2Br_2$ surface.[62] These –Cl/–Br groups can be substituted with –O, –S, or –Se groups using Li_2O, Li_2S, or Li_2Se salts at high temperatures, while LiH eliminates surface terminations. Active ionic compounds readily replace surface terminations because of weak bonding between halogen and transition metal atoms. This enables substitution or elimination of terminations on the MXene surface, offering versatile surface chemistry control. The method is safer and suits more MAX precursors, though resulting MXenes are less hydrophilic and require complex experimental conditions.

2.5. Alkali etching

Alkali etching has become a secure and eco-friendly technique for creating MXenes with –O and –OH surface terminations, increasing their hydrophilicity. Despite advantages, alkali-based synthesis of MXenes is challenging as reactions occur spontaneously at high temperatures, making oxidation control difficult at low concentrations. MXenes produced *via* alkali etching show low stability because –OH terminations accelerate oxidation. Alkali compounds like KOH and NaOH were used at high temperatures to remove Al layers, particularly in Ti_3AlC_2, because of OH^- binding with Al atoms. The alkali-assisted hydrothermal method, using NaOH and NaClO, offers a fluorine-free alternative and forms TiO_2 *in situ*, preventing $Ti_3C_2T_x$ layer stacking.[63] MXene nanoribbons could be synthesized *via* the hydrothermal method by etching Ti_3AlC_2 at 180 °C for 24 h in concentrated KOH solution (≈93.3 wt%).[64] Li *et al.* achieved multilayer $Ti_3C_2T_x$ (T = –O, –OH) MXene at 270 °C in 27.5 M NaOH solution with ~92 wt% purity.[65] The synthesized $Ti_3C_2T_x$ shows a {002} plane spacing of 24 Å, which was larger than that of $Ti_3C_2T_x$ (20 Å), produced *via* HF-based methods, suggesting Na^+ ion intercalation from concentrated NaOH solution. XPS data confirmed reduced Al and Na contents in the final $Ti_3C_2T_x$ product (Fig. 2j). The reaction temperature and alkali concentration are crucial for forming hydrophilic MXenes with high purity. However, these factors restrict large-scale MXene production. Alkali etching works best on Al-containing MAX phases because concentrated bases (NaOH and KOH) react with Al layers in a specific way to produce soluble aluminate species like $[Al(OH)_4]^-$. The Al "A-layer" may be effectively removed due to its high solubility, which yields the corresponding 2D MXene nanosheets. In contrast, the MAX phase containing other A layers of Si, Ga, and Ge generates extremely stable oxides or hydroxides (*e.g.*, SiO_2, Ga_2O_3) that are chemically resistant to dissolution under alkaline conditions. Under alkali circumstances, these compounds' weak solubility and inertness restrict successful 2D MXene production and full etching.[39] These point out that the alkali etching technique works only for Al-containing MAX phases, limiting broader MXene family preparation.

2.6. Electrochemical etching

The electrochemical etching route shows promise for selectively extracting nanolaminate materials from MAX phase precursors. Sun *et al.* performed electrochemical etching of the Ti_2AlC MAX phase at 0.6 V (*vs.* Ag/AgCl) in a three-electrode setup.[66] Yang *et al.* introduced a fluorine-free strategy using anodic corrosion of the Ti_3AlC_2 Max phase in a mild alkaline solution.[67] The solution contains ammonium chloride (NH_4Cl) and tetramethylammonium hydroxide (TMAOH) as a binary aqueous electrolyte. Ti_3AlC_2 served as both the anode and cathode. Cl^- ions in the electrolyte caused rapid Al corrosion in the anode, breaking Ti–Al bonds. The XRD patterns showed the (002) peak of Ti_3AlC_2 shifting to a lower angle, corresponding to an increase in *c*-lattice parameter from 18.0 to 22.6 Å, because of termination groups and NH_4OH molecule intercalation between $Ti_3C_2T_x$ layers (Fig. 2k(i and ii)). The intercalated NH_4OH molecules open the etched $Ti_3C_2T_x$ anode edges, facilitating further etching. The Ti_3AlC_2 anode etches fully within 5 h under ambient conditions. The process yields over 90% monolayer or bilayer materials with lateral dimensions above 2 μm, larger than those for traditional HF etching methods. SEM images show that electrochemically etched $Ti_3C_2T_x$ remains tightly stacked with a multilayered structure, unlike accordion-like HF-etched $Ti_3C_2T_x$ structures, resembling bulk Ti_3AlC_2 (Fig. 2k(iii and iv)). Al layer dissolution and NH4OH intercalation produce $Ti_3C_2T_x$ flakes (T = –O, –OH) up to 18.6 μm with high yield (>90%) of mono- or bilayer sheets. Electrochemical etching offers a rapid route for fluorine-free MXene synthesis. However, electrolytes require careful selection because of TMAOH

safety concerns, and reaction time and etching potential significantly affect the final MXene structure.

2.7. Halogen etching

Halogens have been explored as etchants for the MAX phase. Shi *et al.* demonstrated using iodine to etch Ti_3AlC_2 in anhydrous acetonitrile (CH_3CN) at 100 °C, producing accordion-like $Ti_3C_2I_x$.[68] The product was treated with 1 M HCl to eliminate the AlI_3 byproduct from the etching reaction. The –I terminations were unstable and transformed to –OH and –O groups in HCl solution, leading to oxygen-rich $Ti_3C_2T_x$ (T = –OH, –O) MXene sheets with high yield (71%), large lateral size (1.8 μm), and ultrathin structure (<5 nm). As shown in Fig. 2l(i–vi), the iodine-etched MXene sheets maintained excellent structural integrity and showed stability in water for over two weeks compared to fluoride-terminated MXenes from traditional methods. This technique needs expansion for synthesizing other MXenes, such as V_2CT_x, Cr_2CT_x, *etc.*

2.8. Non-etching methods

The bottom-up technique can enable the fabrication of defect-free 2D monolayer MXene crystals, unlike the top-down method. Xu *et al.* synthesized large-area, ultrathin Mo_2C crystals through chemical vapor deposition (CVD) at 1085 °C.[69] Methane served as the carbon source, while Cu/Mo foil acted as the substrate. The Mo_2C crystals were nanometers thick with a lateral size of ~100 μm and good structural stability under ambient conditions. MAX and MXene thin film composites were fabricated using a two-step method involving ion beam sputtering.[70] A low-energy ion facility (LEIF) using heavy ions was developed. Low-energy DC ion beam sputtering of elemental targets forms uniform layers of mixed phases or multilayers of individual phases; thermal annealing under vacuum enables diffusion and phase interactions to form desired composites. The first Ti-based MAX and MXene carbide (Ti_2SnC and Ti_2C) composite thin films were produced. However, MXenes prepared by bottom-up methods typically lack surface terminations and suffer from low yield and sophisticated equipment requirements. The Y_2CF_2 crystal, a stack of MXene-like sheets with fluorine terminations, was directly synthesized through solid-state reaction at high temperature without air and water.[71] The unit cell of the 3D crystal was isostructural to MXene, but the layers are held together by ionic bonds. The yttrium carbide layers were electrically isolated by the fluorine layers, providing 2D-like electronic transport properties to this 3D crystalline material.

MXenes' surface chemistry, structural integrity, and effectiveness as nanozymes are all determined by their synthesis process. For example, –O, –OH, and –F-terminated surfaces are commonly produced by standard HF and *in situ* HF etching; an excess of –F can impede electron transmission and lower catalytic performance. On the other hand, fluoride-free techniques, including halogen etching, electrochemical etching, alkali, or molten salt, frequently provide O-rich MXenes with better conductivity, redox activity, and environmental durability, which makes them more appropriate for catalytic and sensing applications (Table 1). Furthermore, considerations of safety, scalability, and cost vary widely across methods, with molten salt and *in situ* HF approaches showing the greatest promise for real-world applications.[39,57] Therefore, the choice of synthetic protocol not only determines the characteristics of MXene but also plays a crucial role in determining its long-term viability and performance in nanozyme-based technologies.

3. MXzyme classifications

There are numerous ways to classify nanozymes. In their work, M. Zandieh *et al.*[72] divided nanozymes into two

Table 1 Comparison of MXene synthesis protocols, their influence on their properties, scalability, and limitations

Method	Etching source	Surface terminations	MXene features	Scalability and limitations
Direct HF etching	HF acid	–F, –OH, –O	High yield; generates stable multilayer MXenes; conductivity is decreased by F-rich surfaces	Scalable yet risky because of HF handling, safety, and sustainability problems
In situ HF etching	LiF/HCl, NH_4F/HCl	Tunable –O /–OH/–F ratios	Improved hydrophilicity; enhanced interlayer spacing from ion intercalation	Safer than direct HF; moderately scalable; properties depend on cation type
F-free acid etching	HCl	–Cl dominant, some –OH, –O	Controlled layer removal	Safer than HF; termination control is limited
Molten salt etching	KF, and NaF	–O, some –F	F-free MXenes; enhanced conductivity, thermal stability, and oxidation resistance	Large-scale potential; requires high temperatures and careful handling
Alkali etching	NaOH and KOH	–OH and –O	Produces MXenes with minimal –F; improved catalytic and electronic properties	Limited to Al-containing MAX phases; harsh conditions; scalability still under evaluation
Electrochemical etching	Electrochemical equipment	–OH and –O rich, fewer –F	Eco-friendly; control and precise etching; good for fine-tuning surface states	Low yield is not suitable for bulk production
Halogen etching	I_2	–OH and –O	Unique surface with good stability	Challenging to synthesize and needs more safety precautions
Non-etching methods	CVD, and ion beam sputtering	Customized terminations	High purity and tunable terminations	Early processes; costly, difficult, and at present limited in scalability

categories based on development history. The first decade was dominated by type 1 nanozymes, which are catalysts or enzymes immobilized on nanomaterials since 2004. Type 2 nanozymes, extensively studied in the past decade, are based on the self-catalytic characteristics of inorganic nanomaterial surfaces. MXzymes with catalytic activity can be divided into three types: POD, oxidase (OD), and other catalytic nanozymes like catalase (CAT) and superoxide dismutase (SOD).[73,74] Hydrolases work like phosphatases, nucleases, proteases, and other enzymes in catalyzing hydrolysis. CAT-like and SOD-like nanozymes are less common in colorimetric sensing as they are mainly used in biomedical applications for removing reactive oxygen species (ROS) and protecting cell membranes.[73–75] It is important to note that CAT-like nanozymes exhibit relatively lower catalytic turnover in the absence of high H_2O_2 concentrations, which restricts their applicability in typical biosensing environments. Similarly, SOD-like activity is mechanistically more complex and often requires precise superoxide generation and detection systems, making it less suitable for straightforward sensing platforms compared with POD- and OD-like systems.[1,75] Thus, POD-like and OD-like nanozymes are our main investigation focus.[76,77]

In biosystems, oxidative enzymes POD and OD catalyze substrate oxidation under mild circumstances by activating H_2O_2/O_2.[36,79] MXenes' large specific areas make them suitable supports for enzymatic events, with physical and chemical features enhancing supported NP stability and POD catalysis.[78] O_2 is the oxygen supply used by OD to catalyze oxidation.[36] Jin *et al.*[79] hydrothermally treated $Ti_3C_2T_x$ MXene to create TiO_2-loaded carbon quantum dots (TiO_2/C-QDs), an active OD nanozyme, developing a quick colorimetric technique for GSH identification. CATs and SODs are antioxidant enzymes crucial in scavenging excess ROS and preserving redox balance. These nanozymes catalyze O_2 conversion into H_2O_2 and O_2, created by O_2 and H_2O breakdown and OH radical scavenging.[80,81] Nb_2C nanosheets modified with polyvinylpyrrolidone (PVP) were created by liquid-phase exfoliation, showing SOD-like features from surface oxidation.[82] Several MXene-based nanozymes exhibit multiple enzymatic activities.[83–85] V_2C-based nanozymes demonstrate six enzyme-like properties (SOD, CAT, POD, GPx, TPx, and HPO), enabling biocompatibility and cytoprotection against oxidative stress.[29]

4. Factors affecting MXzyme-based sensors

MXzyme's enzymatic activity is influenced by its composition, oxidation state, and surface structure. The inclusion of transition metals like Nb and Ti in MXene could assist in transferring electron activities, crucial for reaction catalysts.[38] The catalytic functionalities of MXene-based nanozymes can be modulated by altering MXene components. MXzymes can generate hybrids with improved catalytic activity.[37,38] Additionally, MXene's layered structure offers a vast surface area and improved catalytic activity. Because thinner nanosheets provide more surface area and catalytically active sites, the lateral dimension and thickness of MXene nanosheets influence enzymatic activity. Altering electrical characteristics and active site accessibility directly influences enzyme functioning. MXzyme' catalytic activity can be impacted by surface alterations, including functional groups and surface charges.[38] The synthesis conditions and chemical treatment can accommodate various functional groups on the MXene surface, including –O, –F, and –OH. The pH and temperature regulate the catalytic activity of nanozymes based on MXene.[86] pH has a significant effect on catalytic properties. The catalytic capabilities can be controlled using photo-responsive technology. Under near-infrared (NIR) irradiation, the catalytic capabilities of MXzymes increase owing to high photothermal conversion efficiency in the NIR range.[37] MXene's enzyme-like activity can be enhanced by considering and refining these enzymatic qualities.

5. MXzyme-based sensor classification

Based on the enzyme mimic features and detection modes of MXene supported nanostructured materials, various sensing platforms such as colorimetric, smartphone assisted colorimetric, fluorescence, chemiluminescence, electrochemiluminescence, electrochemical, and SERS sensors have been explored for the detection of a wide range of analytes. The following sections will comprehensively discuss these sensing systems in detail.

5.1. MXzyme colorimetric sensors

In chemical analysis, naked-eye visual analysis is a strong method that determines substance concentration by measuring solution color intensity through color absorption.[87,88] Reliability, affordability, and convenience are its main advantages, driving advancements in biomolecule identification.[88,89] ELISA, which uses an enzyme to activate a chromophore and produce a discernible color shift in solution, is among the most widely used methods.[90] This change is visible to the naked eye or can be evaluated using a spectrometer. This method is used for quick detection in sensor technologies and is effective.[91,92] However, detection sensitivity is limited by the low extinction coefficient of organic chromophores, which presents a problem.

The following elements are typically included in colorimetric observing mechanisms, depending on the kinds of substances or reactions employed to fabricate colorimetric sensors:

(i) Target-induced changes in interparticle distance, size, shape, or composition cause the plasmonic NPs (such as Ag and Au NPs) to change color through surface plasmon resonance (SPR).[91,92]

(ii) Fluorescent on–off switching or photonic crystal color changes in the direction of targets.[93,94]

(iii) Catalyzed by natural enzymes, enzyme mimics, synthetic enzymes, or nanozymes, the chromogenic reaction of several substrates, including 3,3′,5,5′-tetramethylbenzidine (TMB).[15]

(iv) The direct or indirect production of colored products or the colorimetric alteration of chromogenic agents brought on by the targets through non-enzymatic processes.[95]

Enzyme mimic-based colorimetric sensors are recent developments in this field.[37,96–98] A substrate is converted by nanozymes into an optically detectable product, producing a quantifiable signal. Catalytic turnover, where a single nanozyme speeds up many substrate-to-product conversion events, causes signal amplification that increases recognition sensitivity.[97,98] Compared to conventional noncatalytic AuNPs, nanozymes with intrinsic optical characteristics provide increased detection sensitivity, improving the detection limit by up to 10 times.[96] The optical contributions of nanozymes in colorimetric assays extend beyond catalysis. An improvement in detection limit can significantly impact assay diagnostic precision. Advancements are underway to engineer nanozymes with superior optical features by tuning their physical attributes (size, shape) and chemical composition (element distribution).[15,99,100] Table 2 summarizes the substrates for these enzyme mimic catalyzed reactions, which are chromogenic compounds.

5.1.1. Heavy metal ions. Globally, the environment is polluted by heavy metal ions because of mining operations, production, subsurface water extraction, depleted groundwater supplies, and unregulated factory waste. Substances containing harmful metal ions (Hg^{2+}, Cr^{3+}, Cr^{6+},

Table 2 Nanozyme substrates are utilized for different analytical sensors

Substrate	Product	Colorimetric signal	Detection platforms
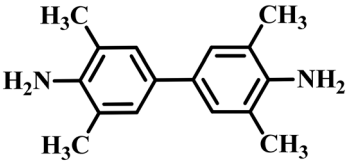 (TMB)	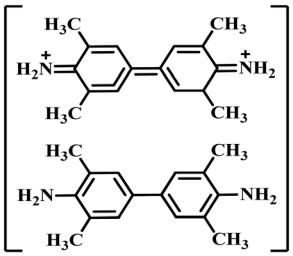 (TMBox)	TMB is colorless, oxidized TMB displays a blue color	Colorimetric, fluorescence, and SERS sensors. Notably, these are further developed to be operated by smartphones
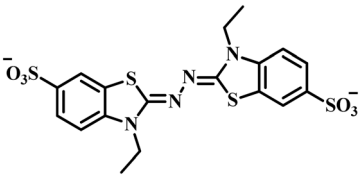 (ABTS)	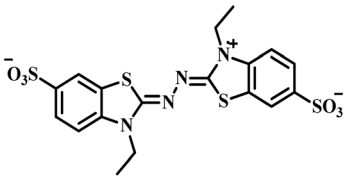 (ABTSox)	Oxidized product APTSox exhibits a green color	Colorimetric and electrochemical sensors
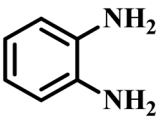 (OPD)	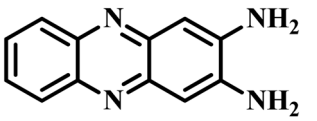 (OPDox)	Oxidized OPD has a yellow color and shows an emission around 550 nm	Colorimetric, smartphone, and fluorescence sensors
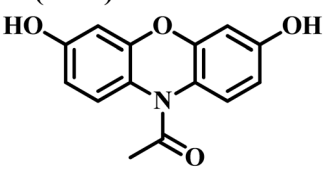 (Amplifu red)	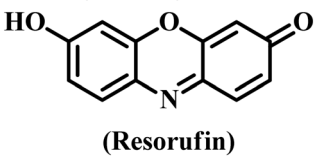 (Resorufin)	Oxidized Amplifu red displays fluorescence maximum at 585 nm	Fluorescence-based chemo-biosensors
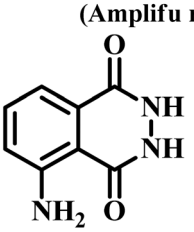 (Luminol, (LH))	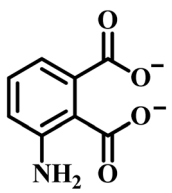 (3-Aminophthalate, (AP))	LH is oxidized into AP, which offers a chemiluminescent indicator	Chemiluminescent assays

Pb^{2+}, *etc.*) will be distinguished.[15] For example, Pt NPs on $Ti_3C_2T_x$ MXene nanoribbons ($Ti_3C_2T_x$ MXene NR) were synthesized by the hydrothermal method to detect Hg^{2+} ions.[101] The nanozyme activity was suppressed by Hg^{2+} ions, while Pt–Hg amalgam formed, allowing for a POD-like colorimetric detection technique with a 15 pM LOD (Fig. 3a). A hydrogel-based sensor with smartphone assistance was created, attaining a 26 pM detection limit. Next, a DNA-encoded MXene–Pt nanozyme was developed for sensitive colorimetric detection of Hg^{2+} ions.[102] Researchers used a DNA-mediated seed-growth technique to overcome pristine MXenes' drawbacks. The POD activity of these nanocomposites was inhibited by Hg^{2+} because of its binding and reduction to Hg^0 on the hybrid interface of Pt NPs (Fig. 3b). Quick, high-throughput, point-of-care mercury detection was enabled by the nanozyme's integration with a centrifugal microfluidic device. Xun Zhou *et al.* explored a $Ti_3C_2T_x$ MXene NR hybrid decorated with self-reduced AuNPs for POD-like colorimetric detection of Hg^{2+} ions and cysteine (Cys) (Fig. 3c).[103] They created the $Ti_3C_2T_x$ MXene NR hybrid using the self-reducing characteristics of $Ti_3C_2T_x$ MXene. These NPs showed increased POD activity with Hg^{2+} ions as Au–Hg amalgam formed. TMB's oxidation was catalyzed, causing a visible transformation from colorless to dark blue, while the absorbance spectral wavelength at 653 nm was enhanced (Fig. 3c(i and ii)). The reaction was reversed by Cys's reducing qualities, returning the color to its initial state. This sensor outperformed earlier colorimetric techniques with selectivity, sensitivity, and a low detection limit for Hg^{2+} ions (0.054 nM). A smartphone-based detection device was created for real-time measurement of Cys and Hg^{2+} ions. For hexavalent Cr detection, Fe_3O_4@MXene quantum dots with enhanced POD activity were reported.[104] The hybrid material was created using an ultrasonic technique and could catalyze H_2O_2 breakdown into reactive hydroxyl radicals. A colorimetric sensor with a 0.26 μM detection limit was created using Fe_3O_4@MXene quantum dots. The results showed that Fe_3O_4@MXene quantum dots can be useful for pollution detection and environmental monitoring.

5.1.2. Biothiols. Biothiols are molecules containing a free thiol group, including glutathione (GSH), homocysteine (HCy), and Cys. These thiols in appropriate amounts are crucial for metabolic functions in living things. Owing to their impact, sensitive sensing of thiols is important.[105] Mo atom nanoclusters/N–$Ti_3C_2T_x$ MXzymes were fabricated for

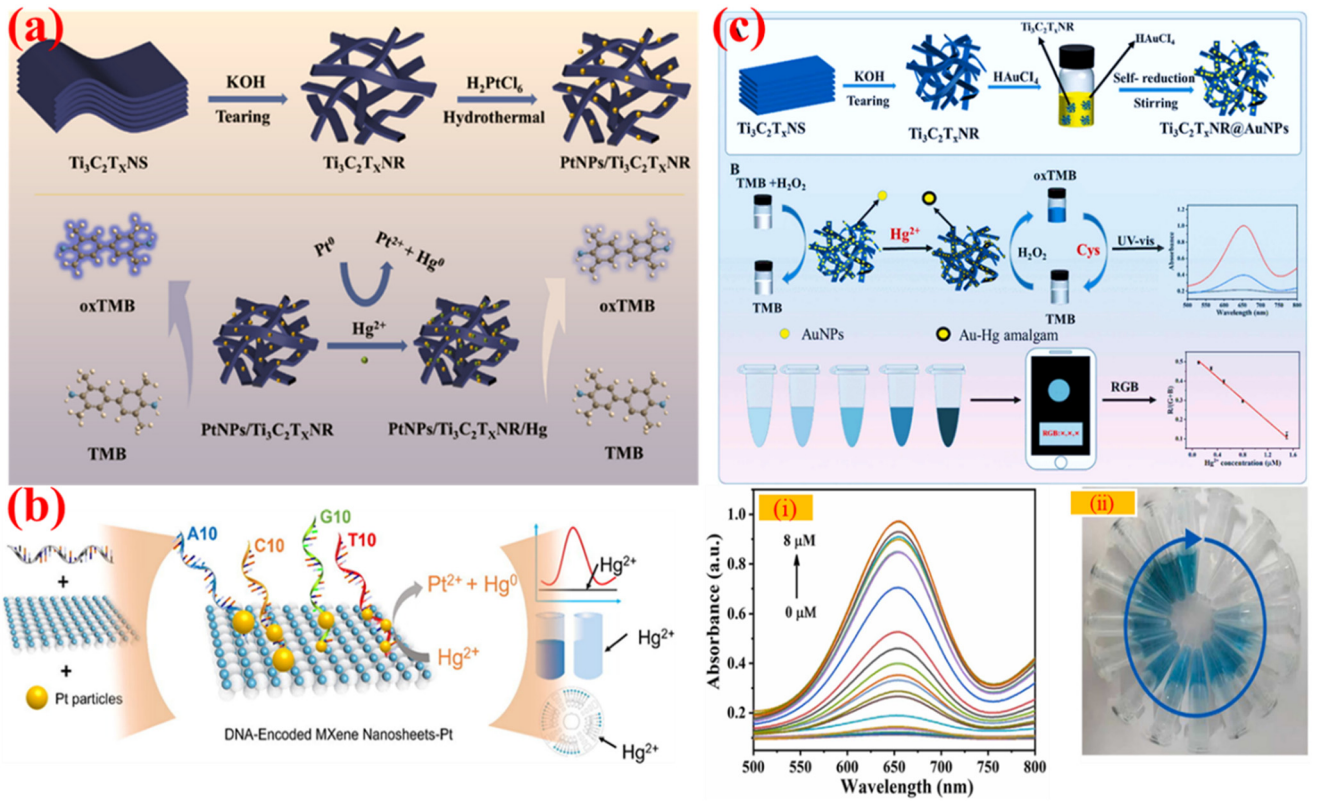

Fig. 3 MXzyme-based colorimetric detection of heavy metal ions. (a) Pt NPs on $Ti_3C_2T_x$ MXene nanoribbons ($Ti_3C_2T_x$ MXene NR) were synthesized by the hydrothermal method and utilized to detect Hg^{2+} ions by POD activity [reproduced from ref. 101 with permission from Elsevier, copyright 2024], (b) DNA-encoded MXene–Pt nanozyme for highly sensitive colorimetric detection of Hg^{2+} ions by POD activity [reproduced from ref. 102 with permission from Elsevier, copyright 2022], and (c) $Ti_3C_2T_x$ MXene NR hybrid decorated with self-reduced AuNPs for highly sensitive POD-like colorimetric detection of Hg^{2+} ions and Cys [reproduced from ref. 103 with permission from Elsevier, copyright 2023]. In (i) and (ii), the absorbance spectral profile at 652 nm and colorimetric changes (Au/$Ti_3C_2T_x$ MXene NR + TMB + H_2O_2) with various concentrations of Hg^{2+} ions are represented, respectively.

sensitive colorimetric detection of GSH.[106] By creating Mo NCs/N–$Ti_3C_2T_x$ MXzymes with increased POD-like activity, researchers found that they outperformed natural HRP (Fig. 4a). The study showed that nitrogen doping and Mo atom clusters increased catalytic efficiency by altering electron–metal-carrier interactions. Furthermore, this work's experimental and theoretical findings jointly indicate that N doping reduces the strong bonds between OH groups and Mo atoms, significantly enhancing the POD-like catalytic activity of Mo NCs/N–$Ti_3C_2T_x$ MXzymes. The nanozyme demonstrated stability and recyclability, allowing GSH detection with a 0.29 μM detection limit. The process relied on TMB oxidizing with H_2O_2, and colorimetric changes correlated with GSH levels. The technique effectively identified GSH with high sensitivity in biological fluids like human serum and urine. Based on this concept, Wenjing Wang's team established polydopamine-functionalized MXene/Carbon Dots (CDs) for POD visual detection of GSH in biological fluids with LOD 0.12 μM.[107] In a similar TMB-based POD activity, J. Wang *et al.* reported visual detection of GSH and H_2O_2 by MXene@Fe_3O_4 nanocomposites.[108] The sensor showed selectivity in biological samples, with detection limits of 0.4 mM for H_2O_2 and 0.5 mM for GSH. Several MXene-supported nanozymes were demonstrated for GSH quantification using TMB substrate-based POD performance.[104,109,110] Another example is detecting biothiols using POD-mimicking AgNPs on $Ti_3C_2T_x$ MXene nanosheets (AgNPs@$Ti_3C_2T_x$ MXene NSs).[111] These nanocomposites showed enhanced POD-like activity, catalyzing OPD oxidation with H_2O_2. This activity was reduced by biothiols, enabling color-change-based detection. The method showed linear ranges (50 nM to 50 μM for Cys, 10 nM to 250 μM for HCy, and 10 nM to 50 μM for GSH) with low detection limits (48.5 nM for Cys, 5.5 nM for HCy, and 7.0 nM for GSH). The detection of Cys in diluted human serum samples produced high recovery rates. TiO_2-loaded carbon quantum dots (TiO_2/C-QDs) were created by Jin *et al.*[79] by hydrothermally treating $Ti_3C_2T_x$ MXene, and they demonstrated a strong OD-like nanozyme activity (Fig. 4b). Catalytic efficiency was increased by the creation of TiO_2 nanoparticles anchored on conductive C-QDs, which offered a large number of active sites and sped up electron transmission. This hybrid nanozyme was used to provide a quick colorimetric technique for detecting GSH (Fig. 4b(i)). The oxidation of chromogenic substrates was catalyzed by the oxidase-mimicking TiO_2/C-QDs, resulting in a unique

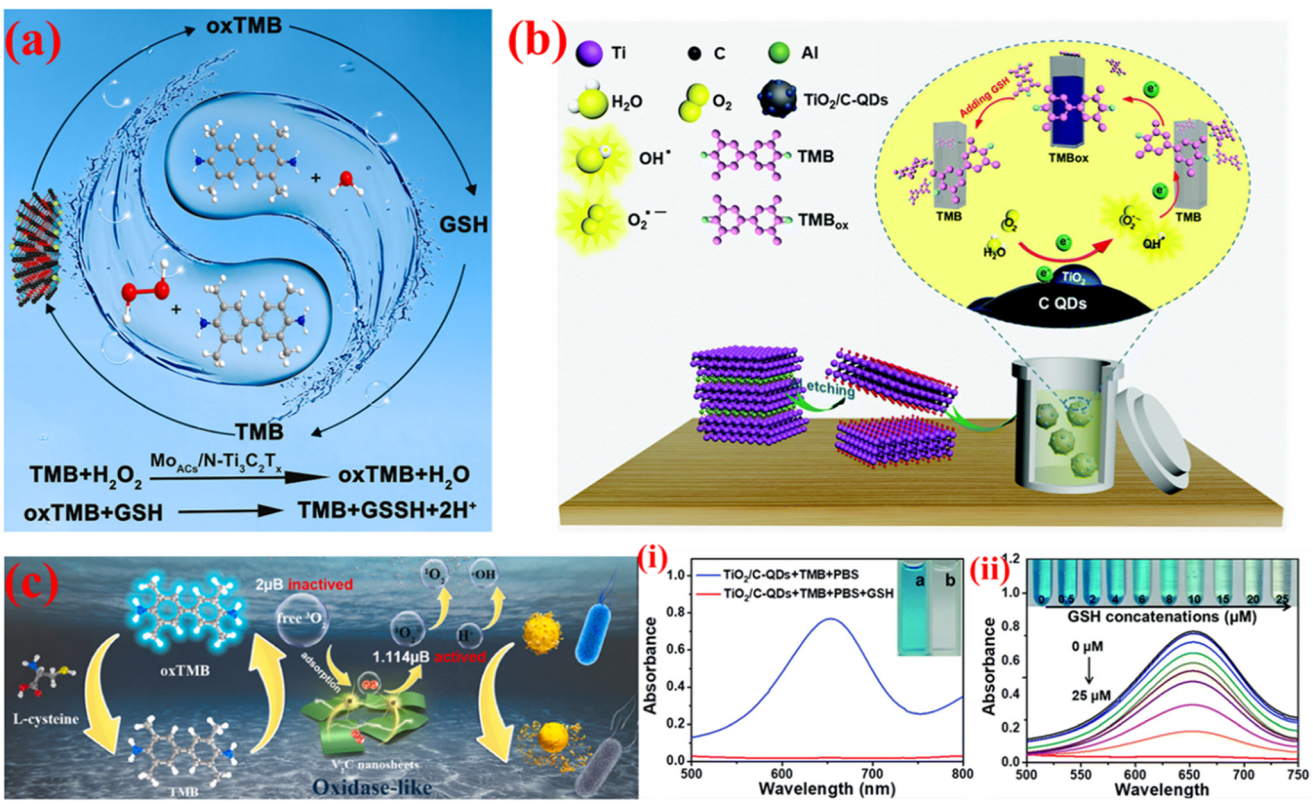

Fig. 4 MXzyme-based colorimetric detection of biothiols. (a) Mo atom nanoclusters/N–$Ti_3C_2T_x$ MXzymes based POD-like sensing of GSH [reproduced from ref. 106 with permission from Elsevier, copyright 2024], (b) TiO_2/C-QDs-$Ti_3C_2T_x$ MXene composite MXzyme based OD-like sensing of GSH, and (i) and (ii) represent the OD-like behavior of the TiO_2/C-QDs-$Ti_3C_2T_x$ MXene composite and sensitive detection of GSH at increasing concentrations, respectively [reproduced from ref. 79 with permission from Royal Society of Chemistry, copyright 2020]. (c) OD-like V_2C MXzyme with antibacterial qualities for colorimetric sensing application of Cys [reproduced from ref. 112 with permission from Elsevier, copyright 2023].

color signal that was selectively quenched by the potent reducing activity of GSH (Fig. 4b(ii)). This allowed for sensitive and specific detection that is pertinent to biological diagnostics. The fabrication of an OD-like V_2C MXzyme with antibacterial properties for colorimetric sensing was discussed by Da Chen's research team.[112] Using intercalation and stripping, researchers constructed V_2C MXene nanosheets that could accelerate TMB oxidation without H_2O_2. The study showed the nanozyme activated oxygen on the surface, causing structural changes that enhanced catalytic effectiveness (Fig. 4c). V_2C MXene demonstrated antibacterial action by producing ROS, which stopped the growth of both Gram-positive and Gram-negative bacteria. Based on this nanozyme, an OD-like colorimetric sensor was developed, enabling sensitive detection of Cys with a 30.0 nM detection limit.

5.1.3. Biological analytes and small molecules. H_2O_2 is utilized in various productions and can originate in biotic settings, water and air. Within certain levels, H_2O_2 can be hazardous to human health. For safety and diagnostic reasons, determining its concentration is essential. A heterostructure Au@Pt/Nb_2C-MXene nanocomposite for

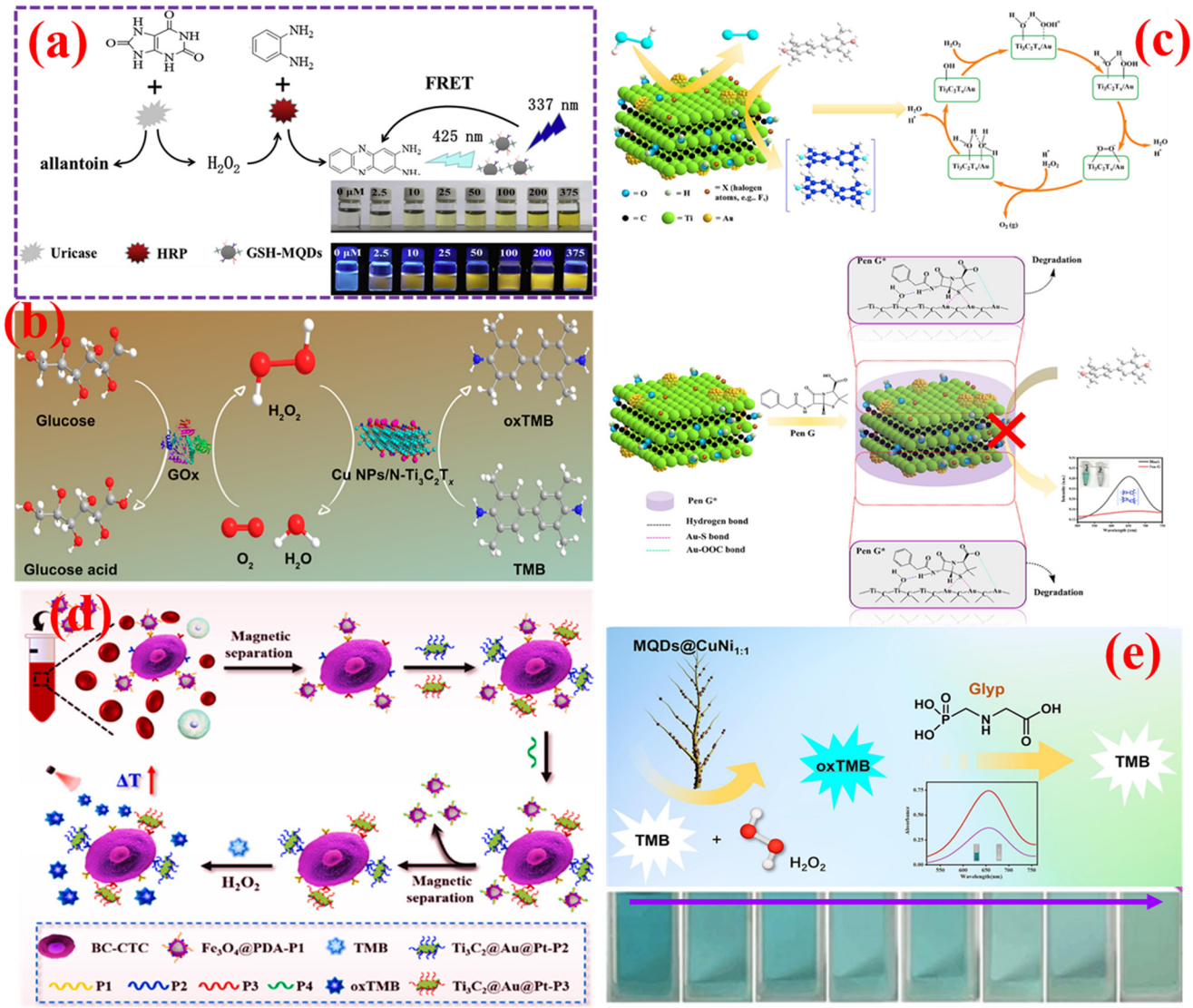

Fig. 5 MXzyme-based colorimetric sensors for biologically important analytes. (a) Colorimetric and ratiometric fluorescence probe for detecting UA by GSH-functionalized $Ti_3C_2T_x$ MXene QDs, and the inset shows colorimetric changes of nanozyme with different quantities of UA under daylight and UV light [reproduced from ref. 115 with permission from Elsevier, copyright 2020], (b) POD-like activity-based colorimetric sensing strategy for glucose using CuNPs/N-doped $Ti_3C_2T_x$ MXene hybrids [reproduced from ref. 119 with permission from American Chemical Society, copyright 2022], (c) $Ti_3C_2T_x$ MXene/AuNPs heterostructure nanozyme-based detection of penicillin G and the possible sensing mechanism [reproduced from ref. 125 with permission from Elsevier, copyright 2024], (d) $Ti_3C_2T_x$ MXene supported-Fe_3O_4@PDA-aptamer capture nanoprobe for direct capture and detection of BC-CTCs [reproduced from ref. 128 with permission from Elsevier, copyright 2023], and (e) dendritic-like Ti_3C_2-T_x MXene QDs@CuNi nanozyme-based colorimetric detection of glyphosphate, and the inset shows the colorimetric changes in the various concentrations of glyphosphate [reproduced from ref. 133 with permission from Elsevier, copyright 2024].

colorimetric identification of H_2O_2 was developed based on POD-like activity.[113] This nanocomposite was created using interfacial electrostatic attraction to decorate Au@Pt core–shell NPs on 2D Nb_2C-MXene nanosheets. Owing to synergistic electron transfer and photothermal effects, the nanocomposite showed improved POD-mimicking activity, accelerating TMB oxidation with H_2O_2. Kinetic investigations following the Michaelis–Menten model showed high catalytic affinity. The technique demonstrated promise for biosensing applications when used to detect H_2O_2 in biological samples.

The need for quick, sensitive, and consistent uric acid (UA) detection has grown because of increasing cases of conditions like osteoarthritis linked to abnormal UA levels.[114] Sensor materials have attracted interest owing to affordability, ease of use, and electromagnetic interference resistance. Research has focused on UA direct identification for continuous monitoring and quick diagnosis. A "naked-eye" colorimetric and ratiometric fluorescence probe using GSH-functionalized $Ti_3C_2T_x$ MXene quantum dots was developed.[115] The technique used uricase to oxidize UA, yielding H_2O_2 and allantoin, which oxidized OPD to 2,3-diaminophenazine. The UV absorption of oxOPD at 425 nm matched the fluorescence emission of GSH-$Ti_3C_2T_x$ MXene QDs at 430 nm, enabling ratiometric UA measurement and FRET (Fig. 5a). The probe showed stability, selectivity, and a LOD of 125 nM. N and S co-doped $Ti_3C_2T_x$ MXene nanosheets were developed for UA detection using TMB oxidation.[116] Thiourea enhanced the material's POD-like activity by improving active sites and electron transport. The catalytic mechanism involved protonating TMB and H_2O_2 dissociation. The ZnO–Co_3O_4 nanofiber/MXene composite's POD-like colorimetric features detected ascorbic acid (AA).[117] The MXene-supported nanocomposite showed rapid reaction kinetics and proved suitable for food analysis through orange juice testing.

Glucose is the primary energetic source in our bodies and is essential to metabolic processes. Diabetes prevalence is rising in emerging nations because of economic growth and urbanization. Insulin dosages can be modified to maintain glucose levels within permitted limits and reduce complications through accurate glucose assessment.[118] A POD-like activity-based colorimetric sensing strategy for glucose using CuNPs/N-doped $Ti_3C_2T_x$ MXene hybrids was established.[119] CuNPs were anchored onto N-doped $Ti_3C_2T_x$ MXene through simple synthesis, producing a nanohybrid with stable structures and significant catalytic power (Fig. 5b). The oxidation of TMB with H_2O_2 resulted in a blue oxidized product with absorbance at 652 nm. The glucose sensor showed excellent sensitivity, specificity, and reliability with a LOD of 5 μM. It retained POD-like properties after a month of storage. Similarly, Pt/$Ti_3C_2T_x$ MXzyme was applied for glucose and GSH detection.[109] The optimized Pt/$Ti_3C_2T_x$ MXzyme showed POD-like activity 7.9 times higher than that of Pt alone under NIR radiation, and six times higher in the dark. Yu He's team reported $Ti_3C_2T_x$ MXene/Co nanosheet hydrogel sensors for glucose recognition *via* smartphone-based point-of-care testing.[120] The $Ti_3C_2T_x$ MXene/Co nanosheet material catalyzed TMB by H_2O_2, producing a blue-colored product. A sodium alginate hydrogel-embedded $Ti_3C_2T_x$ MXene/Co nanosheet sensor enables real-time glucose measurement using RGB analysis and a smartphone app. G. Yang's team developed a glucose-sensing method through an immunoassay for IR-β detection using $Ti_3C_2T_x$ MXene's catalytic activity.[29] These studies showed MXene-based nanozymes' potential for rapid, portable glucose sensing.

Cholesterol is necessary for human survival, but can pose serious health risks when accumulated beyond certain thresholds. Keeping cholesterol intake regulated is essential for maintaining key physiological processes.[121] Y. Chen *et al.* described an Ag/$Ti_3C_2T_x$ MXzyme with boosted POD-mimicking activity for antibacterial applications and cholesterol sensing.[122] The Ag/$Ti_3C_2T_x$ MXzyme produced by *in situ* reduction indicated higher catalytic efficiency. Both Gram-positive and Gram-negative bacteria were inhibited by their conversion of H_2O_2 into hydroxyl radicals, which disrupted bacterial biofilms. The Ag/$Ti_3C_2T_x$ MXzyme's POD-like activity was coupled with cholesterol oxidase to create a TMB-based colorimetric biosensor. This sensing technique showed accuracy when used to detect cholesterol in human blood specimens. According to TMB oxidation, Y. Li *et al.* reported an MXene-supported CuS nanozyme for cholesterol sensing.[123]

5.1.4. Antibiotic compounds. Antibiotics have gained interest as novel organic contaminants because of their widespread use and possible adverse effects.[124] Penicillin G, an antibiotic used to treat bacterial infections in animals, can contaminate animal products when used excessively. Consuming foods tainted with antibiotics can lead to accumulation and health risks. For penicillin G detection, a colorimetric sensor using $Ti_3C_2T_x$ MXene/AuNPs heterostructure with catalase-mimic activity was developed.[125] This nanocomposite catalyzed TMB oxidation with H_2O_2, producing a greenish-blue color at 652 nm. Penicillin G suppressed this response, enabling sensitive detection with an LOD of 7.51 nM. The tests worked on food samples, notably milk, with good recovery rates and showed high selectivity against other antibiotics. The authors suggest that penicillin G molecules could adsorb onto Au through hydrogen bonding and Au–S interactions in acidic environments, based on known interactions between Au and ampicillin, and hydrogen bonding between TiO_2 and penicillin G (Fig. 5c). This adsorption may block $Ti_3C_2T_x$/AuNPs' active sites, inhibiting TMB oxidation and color change. Using the $Ti_3C_2T_x$ MXene/AuNPs nanocomposite TMB-based POD-like colorimetric sensing of ampicillin in plasma samples was reported by Wanqing Yue's research group.[126] Sulfur atoms in ampicillin formed Au–S bonds with the nanocomposite, reducing catalytic function and causing color fading for detection. Kanamycin (KA), an aminoglycoside antibiotic, treats Gram-negative bacterial infections. A colorimetric biosensor using oxygen-

terminated few-layered $Ti_3C_2T_x$ MXene nanosheets as POD-mimic nanozyme was developed for kanamycin detection.[127] OFL-$Ti_3C_2T_x$MXene nanosheets catalyzed TMB oxidation with H_2O_2, causing a bluish-green color change. Adding kanamycin prevented this reaction, causing color fading. This created a sensitive biosensor with a 15.28 nM–46.14 μM dynamic range and 15.28 nM detection limit. The research explained kanamycin's antibacterial action through its inhibitory effect on POD-like activity.

5.1.5. Cancer cells and pathogens. The most prevalent malignancy worldwide is breast cancer (BC), and migrating tumor cells (CTCs) are trustworthy indicators for harmless early-stage breast cancer screening. Isolating BC-CTCs from human blood samples and detecting them sensitively using portable gadgets remains challenging.[128] Feng Li *et al.* established the $Ti_3C_2T_x$ MXene supported-Fe_3O_4@polydopamine (PDA)-aptamer capture nanoprobe for direct capture and detection of BC-CTCs.[128] A 2D core–shell structured multifunctional $Ti_3C_2T_x$ MXene@Au@Pt nanozyme was developed by integrating an efficient photothermal nanomaterial with POD-like catalytic activity. This nanozyme catalyzed the oxidation of TMB to produce oxTMB, which subsequently interacted with $Ti_3C_2T_x$ MXene@Au@Pt to amplify the photothermal signal and enhance the detection sensitivity. The Fe_3O_4@PDA-P1 capture nanoprobe attached to the cell surface in the presence of BC-CTCs through specific recognition. After magnetic separation, $Ti_3C_2T_x$ and $Ti_3C_2T_x$ MXene@Au@Pt–P2, @Au@Pt–P3 were found on the BC-CTC surface. Fe_3O_4@PDA-P1 was liberated from the captured BC-CTCs by strand displacement reaction with P4, as shown in Fig. 5d. The sensor enabled sensitive identification of BC-CTCs in blood specimens with a LOD of 50 cells per mL and high specificity. This revealed a non-surgical detection method for breast cancer that is sensitive and user-friendly.

Hepatitis B virus (HBV) infection is linked to human hepatitis disorders, including chronic hepatitis, liver fibrosis, cirrhosis, and hepatoma. Researchers introduced a CRISPR-Cas12a-based colorimetric biosensor using the DNA-modulated POD-mimic activity (TMB) of $Ti_3C_2T_x$ MXene–Ag/Pt nanohybrids.[129] A colorimetric reaction occurred when Cas12a enzyme triggered *trans*-cleavage with HBV DNA, breaking down the DNA probe and inhibiting the nanohybrid's catalytic activity. The biosensor tested human serum samples with excellent sensitivity and sub-picomolar LOD. A smartphone-based platform enabled real-time, visible detection suitable for field use.[88] This work demonstrated sensitive viral DNA detection by combining CRISPR technology with nanozymes. Wenhai Wang *et al.* developed a dual-mode aptasensor for detecting *Vibrio parahaemolyticus* (V.P.) using Pt, phenyl boric acid (PBA), and a ferrocene-modified $Ti_3C_2T_x$ MXene nanoprobe (PBA-Fc@Pt@$Ti_3C_2T_x$ MXene).[130] The aptasensor collected bacteria using an aptamer-functionalized electrode, combining colorimetric and electrochemical detection. The PBA-Fc@Pt@$Ti_3C_2T_x$ MXene nanohybrid formed a sandwich complex, catalyzing TMB oxidation with H_2O_2 to generate visible and electrochemical signals. Detection limits were 30 CFU mL^{-1} in colorimetric mode and 5 CFU mL^{-1} in electrochemical mode. The platform could detect other diseases by changing the aptamer, offering a versatile tool for pathogen screening.

5.1.6. Pesticides. Most commonly employed in agriculture, organophosphorus pesticides (OPs) can be hazardous to human health and food safety because of their residues. Monitoring OP amounts in food samples is crucial. Distinguishing between OP species with comparable chemical structures remains difficult.[131] The synthesis of Prussian blue (PB)-$Ti_3C_2T_x$ MXene hybrid nanocomposites (PB@$Ti_3C_2T_x$ MXene) enabled dual-functionality for H_2O_2 and pesticide (malathion) detection.[132] The PB@$Ti_3C_2T_x$ MXene hybrid showed strong POD-like activity of TMB for colorimetric detection of H_2O_2 with an extensive linear range and sensitivity. An acetylcholinesterase (AChE)-modified PB@$Ti_3C_2T_x$ MXene hybrid electrode was developed for malathion recognition. Applied to actual food samples, it demonstrated outstanding stability, selectivity, and repeatability. Ke Chu's research group developed dendritic-like $Ti_3C_2T_x$ MXene QDs@CuNi *via* the hydrothermal method for glyphosate detection.[133] The $Ti_3C_2T_x$ MXene QDs@CuNi nanocomposites showed greater POD-like activity of TMB, catalyzing H_2O_2 decomposition and generating –OH radicals. Upon glyphosphate interaction, the blue color disappeared (Fig. 5e and inset).

According to theoretical calculations, the interaction between CuNi bimetal and MXene quantum dots, which promoted H_2O_2 activation, caused the high catalytic efficiency. Using this strategy, $Ti_3C_2T_x$ MXene-supported nanostructured materials showed POD-like catalytic performance for detecting dipterex, astaxanthin, and guanosine 5′-monophosphate.[134–136] MXzyme-based colorimetric sensors primarily use Ti-based MXenes, limiting their usefulness. Exploring Mo, V, and Nb MXenes may reveal improved catalytic activity, permanency, and discrimination, expanding detection applications. These alternate MXenes have diverse electronic structures and surface chemistries, which may improve sensitivity and detectability. Extending beyond Ti-based MXzymes can revolutionize colorimetric sensing, enabling next-gen, quick, cost-effective detection systems in environmental and biomedical areas.

5.2. MXzyme-based smartphone-integrated colorimetric sensors

Using colorimetry, which compares or measures the color depth of colored substances, one can ascertain the concentration of the targets based on the chromogenic reaction of colored compounds.[137–139] Colorimetric sensors operating on smartphones can be exploited away from a lab to satisfy critical requirements, such as on-site monitoring and clinical testing. By adjusting parameters and accessories, researchers can maximize colorimetric image quality, which correlates with detection sensitivity.[140] This smartphone sensor can recognize various colors, determine object hues, and assist visually impaired or color-blind people. Colors are

captured by a smartphone camera after generation.[141] After converting the image to color values like red, green, and blue (RGB), finding the ideal mathematical connection follows. In smartphone colorimetric technology, 0,0,0 and 255,255,255 signify absolute white and black. Smartphone technology is more useful than computer programs as it requires no data transmission and is easily accessible on phones.[142,143] Commercial apps like home-grown, Color Picker, and Color Grab, built for iOS and Android, serve as examples.[4] Most colorimetric sensors based on nanozymes rely on colorimetric fluctuations visible to the naked eye. However, subtle color variations cannot be seen by the naked eye.[142] Smartphones have examined MXene-supported composite materials using enzyme-mimic colorimetric sensing to maintain detection accuracy. Colorimetric study depends on factors like ambient light intensity, label-to-background contrast, and human visual perception alongside NP optical properties. Portable detectors increase measurement reliability and reduce subjective interpretation.

One endogenous plasma component considered as a possible cardiac biomarker is hypoxanthine (1,7-dihydro-6*H*-purin-6-one, Hx), which is generated after the ATP breakdown process. After 15 minutes of heart ischemia, the blood's Hx content rises, making it more responsive to acute myocardial infarction than conventional protein indicators. As a result, Hx is a perfect fit for cardiac indicators that will help detect acute myocardial infarction early and treat it quickly.[144] In light of this, a Cu nanocluster (CuNC)-decorated $Ti_3C_2T_x$ MXene nanosheet composite with tetra-enzyme mimic activities for detecting Hx with the assistance of a

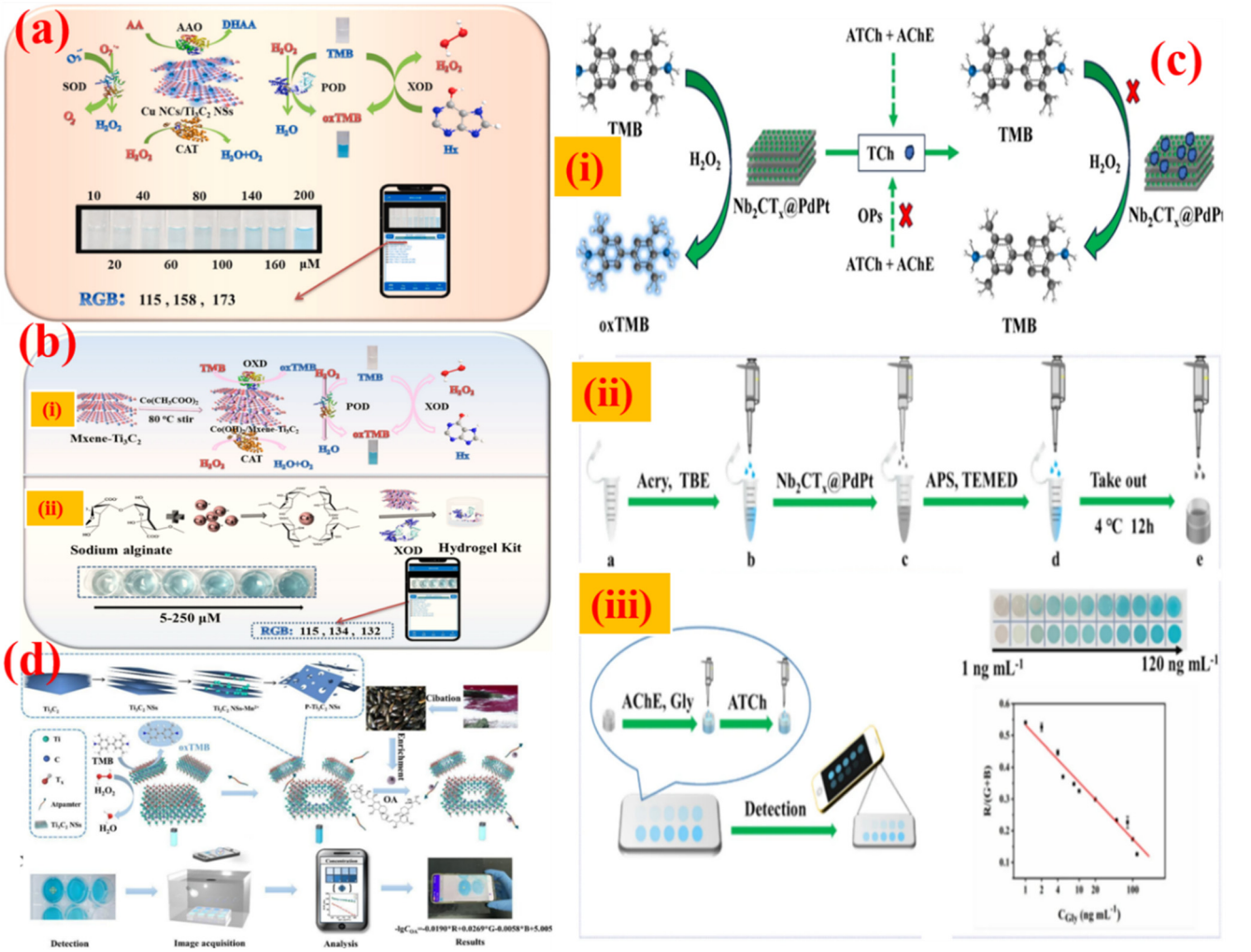

Fig. 6 MXzyme-based smartphone colorimetric detection of potent analytes. (a) CuNC-decorated $Ti_3C_2T_x$ MXene nanosheet composite with tetra enzyme mimic activities for detecting Hx with the assistance of a smartphone [reproduced from ref. 145 with permission from Elsevier, copyright 2022], (b) (i) and (ii) represent the synthesis and nanozyme activity for smartphone colorimetric sensing of Hx by using the $Co(OH)_2/Ti_3C_2T_x$ MXene nanocomposite and sodium alginate hydrogel embedded $Co(OH)_2/Ti_3C_2T_x$ MXene nanocomposite, respectively [reproduced from ref. 146 with permission from Springer Nature, copyright 2022], (c) (i) Nb_2CT_x@PdPt nanozyme based POD mimic activity based sensing of OPs, (ii) preparative protocol for the hydrogel, and (iii) smartphone-based sensing of OPs with the corresponding calibration plot [reproduced from ref. 149 with permission from Springer Nature, copyright 2024], (d) synthesis and POD activity based smartphone colorimetric sensing of OA [reproduced from ref. 155 with permission from Elsevier, copyright 2025].

smartphone was developed and is displayed in Fig. 6a.[145] Ascorbic acid oxidase (AAO), POD, (CAT), and SOD mimic activities were demonstrated by the (CuNC)-decorated $Ti_3C_2T_x$ MXene nanosheets; the synergistic impact increased catalytic efficiency. This sensing study developed a quick, smartphone-supported colorimetric Hx sensing technique that achieved a LOD of 0.25 μM and a detection range of 5–200 μM. Using a smartphone app, the sensor converted discernible color changes into numerical RGB values, enabling real-time Hx monitoring in aquatic products. Enhanced electron transfer was identified as the catalytic mechanism of the POD-mimic activity instead of the production of hydroxyl radicals. According to the study's findings, CuNC-decorated $Ti_3C_2T_x$ MXene nanosheets offer a portable, quick, and affordable sensing platform for applications involving food safety. The next example is the development of a $Co(OH)_2/Ti_3C_2T_x$ MXene nanocomposite with triple-enzyme mimic activities, including OD, POD, and CAT, for the smartphone-integrated colorimetric detection of Hx.[146] A sodium alginate hydrogel was used to embed the $Co(OH)_2/Ti_3C_2T_x$ MXene nanocomposite, resulting in a hydrogel-assisted detecting device for on-time sensing of Hx (Fig. 6b). This investigation established that Hx was catalyzed by xanthine oxidase (XOD) to yield H_2O_2, which reacted with TMB in the presence of the $Co(OH)_2/Ti_3C_2T_x$ MXene nanocomposite, producing a visible blue color at a wavelength of 650 nm. The researchers also utilized sodium alginate hydrogel, a colorimetric signal as an indicator for Hx detection, which was further integrated with a simple smartphone. Rapid Hx quantification was made possible by the smartphone-based detection approach, which achieved a LOD of 0.2 μM and a linear range of 5–250 μM. High selectivity, stability, and repeatability were demonstrated by the sensor, and its practical usefulness was confirmed by real sample analysis in aquatic products. Using a similar TMB oxidation, Xuemin Zhou's research group developed a smartphone-aided colorimetric detection of glucose based on the Fe_3O_4@MXene–Au nanocomposites with high POD-like activity.[147] With a high recovery rate, it was able to identify glucose in human whole blood samples. Furthermore, a portable detection technology based on agarose hydrogel was created for real-time analysis, enabling glucose quantification using a smartphone. This Fe_3O_4@MXene–Au nanocomposite-based nanozyme glucose biosensor demonstrated a linear range from 0 to 1.4 mM and a LOD of 0.11 mM.

Although the widespread use of organophosphate pesticides (OPs) has seriously harmed both human health and the environment, it is still very difficult to identify them on-site and with high effectiveness.[148] In this connection, a colorimetric detection method for OPs using Nb_2CT_x MXene is integrated with a PdPt nanozyme and hydrogel for smartphone-assisted analysis. Using a self-reduction technique, the Nb_2CT_x@PdPt nanozyme was produced and demonstrated potent POD-like activity.[149] According to this work's findings, the Nb_2CT_x@PdPt nanozyme's catalytic activity was suppressed in the presence of acetylcholinesterase (AChE) and acetylcholine chloride (ATCh), but it was restored upon exposure to OPs, enabling extremely sensitive detection (Fig. 6c(i)). The established glyphosphate distinguishing platform attained a linear range of 1.0 ng mL^{-1} to 1.0 μg mL^{-1} with a LOD of 0.419 ng mL^{-1}. The hydrogel-based sensor provided a practical and portable detection approach by increasing stability and enabling real-time analysis through smartphone images. Nb_2CT_x@PdPt nanozyme, working together with a smartphone-based platform, was found to be an efficient, inexpensive, and quick on-site monitoring tool for food safety applications (Fig. 6c(ii and iii)). Furthermore, $Ti_3C_2T_x$ MXene modified with platinum nanoparticles was utilized for the detection of pesticide-like chloramphenicol (CAP) in animal-derived foods.[150] Based on this AChE activity, a Pd–Pt bimetallic-modified MXzyme was developed for the highly sensitive portable device (paper and smartphone) integrated colorimetric detection of AChE inhibitors, which are critical in Alzheimer's disease (AD) treatment.[151] For real sample analysis, a paper-based sensor device was created, facilitating quantitative detection using a smartphone. The technique effectively identified AChE inhibitors in pharmaceutical tablets and extracts from medicinal plants, exhibiting great sensitivity, specificity, and stability. It is well known that Hg^{2+} ions are highly toxic. For the detection of Hg^{2+} ions, a smartphone-assisted fluorescence and colorimetric method was developed for on-site detection of Hg^{2+} and Cl^- using the oxidase-like activity of Au–Hg alloys on Au/Cu/$Ti_3C_2T_x$ MXene nanosheets.[152] Upon adding Hg^{2+} ions, Hg–Au alloys catalyzed OPD oxidation, producing a fluorescence signal at 570 nm, permitting turn-on detection of Hg^{2+} ions. Then, the introduction of Cl^- quenched the fluorescence of 2,3-diaminopenazine, allowing turn-off detection of Cl^-. A smartphone-based colorimetric analysis further facilitated on-site monitoring. The Au/Cu/$Ti_3C_2T_x$ MXene nanosheet-based approach enhanced environmental sensing applications. Furthermore, metal–carbon showed POD activity of TMB-based nanozymes and is also utilized for the smartphone-assisted colorimetric detection of pyrophosphate anions.[153] This work illustrated the growing use of nanozymes with POD-like activity in pyrophosphate synthesis and will accelerate the development of useful sensors while ensuring environmental safety. The main toxin responsible for diarrheal shellfish poisoning is okadaic acid (OA), which is extremely dangerous to human health.[154] To detect OA, a smartphone-assisted colorimetric aptasensor was developed for the ultrasensitive detection of OA using DNA-encoded porous $Ti_3C_2T_x$ MXzymes (Apt-P-$Ti_3C_2T_x$ MXene).[155] The porous $Ti_3C_2T_x$ MXene was synthesized *via* microwave combustion, creating unsaturated Ti center edges and residual Mn^{2+}, which enhanced the POD-like catalytic activity of TMB. A detectable colorimetric shift resulted from the presence of OA, which decreased Apt-P-$Ti_3C_2T_x$ MXene's

catalytic effectiveness, which was integrated with a portable smartphone (Fig. 6d).

By achieving great sensitivity, mobility, and real-time detection, these research works did away with heavy laboratory equipment. Smartphone imaging strengthened its role in next-generation biosensors by enabling quick and affordable analysis for environmental monitoring, diagnostics, and food safety. Real-time detection will be transformed by future developments in smartphone-assisted MXene-based biosensors, which will combine multi-target sensing, IoT connectivity, and AI-driven analytics for unmatched precision in environmental monitoring, food safety, and healthcare. Enhanced nanozyme engineering and miniaturized platforms will drive ultra-sensitive, portable diagnostics, enabling rapid, cost-effective, and data-driven decision-making on a global scale.

5.3. MXzyme-based luminescence sensors

Among the different analytical approaches, the fluorescence spectral technique is a good choice for the detection of potential analytes because of its simple setup, good spectral resolution, efficiency, 100-fold higher sensitivity than colorimetric approaches, and excellent specificity.[156–158] Chromogenic compounds have been utilized as substrates in the majority of nanozyme tests because they can react to modify wavelength in the visible range (350 nm to 800 nm). As a chromogenic substrate, TMB is most frequently used in colorimetric nanozyme sensors.[159] Tragically, the lack of fluorescence in this molecule led scientists to hunt for alternative chemical substrates.[159–161] Fluorescent and luminous signals are necessary for some applications, like bioimaging. In this regard, both OD and POD enzymes most frequently utilize Amplex red (AR) as a fluorogenic substrate.[162] At neutral pH, its oxidation product, resorufin, exhibits a bright orange fluorescence peak at 585 nm; however, the fluorescence yield sharply declines at decreasing pH. The second of these fluorescence nanozyme substrates is *O*-phenylenediamine (OPD). It is a naturally occurring aromatic diamine. OPD is catalytically oxidized by hydroxyl radicals formed when H_2O_2 peroxidase is reduced, resulting in the formation of 2,3-diaminophenazine, which is highly fluorescent. OPD is excited with a wavelength of 365 nm, and its maximum emission intensity is reported at wavelength λ = 568 nm.[163,164] OPD's primary drawback is associated with the nonspecific character of its oxidation. OPD is simply oxidized not only by H_2O_2 but also by other oxidizing agents. D-Luciferin and luminol molecules were frequently utilized in bio and chemiluminescence, respectively.[159]

The basic process that produces an analytical signal is used to classify nanozyme-based fluorescence sensors. The first class includes fluorescence sensors in which the chemical relationship between the potential analytes and the catalytic substrate affects the emission maximum intensity. These sensors frequently support cascade catalytic events by using both natural enzymes and nanozymes. Enzymes such as glucose oxidase, uricase, and choline oxidase adjust H_2O_2 generation, which in turn disturbs the emission signal variation.[163,164] The second group comprises fluorescence sensors where fluorescence is dictated by the direct interface between the impact analytes and nanozymes. The analytes can interact with catalytic nanostructured materials, fluctuating their enzyme-like activity.[165] The interaction between the nanozyme and the analyte can boost or reduce the fluorescence of the nanozyme itself. Furthermore, the analyte could influence enzyme mimetic performance through interactions with the reaction's intermediate products.[166] The third group includes nanosensors in which the analyte–catalytic product interactions modify luminescence. The analyte uses an "on–off–on" process to restore light emission after quenching agents are frequently added.[167,168] Nanozymes pre-functionalized with recognition molecules (such as aptamers or antibodies) produce luminescence proportionate to analyte binding in the fourth category of bio-specific nanozyme sensors.

The previously stated chromogenic compounds serve as substrates for nanozymes that resemble OD and POD activity-based fluorescence sensors. Similarly, such substrates can be modified for luminescence-based detection by the use of different nanozymes, such as metal nanoparticles, metal oxide nanoparticles, carbon-based nanomaterials, MXene, graphene, and metal–organic frameworks.[168–172] The detection of various ions, chemicals, and proteins is made possible by these nanozymes, either by themselves or in combination with recognition molecules such as aptamers and antibodies.[169] Since the majority of fluorescent nanozyme systems function *via* oxidation reactions, they are extremely vulnerable to antioxidants, which can considerably reduce the oxidation of luminescent substrates.[160] Furthermore, the surface properties of nanozymes affect their catalytic activity, which enables the selective detection of analytes by activity modulation. The creation and use of nanozymes based on composite materials developed from MXene have garnered much attention to date.[160,173,174] Therefore, nanozymes are used based on composite materials obtained from MXene in chemical and biological sensing through luminescent transduction.

As a potent antioxidant that is soluble in water, ascorbic acid (AA) can lessen the harm that ROS does to DNA, lipids, and proteins. However, diarrhea, urinary tract stones, and stomach irritation can readily result from consuming excessive amounts of AA.[175] Therefore, developing efficient methods for measuring AA in actual samples is essential. For the selective detection of AA, J. Huang *et al.* created a fluorescence-based sensor by incorporating Cu nanoparticles (CuNPs) into nitrogen-doped $Ti_3C_2T_x$ (N–$Ti_3C_2T_x$) MXzymes.[176] Because of the CuNPs/N–$Ti_3C_2T_x$ nanocomposite's potent ascorbic acid oxidase (AAO)-like catalytic activity (Fig. 7a), AA was oxidized to dehydroascorbic acid (DHAA), which then interacted with OPD to generate a fluorescent molecule. This mechanism enabled a sensitive detection method of AA with a linear range of 5–150 μM and

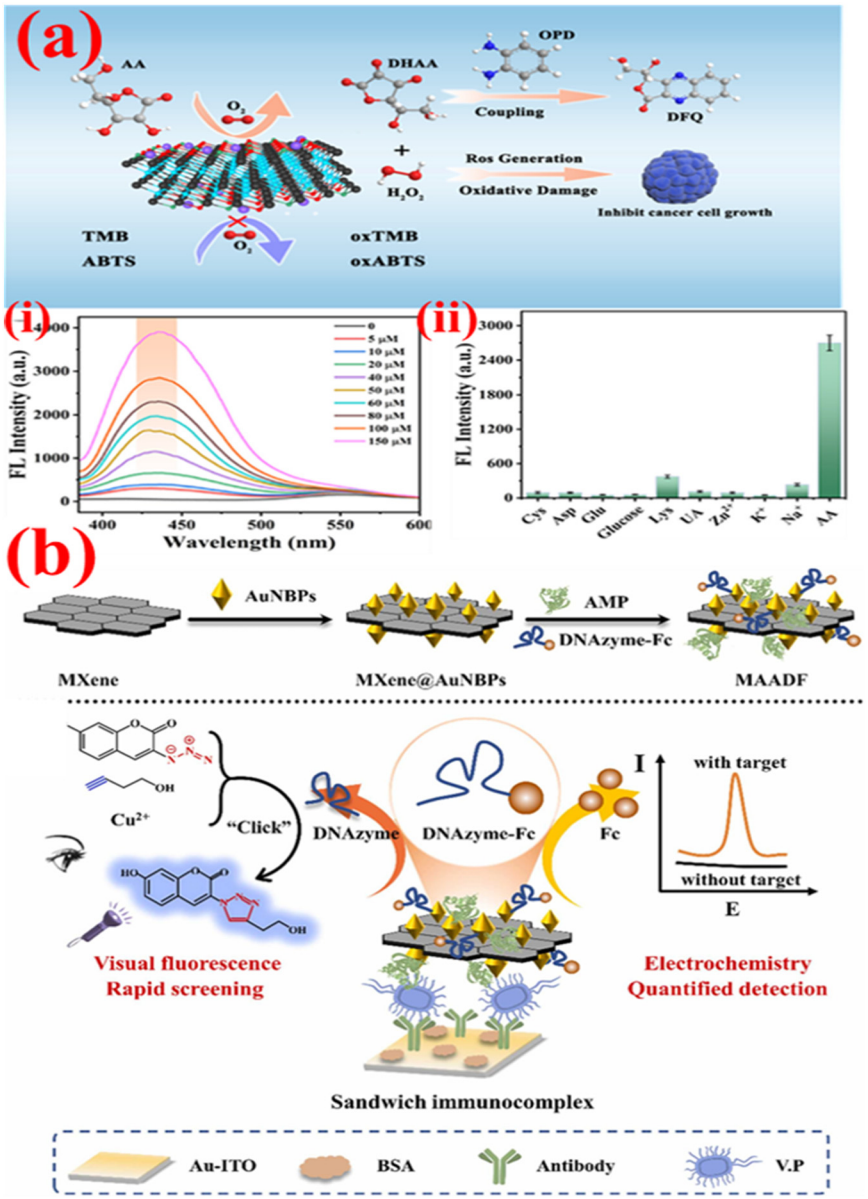

Fig. 7 MXzyme-supported fluorescence sensors for potent analytes. (a) CuNPs/N–$Ti_3C_2T_x$ nanocomposite's potent AAO-like catalytic activity-based fluorescence detection of AA, and (i) and (ii) sensitive and selective detection of AA, respectively [reproduced from ref. 176 with permission from the American Chemical Society, copyright 2023]. (b) DNAzyme-ferrocene-modified $Ti_3C_2T_x$ MXene/Au nano bipyramid/antimicrobial peptide-based sensing of food-borne pathogen [reproduced from ref. 178 with permission from Elsevier, copyright 2023].

a LOD of 0.437 μM (Fig. 7a(i)). This research showed its excellent specific detection of AA (Fig. 7a(ii)). Furthermore, the MXzyme efficiently produced ROS, inhibiting the growth of cancer cells while posing little threat to healthy cells. While theoretical studies demonstrated how nitrogen doping can improve the material's performance, advanced characterization techniques verified the material's structural integrity and catalytic effectiveness. Through ROS-mediated cytotoxicity, this research showed the dual utility of CuNPs/N–$Ti_3C_2T_x$ for biomedical applications, providing a promising strategy for both AA sensing and cancer therapy.

As a major global public health concern, foodborne microorganisms in human food cause dangerous and deadly infectious illnesses, including fever, diarrhea, and even death.[177] At this point, scientists constructed a dual-signal biosensing approach for the quick screening and quantitative identification of the common foodborne pathogen *Vibrio parahaemolyticus* (V.P.).[178] The signal probe was a DNAzyme-ferrocene-modified $Ti_3C_2T_x$ MXene/Au nano bipyramid/antimicrobial peptide (MAADF) nanocomposite, which combined fluorescence and electrochemical detection. When it interacted with V.P., a sandwich immunocomplex developed on the sensing electrode, allowing for the production of a fluorescent signal for visual screening through a catalytic click reaction and an electrochemical signal for accurate quantification from the ferrocene

component (Fig. 7b). The accuracy of detection was greatly increased by the integrated cross-reference correction. The biosensor demonstrated a low detection limit of 6 CFU mL^{-1} and a wide detection range of 10–10^8 CFU mL^{-1}. High specificity, stability, and reproducibility were displayed by the created sensor, which also showed little interference from other microorganisms. Additionally, real seafood samples were used to validate its efficacy, and good recovery rates were obtained. This strategy provided benefits like dual-mode precision, on-site applicability, and quick reaction as compared to traditional techniques. According to this study's findings, this biosensor offered a viable and effective way to identify foodborne pathogens, and by altering the capture probes, it might be further tailored to additional bacterial targets.

Aflatoxin B1 is extensively found in agronomic products (such as corn, peanuts, soybeans, *etc.*) and nutrition.[179] The World Health Organization's cancer research department has classified AFB1 as a Class I carcinogen, making it one of the most dangerous mycotoxins with exceptionally high cancer risk, genetic mutation, fetal harm, and other toxicities, posing a serious threat to human health.[180] The food industry needs to develop affordable, portable, rapid, accessible, and ultrasensitive approaches for AFB1 detection immediately. To detect AFB1 in peanuts with high sensitivity, the X. Li research group created a multimodal biosensor based on $Ti_3C_2T_x$ MXene-based nanozymes.[181] Fluorescence-quenching $Ti_3C_2T_x$ MXzymes with POD-like activity were created and functionalized using an AFB1-specific fluorescein-labeled aptamer (Fig. 8a). By using colorimetric, fluorescence, and smartphone-based detection techniques, this sensor was able to achieve LODs of 0.09 ng mL^{-1}, 0.61 ng mL^{-1}, and 0.96 ng mL^{-1}, respectively. The fluorescence detection relied on the quenching effect of $Ti_3C_2T_x$ MXene on the carboxyfluorescein-labeled (ssDNA-FAM)-aptamer, which was reversed upon AFB1 binding. The POD-like activity of $Ti_3C_2T_x$ MXene, which oxidized TMB and produced a color shift regulated by aptamer binding to AFB1, served as the basis for the colorimetric assay (Fig. 8a). The smartphone mode used a calibration model to translate color intensity into AFB1 quantities. The described sensor exhibited great stability over seven days and outstanding selectivity against probable interferents. Analyzing spiked peanut samples confirmed its accuracy and demonstrated its practical usefulness, producing recoveries exceeding 102%. This sensing protocol highlighted the potential of $Ti_3C_2T_x$ MXene-based nanozymes for multiplexed toxin quantification and underlined the need for further improvements to enhance stability for long-term storage under ambient conditions. The same research group established the improvement of a novel biosensor based on V_2C MXzyme materials (V_2C MNs) for the detection of AFB1 in peanuts.[182] Using 6-carboxyfluorescein-labeled aptamers

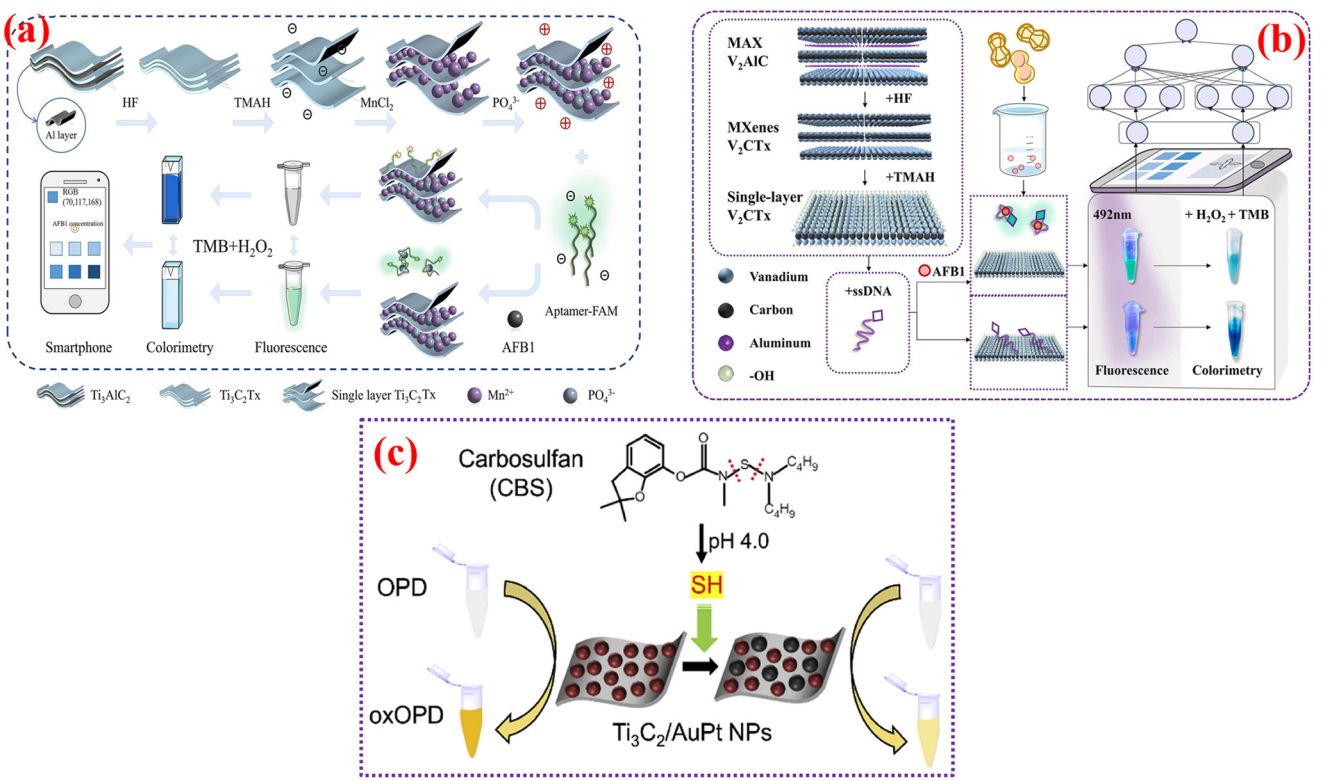

Fig. 8 MXene-supported fluorescence sensors for potent analytes. (a) Synthesis and $Ti_3C_2T_x$ MXene-based nanozymes for the multimodal detection of AFB1 [reproduced from ref. 181 with permission from Elsevier, copyright 2023]. (b) Artificial neural networks are involved in V_2C MXzyme materials (V_2C MNs) for detecting AFB1 in peanuts [reproduced from ref. 182 with permission from Elsevier, copyright 2024]. (c) POD-like activity of Ti_3C_2 MXene/AuPt nanozymes based sensing of carbosulfan [reproduced from ref. 187 with permission from Elsevier, copyright 2025].

(ssDNA-FAM), the researchers altered V_2C MNs with exceptional suppression of fluorescence and POD-like function to produce a sensor called V_2C@ssDNA-FAM. This sensor demonstrated high sensitivity with an LOD of 0.0477 ng mL^{-1} in fluorescence mode and 0.2789 ng mL^{-1} in colorimetric mode (Fig. 8b). In addition, a detection platform utilizing artificial neural networks (ANNs) was created to examine colorimetric and fluorescence signals, with detection limits of 0.6845 ng mL^{-1} and 0.0905 ng mL^{-1}, respectively. In addition, a detection platform utilizing artificial neural networks (ANNs) was created to examine colorimetric and fluorescence signals, with detection limits of 0.6845 ng mL^{-1} and 0.0905 ng mL^{-1}, respectively. Through automated data analysis and a decrease in false positives and negatives, the ANN-based method improved accuracy (Fig. 8b). The study emphasized the sensor's potential in food safety applications by highlighting its higher accuracy when compared to current techniques. This investigation recommended that the combination of nanomaterials and artificial intelligence (AI) could transform toxin detection in food, offering a real-time, intelligent, and highly sensitive method for ensuring food safety.

Metals having large atomic weights and high relative densities that can be hazardous to living things and the environment, even at trace levels, are known as heavy metals. Lead (Pb^{2+} ions) is one of the most pervasive and harmful environmental contaminants on the globe. One heavy metal with a reputation for harming both the environment and human health is Pb^{2+} ions.[183,184] The industrial use of Pb^{2+} ions has increased dramatically in recent years, highlighting the critical need for effective measuring techniques. H. Jin and co-workers examined a dual-mode biosensor using bifunctional $Ti_3C_2T_x$ MXene@PtPd NPs for sensing Pb^{2+} ions in environmental and food specimens.[185] Researchers synthesized $Ti_3C_2T_x$ MXene@PtPd NPs with luminescence quenching and POD-like activity, participating in nanozyme recognition and magnetic separation for accurate detection of Pb^{2+} ions. The colorimetric and fluorescence modes exhibited LOD values of 23 pM L^{-1} and 74 pM L^{-1}, respectively. Real sample analysis confirmed the biosensor's dependability, demonstrating recoveries ranging from 95.4% to 111.1%. The investigation demonstrated the sensor's utility in food safety monitoring by highlighting its reliability, strength, and affordability. This investigation demonstrated the sensor's utility in food safety monitoring by highlighting its reliability, strength, and affordability. The dual-mode approach reduces ambient interferences and increases selectivity, making it a promising advancement in the detection of Pb^{2+} ions. The detection method depended on catalytic signal amplification and nanozyme recognition. The DNAzyme split its substrate strand in the presence of Pb^{2+}, producing single-stranded DNA that then merged with a luminously tagged sensor to recover fluorescence. Concurrently, the POD-like activity of the $Ti_3C_2T_x$ MXene@PtPd NPs catalyzed the oxidation of TMB in the colorimetric mode, resulting in a visible color change. Both sensing modes were able to function independently thanks to magnetic isolation, which decreased background interference and improved detection accuracy. $Ti_3C_2T_x$ MXene played a crucial role in analyte sensing by acting as a fluorescence quencher *via* Förster resonance energy transfer (FRET) and a nanozyme with POD-like catalytic activity.

Because of its great effectiveness and brief residual time, carbosulfan (CBS) is one type of carbamate pesticide frequently employed in farming to control pests. The safety of food and human health is seriously threatened by CBS residues in fruits, vegetables, and water resulting from abuse or excess.[186] Consequently, the protection of the environment and human health greatly depends on the precise and reliable identification of CBS. Z. Lei reported a specific and sensitive naked-eye visual approach for sensing CBS based on its hydrolysis behavior and the POD-like activity of Ti_3C_2 MXene/AuPt nanozymes.[187] Because it breaks down into poisonous carbofuran, CBS, a common carbamate insecticide, offers a serious health concern. Rapid detection is difficult with traditional detection methods because they need costly equipment and intricate sample preparation. Using a one-step self-reduction method, this strategy produced Ti_3C_2 MXene/AuPt nanozymes with increased catalytic activity. In an acidic environment, CBS hydrolyzed and generated thiol linkages that coupled with Pt atoms to prevent Ti_3C_2 MXene/AuPt nanozymes from catalyzing (Fig. 8c). Using a technique based on color that tracked the oxidation of OPD, this inhibition was used to detect CBS. This technique proved a wide linear range (0.5 ng mL^{-1} to 5 μg mL^{-1}), a LOD of 0.342 nM, and brilliant discrimination against interfering constituents. Real lake water samples were used to confirm the technique's viability, and the results showed reasonable recoveries. In contrast to traditional assays that rely on acetylcholinesterase (AChE), the advantage of the AChE-free method is enhanced specificity, decreased expenses, and streamlined detection. This study offered a new approach for creating nanozyme-based colorimetric sensors for various toxicants and demonstrated the potential of Ti_3C_2 MXene/AuPt nanozymes for environmental utility and pesticide residue analysis.

Cyanobacteria create a class of secondary metabolites called microcystins (MC-LR), which have cyclic heptapeptide sequences and can seriously impair both human and animal health.[188] Consequently, the WHO established that 1 μg L^{-1} is the maximum permitted tolerable limit of MC-LR in drinking water.[189] Thus, the development of trustworthy techniques for the sensitive and precise detection of MC-LR is imperative. Z. Lei's research group reported the POD-like activity of Ti_3C_2 MXene nanosheets (Ti_3C_2 NSs) and their utility in an aptasensor for sensing MC-LR, a toxic cyanobacterial metabolite.[190] Through a variety of tests, the catalytic mechanism of Ti_3C_2 NSs was investigated, and it was discovered that the production of reactive species, such as holes and superoxide anion radicals, and electron transfer accelerated by nanozymes controlled their activity. Kinetic investigations were used to extensively describe the POD-like

activity, revealing Michaelis–Menten kinetics. According to the study, ssDNA prevented substrates from reaching the nanozyme surface, thereby inhibiting the POD activity of Ti_3C_2 NSs. Utilizing this property, a label-free colorimetric aptasensor was designed for MC-LR detection, engaging an MC-LR-specific aptamer that adsorbed onto Ti_3C_2 NSs, suppressing their catalytic activity. The aptamer–nanozyme interaction caused a detectable drop in the OPD colorimetric signal upon binding to MC-LR, making quantification possible. The sensor exhibited a broad linear detection range (0.01–60 ng mL^{-1}), a LOD value (6.5 pg mL^{-1}), and high selectivity against potential interferents. Real water samples that had been tampered with were utilized for validating their practical use, and recoveries ranging from 97.2% to 102.1% were obtained.

Serum overexpression of thrombin (TB) is a crucial biomarker linked to many illnesses with high rates of morbidity and death.[191] Current TB detection methods are laborious, necessitate complex equipment, and involve lengthy sample preparation processes, all of which prolong detection times and raise procedure costs.[192] Clinical interventions begin with an early and easily accessible diagnosis at the point of care, particularly in nations with limited resources. Y. Guo and colleagues[193] synthesized Ti_3C_2 MXene nanosheets (Ti_3C_2 NSs) with intrinsic POD-like activity and used them for colorimetric, label-free protein (TB) detection. Researchers discovered that Ti_3C_2 NSs could catalyze oxidation events by imitating POD enzymes and that the adsorption of single-stranded DNA (ssDNA) greatly increased their catalytic activity. This development was attributed to improved substrate (OPD) affinity and electrostatic interactions between ssDNA and the Ti_3C_2 NSs. Based on these results, this team created a biosensing method for identifying biomolecules. Aptamer-modified Ti_3C_2 NSs saw a decrease in catalytic activity following thrombin binding, enabling TB measurement in a colorimetric biosensor built using TB as an analyte. In real blood samples, the sensor performed satisfactorily and showed a linear detection range of 10 pM to 10 nM. From outcomes, the authors confirmed that Ti_3C_2 NSs are stable, reasonably priced, and highly sensitive nanozymes for biosensing applications. This study demonstrated how Ti_3C_2-based biosensors can integrate particular aptamers to detect a variety of biomolecules. Ti_3C_2/V_2C MXene acted as a significant character as a nanozyme with POD-like action, aiding fluorescence and naked-eye visual approach-based detection approaches. For CBS quantification, Ti_3C_2 MXene/AuPt nanozymes catalytically oxidized OPD, with CBS hydrolysis impeding the chemical response, leading to a computable color variation. In AFB1 determination, Ti_3C_2/V_2C MXene played as both a luminescence quencher and a POD mimic, allowing multimodal detection through aptamer interactions. An aptamer adsorbed onto the surface of Ti_3C_2 hindered its catalytic activity for MC-LR recognition, and target binding further reduced the signal. Across all fluorescence sensing studies, the aptamer-binding ability, high surface area, and catalytic activity of MXene allowed for the sensitive, economical, and selective detection of harmful substances in food and environmental samples. Table 3 summarizes various MXene-conjugated nanostructured materials used in nanozyme-based optical sensing, particularly for detecting important or biologically/chemically relevant analytes. Furthermore, Table 3 highlights the nanozyme activity, target analyte, LOD, linear range, and MXene role in this sensing approach, providing valuable insights for future research and development.

5.4. MXzyme-based chemiluminescence sensors

Chemiluminescence (CL) is a phenomenon that occurs when a species' excited state electronically emits light during a chemical reaction process. In simple terms, when more than one chemical is combined and reacts, some of them, like reactants or intermediates, can be triggered by oxidation to generate a high-energy intermediate that can break down or transfer its energy to fluorescence probes before returning to the ground states and emitting light spontaneously.[194–197] In contrast to luminescence, which is instigated *via* the absorption of light (photons), CL does not necessitate an external light source excitation, discontinuing interference from light scattering and background emission from the sample matrix.[194] Additionally, its optical signal interpretation offers a good signal-to-noise ratio, and its ability to identify high-impact analytes is high. The CL test works by launching a computable association between the CL readout signal and the analyte concentration.[198] This technique also incorporates a biomolecular recognition-based investigation that employs substantially biologically active materials, including DNA, enzymes, antibodies, or antigens, as recognition elements. CL systems act as indication transducers, qualifying the alteration of specific biological reaction identifications into quantifiable CL signals to detect the concentration of target biomolecules.[195,197] Thus, the construction of CL signals is crucial for the accurate and sensitive recognition of a particular analyte.

In the history of CL, initially, in 1877, a chemical reaction involving lophene and H_2O_2 in an alkaline medium produced luminescence that was utilized for army soldiers' lights.[199] An essential factor in the development of CL as a useful tool in analytical chemistry was the synthesis of the CL reagent 3-aminophenylhydrazine (luminol) in 1902 and the discovery of its CL behavior in alkaline environments in 1928.[200] In 1935, the reaction between lucigenin substance (*N*,*N*-dimethyldiacridinium nitrate) and H_2O_2 revealed the lucigenin CL behavior.[201] However, the aforementioned CL signal is relatively weak and transient, and early CL research has advanced slowly, with few significant applications. CL signal pathways can principally be categorized into two categories: direct and indirect CL signals. In a direct CL signal, a CL compound undergoes oxidation, forming a high-

Table 3 Summary of MXene conjugated nanostructured materials for nanozyme-based optical sensing of potential analytes

Material	Nanozyme activity/substrate	Role of MXene	Analyte	Linear range	LOD	Ref.
DNA-$Ti_3C_2T_x$ MXene/Pt	POD/TMB	Catalytic booster	Hg^{2+}	5–50 nM	9 nM	102
$Ti_3C_2T_x$ MXene/AuNPs	POD/TMB	Reducing agent and catalyst	Hg^{2+}	0–2.0 μM	0.054 nM	103
Fe_3O_4/Ti_3C_2 QDs	POD/TMB	Catalytic booster	Cr^{6+}	0–60 μM	0.26 μM	104
Mo NCs/N–$Ti_3C_2T_x$ MXene	POD/TMB	Catalytic supporter	GSH	1–150 μM	0.29 μM	106
$Ti_3C_2T_x$ MXene/carbon dots	POD/TMB	Catalytic booster	GSH	0.3–20 μM	0.12 μM	107
$Ti_3C_2T_x$@Fe_3O_4 nanocomposites	POD/TMB	Catalytic booster	GSH	0.5–10 μM	0.5 μM	108
Ti_3C_2/Pt hybrids	POD/TMB	Synergistic catalyst	GSH	0.4–7 μM	8.9 nM	109
Au/Pt/$Ti_3C_2Cl_2$ nanocomposite	POD/TMB	Structural and catalytic base	GSH	50–10 000 μM and 0.1–20 μM	10.24 μM and 0.07 μM	110
$Ti_3C_2T_x$ MXene/AgNPs	POD/OPD	Catalytic supporter	GSH	10 nM–50 μM	7 nM	111
$Ti_3C_2T_x$ MXene/AgNPs	POD/OPD	Catalytic supporter	Cys	50 nM–50 μM	48.5 nM	111
$Ti_3C_2T_x$ MXene/AgNPs	POD/OPD	Catalytic supporter	HCy	10 nM–250 μM	5.5 nM	111
$Ti_3C_2T_x$ MXene/AuNPs	POD/TMB	Reducing agent and catalyst	Cys	0–100 μM	0.03 μM	103
V_2C MXene	OD/TMB	Catalyst	Cys	0.1–15 μM	30 nM	112
Au@Pt/Nb_2C–MXene nanocomposite	POD/TMB	Conductive materials	H_2O_2	0.3–2.75 M	—	113
GSH-$Ti_3C_2T_x$ MXene QDs	OD/OPD	Nanoprobe	Uric acid	1.2–75 μM	125 nM	115
N, S, doped-$Ti_3C_2T_x$ MXene sheets	POD/TMB	Active nanozyme	Uric acid	1–400 μM	0.19 μM	116
CuNPs/N-doped $Ti_3C_2T_x$ hybrids	POD/TMB	Catalytic booster	Glucose	5–300 μM	5 μM	119
Ti_3C_2/Pt hybrids	POD/TMB	Synergistic catalyst	Glucose	0.04–0.5 μM	0.85 μM	109
MXene–Ti_3C_2/Co nanosheets	POD/TMB	Sensing matrix and catalyst support	Glucose	0.01–0.1 mM	0.001 mM	120
$Ti_3C_2T_x$ MXene/Ag	POD/TMB	Catalytic supporter	Cholesterol	2–800 μM	0.6 μM	122
MXene–Ti_3C_2/CuS	POD/TMB	Catalytic supporter	Cholesterol	10–100 μM	1.9 μM	123
$Ti_3C_2T_x$/AuNPs heterostructure	Catalase/TMB	Catalytic supporter	Penicillin G	35.05–584 nM	7.51 nM	125
$Ti_3C_2T_x$ MXene/AuNPs	POD/TMB	Catalytic supporter	Ampicillin	0.005–0.5 μg mL^{-1}	1.1 ng mL^{-1}	126
Oxygen terminated $Ti_3C_2T_x$ sheets	POD/TMB	Catalyst	Kanamycin	15.28 nM–46.14 μM	15.28 nM	127
Prussian blue–$Ti_3C_2T_x$ hybrid	POD/TMB	Catalyst surface	Malathion	1 fM–1 nM	1 fM	132
Dendritic-like Ti_3C_2 QDs@CuNi	POD/TMB	Catalytic enhancer	Glyphosphate	0–100 μM	1.13 μM	133
$Ti_3C_2T_x$ nanoribbons@AuPt	POD/TMB	Catalytic supporter	Dipterex	1 ng mL^{-1}–1 μg mL^{-1}	0.479 ng mL^{-1}	134
Cu NPs@N–$Ti_3C_2T_x$ nanozyme	POD/TMB	Electron mediator	Astaxanthin	0.01–50 μM	0.015 μM	135
CuNC-decorated $Ti_3C_2T_x$ MXene nanosheets	Tetra enzyme activity/TMB	Catalytic supporter	Hypoxanthine	5–200 μM	0.25 μM	145
$Co(OH)_2/Ti_3C_2T_x$ MXene nanocomposite	Multi nanozyme activity/TMB	Catalytic supporter	Hypoxanthine	5–250 μM	0.2 μM	146
Fe_3O_4@$Ti_3C_2T_x$–Au nanocomposite	OD/TMB	Composite formation supporter	Glucose	0–1.4 mM	0.11 mM	147
Nb_2CT_x@PdPt nanozyme	POD/TMB	Reducing agent and catalyst supporter	Glyphosphate	1 ng mL^{-1}–1 μg mL^{-1}	0.419 ng mL^{-1}	149
$Ti_3C_2T_x$ MXene/PtNPs	POD/TMB	Catalytic carrier	Chloramphenicol	0.0125–1.0 μg kg^{-1}	—	150
Au/Cu/Ti_3C_2 nanosheets	OD/OPD	Detection platform	Hg^{2+}	8.0–200.0 nM	0.8 nM	152
Au/Cu/Ti_3C_2 nanosheets	OD/OPD	Detection platform	Cl^-	5.0–350.0 μM	27 nM	152
DNA-encoded porous Ti_3C_2 nanozyme	POD/TMB	Porous nature	Okadaic acid	10–1000 ng mL^{-1}	0.38 ng mL^{-1}	155
CuNPs/N–$Ti_3C_2T_x$ nanocomposite	OD/OPD	Fluorescence enhancer	Ascorbic acid	5–150 μM	0.437 μM	176
DNAzyme-ferrocene-modified $Ti_3C_2T_x$ MXene/Au nano bipyramid	OD/OPD	Signal mediator	Food pathogen	10–10^8 CFU mL^{-1}	6 CFU mL^{-1}	178
$Ti_3C_2T_x$ MXene labelled with ssDNA-FAM	Multimode/TMB	Nanozyme support	Aflatoxin B1	0.10–400 ng mL^{-1}	0.61 ng mL^{-1}	181
ssDNA-FAM labelled V_2C MXene	POD/TMB	Signal amplifier	Aflatoxin B1	0.1–500 ng mL^{-1}	0.0477 ng mL^{-1}	182
$Ti_3C_2T_x$ MXene@PtPd NPs	POD/TMB	Fluorescence quencher	Pb^{2+} ions	0.5–1000 nM	74 pM	185
Ti_3C_2 MXene/AuPt nanozymes	OD/OPD	Catalytic substrate	Carbosulfan	0.5–5000 ng mL^{-1}	0.342 nM	187
Ti_3C_2 MXene nanosheets	POD/OPD	Catalytic activity modulator	Microcystins	0.01–60 ng mL^{-1}	6.5 pg mL^{-1}	190
Ti_3C_2 MXene nanosheets	POD/OPD	Intrinsic catalyst	Thrombin	10–1000 pM	10 pM	193

energy chemiexcited intermediate. These intermediates emit light as they change to their ground state. Examples of direct CL systems include luminol and luciferin, which are readily oxidized by H_2O_2 or singlet oxygen to produce luminescence. In another type, energy is transferred from a chemiexcited intermediate to adjacent acceptor molecules, like

fluorophores or photosensitizers, in the indirect CL signaling process. A neighboring acceptor molecule is excited to a higher energy state during this procedure by the chemiexcited intermediate, transferring its energy to it (Fig. 9a). As it returns to its ground state, the excited fluorescent molecule releases energy in the form of light. This kind of energy transfer is known as CL resonance energy transfer (CRET) (Fig. 9a).[202,203]

Nanoparticles used in CL amplification systems have received immediate attention since the advent of nanozymes,[204,205] which are nanomaterials having enzyme-like activity. This is because of their advantages, which include being more stable, easily obtained, inexpensive, and controlled. By utilizing the distinct features of different nano-structured materials, materials with nano sizes can be deployed as high catalyst levels for the measurement of CL signals, improving sensitivity and lowering detection limits.[206] This makes it possible to use these novel nano-sensing platforms to create a high-sensitivity CL system for biological analysis. To date, the MXzyme-based CL assay has been getting more attention and utilized for the detection of potential analytes. Won-Yong Lee's research group[207] examined a new electrode strategy for attractive luminol-based electrogenerated CL (Fig. 9b). The researchers developed a glassy carbon (GC) electrode modified with a 2D $Ti_3C_2T_x$ MXene–Nafion composite material. A crucial development for biological and physiological applications, this $Ti_3C_2T_x$ MXene–Nafion composite material showed strong electrocatalytic activity toward H_2O_2 oxidation and O_2 reduction processes, leading to markedly enhanced cathodic

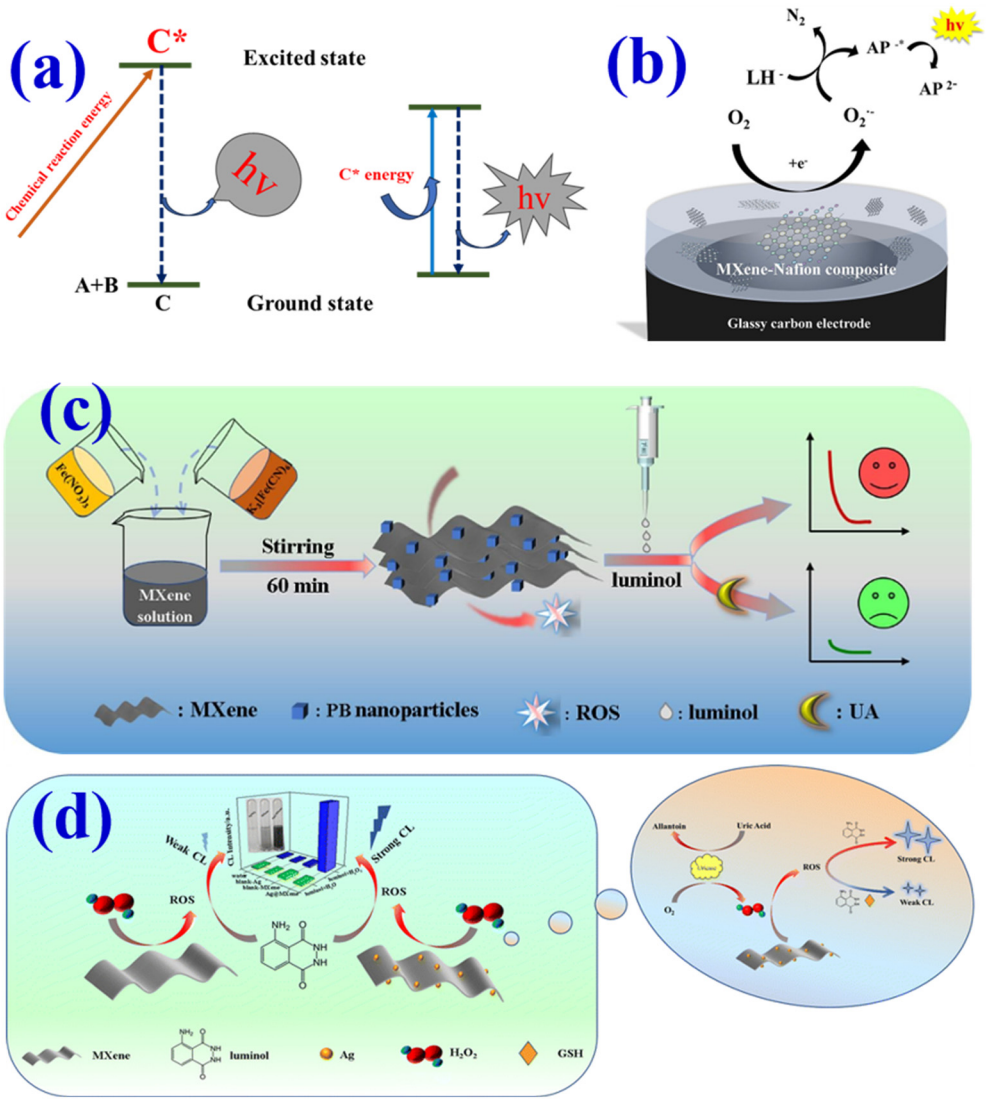

Fig. 9 (a) Schematic illustration of the formation of the CL mechanism. MXzyme-based CL sensors for important analytes. (b) Glassy carbon (GC) electrode modified with a 2D $Ti_3C_2T_x$ MXene–Nafion composite material [reproduced from ref. 207 with permission from Elsevier, copyright 2023], (c) PB/$Ti_3C_2T_x$ MXene nanocomposite-based CL detection of UA [reproduced from ref. 208 with permission from Elsevier, copyright 2024], and (d) Ag/MXene nanozymes for efficient CL sensing of UA and GSH [reproduced from ref. 211 with permission from Royal Society of Chemistry, copyright 2024].

CL emissions in neutral solutions. This study explored the CL-based sensing of H_2O_2, obtaining a detection limit of 3.1 nM and a linear range from 10 nM to 1 mM. The bare and $Ti_3C_2T_x$ MXene–Nafion composite material-modified GC electrodes were outstripped by this electrocatalytic performance. Efficient H_2O_2 quantification in human serum samples, with recovery rates ranging from 98.8 to 104.7%, confirmed the practical applicability. Tests of long-term stability showed that the signal intensity was retained for three weeks at 75.3%. The results, as mentioned above, highlight the potential of the $Ti_3C_2T_x$ MXene–Nafion composite material in the development of stable and sensitive biosensors for environmental and clinical utility.

Xiangjuan Zheng and co-workers reported a novel approach to biosensing through the synthesis of Prussian blue/Ti-based MXene (PB/$Ti_3C_2T_x$ MXene) nanocomposites.[208] The investigators employed the oxidase-like features of the PB/$Ti_3C_2T_x$ MXene nanocomposite to remove the necessity for H_2O_2, a common oxidant in conservative CL systems (Fig. 9c). The PB/$Ti_3C_2T_x$ MXene nanocomposite, acting as both a reducing agent and nanocarrier, significantly raises the CL intensity when mixed with luminol. This allowed for the sensitive detection of uric acid (UA) within a linear range of 0.2–30 μM and a detection limit of 0.19 μM. The sensor exhibited excellent specificity, reliability, and stability, successfully detecting UA in diluted human serum with recoveries ranging from 98.59% to 104.04%. This work followed an oxidase nanozyme-based pathway to produce ROS by triggering dissolved oxygen, which afterward oxidizes the substrate and finishes the whole reaction. The PB/$Ti_3C_2T_x$ MXene nanocomposite catalyzed the reaction, electrocatalytically generating ROS from dissolved oxygen and reacting with just luminol to generate a powerful CL signal without needing H_2O_2 (Fig. 9c). Furthermore, when the concentrations of UA increase in the PB/$Ti_3C_2T_x$ MXene nanocomposite–luminol combination, the added UA can react with ROS. Its CL signal drops when the ROS is used up, allowing for the successful detection of UA. The study highlighted the potential of PB/$Ti_3C_2T_x$ MXene nanocomposite-based materials in the biosensing of UA, offering a greener and more efficient alternative for clinical diagnostics. This work marked a significant advancement in the development of sensitive, cost-effective, and eco-friendly biosensors.

The human body contains two common biomolecules, GSH and UA, which, depending on their levels, are essential for physiological function.[209,210] Due to the biological potential of both biomolecules, early recognition of UA and GSH levels in biological fluids is crucial for public health. By integrating silver nanoparticles (AgNPs) with Ti_3C_2 MXene nanosheets, Xiluan Yan's research group reported an invention of Ag/MXene nanozymes for efficient CL sensing.[211] The Ag/MXene composites, which were created *via* an *in situ* self-assembly technique, demonstrated potent POD-like activity by accelerating the production of ROS from H_2O_2. The synergistic actions of AgNPs and Ti_3C_2 MXene greatly increased the CL intensity, allowing for the very sensitive quantification of UA and GSH (Fig. 9d). These biosensors' linear detection ranges for GSH and UA were 50 nM–20 μM and 1 mM–35 μM, respectively, with LOD as low as 0.83 nM and 0.37 μM. The production of ROS, such as hydroxyl radicals and singlet oxygen, as important reaction intermediates, was validated by mechanistic investigations. Additionally, the sensor demonstrated exceptional stability and selectivity, successfully identifying GSH and UA in human blood serum samples. This work demonstrated the prospective use of MXzyme composites in CL applications and offered a strong biosensing platform.

5.5. MXzyme-based electrochemiluminescence sensors

In recent years, electrochemiluminescence (ECL) sensing devices have become increasingly popular, leading to notable advancements in chemo and biosensors. The utility of advanced signal amplification approaches is crucial to the progress of high-throughput ECL sensors, which will usher in an entirely new phase of sensitive analysis. ECL is the term for light emitted by excited luminophores as a result of electrochemical reactions occurring at an electrode's surface.[212,213] ECL has become an eminent signal transduction system utilized broadly in various eras thanks to its distinct merits, which embrace the lack of a requirement for external light sources, exact control over the spatiotemporal nature of light, low background interference, and exceptional sensitivity.[212–215] Target monitoring of potential analytes has become a significant use for ECL sensors.

Research on ECL has been ongoing since the mid-1960s, when Kuwana, Hercules, Bard, and others began the first investigations on the subject. As a result, ECL (bio)sensors are now a potent analytical tool in the modern world.[216–218] Next, higher detection sensitivity in ECL sensing platforms resulted from the introduction of MXene into the ECL sensing field in 2018.[219] Because of its resistance to excitation light sources and dispersed light, ECL has attracted a lot of interest in clinical diagnostics. Since $[Ru(bpy)_3]^{2+}$ has outstanding ECL efficiency, exceptional biocompatibility, and chemical stability, it is commonly utilized in ECL-based sensing systems.[220–222] Nevertheless, $[Ru(bpy)_3]^{2+}$ has a high-water solubility, which limits the ECL property and makes immobilization on the electrode surface difficult. Many nanocarriers have been researched to address this problem and increase the stability and $[Ru(bpy)_3]^{2+}$-efficacy.[222,223] However, because of their ability to efficiently catalyze the production of hydroxyl radicals, POD mimetic nanozymes have garnered much study interest.[212,224] Under certain reaction settings, it has been established that different metal nanoparticles (MNPs), including Pt, Pd, Ag, and AuNP, may imitate a broad range of enzymes, including CAT, POD, and OD.[224–226] However, the combined activity of two or more MNP components within the same nanozyme makes the hybrid nanosystem-based nanozyme a clear

advantage for biosensing applications.[227] More significantly, as compared to biological enzymes, nanozymes frequently have better catalytic activity. They work better because of their reduced size, which increases the surface area accessible to enzymatic action. They work better because of their reduced size, which increases the surface area accessible to enzymatic action.

Later, a variety of ECL sensors for bioanalysis were created using MXenes and MXene-based composite materials. The catalytic activity of nanozymes, which resembles an enzyme, is combined with the sensitive light-emitting mechanism of ECL to create nanozyme-based ECL.[218,228] Nanozymes expand electron transport, raise fluorescence efficiency, and catalyze the construction of ROS to progress signal amplification. MXzymes' ECL combines ECL technology with the remarkable catalytic capabilities of MXene-derived nanozymes. Because of their high conductivity and adjustable surface chemistry, MXenes catalyze the production of reactive species and facilitate electron transport, which improves the amplification of ECL signals.[218,228,229] This cutting-edge tactic is commonly applied for super-specific and stable quantification in environmental monitoring and biosensors.

A new dual-mode electrochemical (EC) and electrochemiluminescence (ECL) biosensor was developed by Bin Wang *et al.* for the ultrasensitive and real-time detection of H_2O_2, a crucial cancer biomarker.[230] Polycrystalline manganese oxide nanoflowers (MnONFs) were self-assembled on delaminated Ti_3C_2 MXene nanosheet surfaces, leveraging their collaborative interface to improve catalytic efficiency, electron transfer, and stability. The hollow layered structure of Ti_3C_2 MXene offered a high surface area and a conductive pathway, while MnONFs supplied abundant active sites for H_2O_2 oxidation. This composite Ti_3C_2 MXene@MNOFs allowed rapid H_2O_2 determination, attaining an EC linear range of 0.05–650 μM and an ultrasensitive ECL limit of detection of 0.45 nM. This fabricated sensor demonstrated exceptional specificity and anti-interference capabilities in complex biological environments and effectively differentiated cancer cells from normal cells by detecting H_2O_2 effluxes induced by ascorbic acid stimulation. It successfully monitored as few as 20 cancer cells in 1 mL, exhibiting remarkable sensitivity, reproducibility, and stability over extended periods. The integration of EC and ECL readouts minimized false positives and negatives, improving diagnostic accuracy. The study highlighted the potential of this dual-mode sensing platform for early cancer detection, offering a reliable, non-enzymatic alternative for real-time monitoring of ROS. These advancements addressed the limitations of traditional methods, including single-readout systems and complex preparation processes, paving the way for broader applications in biomedical diagnostics and therapy.

One of the most common cancers in men is prostate cancer, and the sensitive marker for detecting prostate cancer is prostate-specific antigen (PSA). To provide a precise and sensitive detection technique for PSA ultra-sensitivity detection, Chuanping Li and colleagues discovered the fabrication of a highly efficient ZIF-67@Ti_3C_2 MXene-based ECL biosensor.[231] Here, researchers established the use of ZIF-67@Ti_3C_2 MXene as a co-reaction accelerator and improved ECL efficacy by up to 830% *via* the specific production of hydroxyl radicals and singlet oxygen. The biosensor effectively detected PSA with an improved detection limit of 0.91 pg mL^{-1}, leveraging a plasmonic NH_2-MIL-88@Pd nanozyme for signal amplification. This study emphasized the incorporation of MXene's conductivity and ZIF-67's stability, offering a super-specific sensing platform for cancer biomarker detection, stability, and excellent sensitivity.

To the best of our knowledge, non-small cell lung cancer[232] is the primary cause of lung cancer-related mortality globally. A tumor marker linked to lung cancer, cytokeratin-19 fragment (CYFRA21-1),[233] is primarily detected in the cytoplasm of tumor cells originating from epithelial cells, including lung and esophageal cancer. In the normal population, it has a reference value of 0–3.3 ng mL^{-1}. Thus, there is some clinical utility for CYFRA21-1 in the treatment, identification, and effectiveness assessment of different kinds of lung cancer. Xian Ren *et al.* demonstrated the development of an ECL immunosensor for CYFRA 21-1 recognition, employing $Ti_3C_2T_x$ MXene@TiO_2–MoS_2 hybrids as co-reactive catalysts and luminol@Au@Ni–Co nanocages as probes.[234] These state-of-the-art nanozyme hybrid materials helped efficient H_2O_2 putrefaction and boosted ECL signal production. The developed sensor established a linear range of 0.1 pg mL^{-1} to 100 ng mL^{-1}, with a LOD of 0.046 pg mL^{-1}, displaying outstanding sensitivity. The incorporation of $Ti_3C_2T_x$ MXenes's high conductivity and MoS_2's catalytic features aided stable, repeatable, and specific CYFRA 21-1 identification analysis, even in complex biological matrices. The strategy offered a strong foundation for the early identification of lung cancer (Fig. 10a). Additionally, this strategy offered a strong foundation for the early identification of lung cancer.

In one of the more recent articles, researchers explored Ti_3C_2-based MXzymes for enhancing ECL glucose biosensing, employing bromophenol blue (BPB) as a co-reaction accelerator and transporter.[235] Delaminated Ti_3C_2-based MXzymes with BPB enabled high loading of luminol and glucose oxidase (GOx), decomposing H_2O_2 to produce hydroxyl radicals, which discriminate ECL signals meaningfully (Fig. 10b). The device demonstrated outstanding rigidity, specificity, and consistency in human serum, with a detection range of 0.1 to 40 000 μM and a LOD of 0.02 μM. Superior sensitivity was attained by minimizing radical breakdown through the proximity of the hydroxyl radicals and the luminophore's upshots. Furthermore, this research effort opened a new door for more sophisticated biosensor designs in clinical diagnostics by demonstrating a potential glucose detection platform.

The broad-spectrum antibiotic chloramphenicol (CAP) has been utilized extensively in the farming of animals because

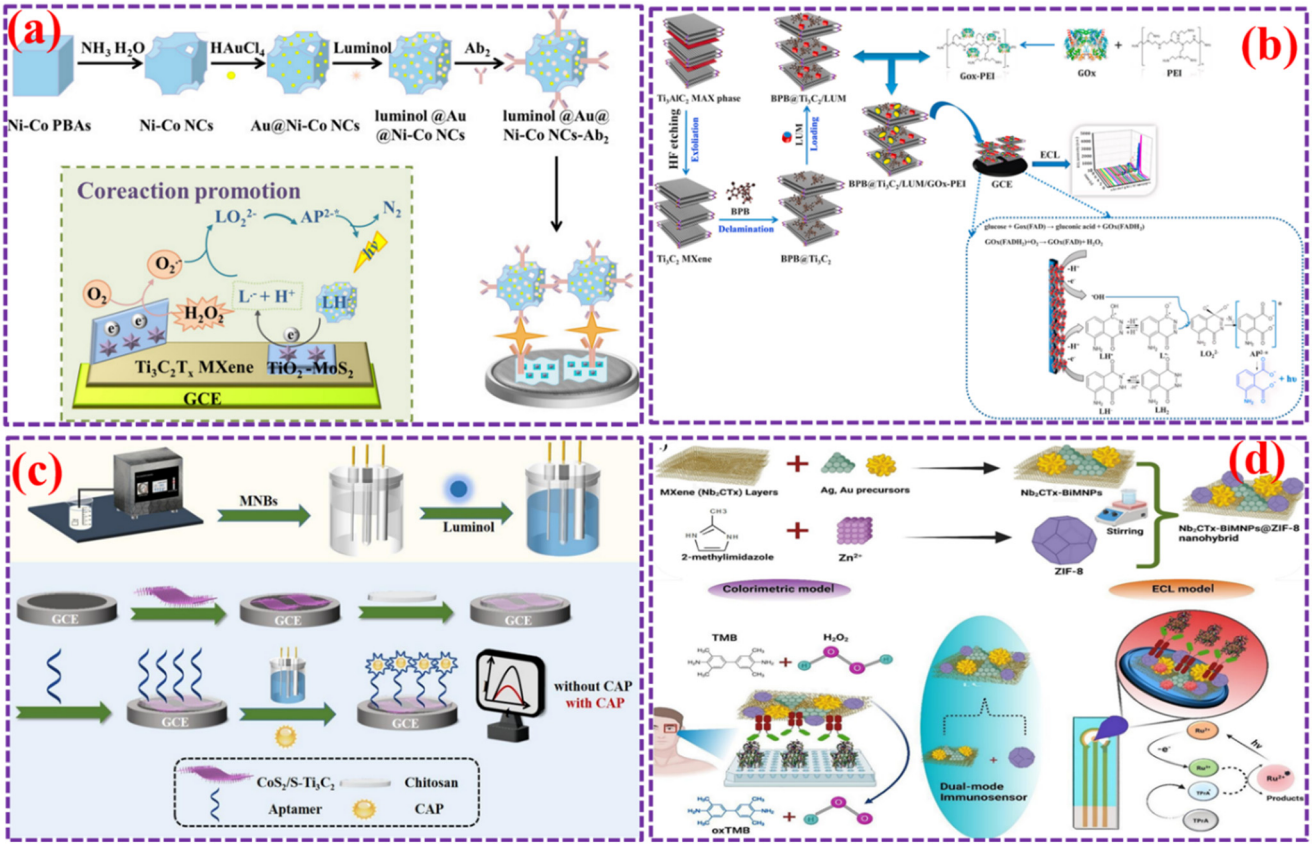

Fig. 10 MXene-supported material-based ECL sensors for the different analytes. (a) $Ti_3C_2T_x$ MXene@TiO_2–MoS_2 hybrids as co-reactive catalysts and luminol@Au@Ni–Co nanocages as an ECL probe for the detection of CYFRA 21-1 [reproduced from ref. 234 with permission from American Chemical Society, copyright 2024], (b) Ti_3C_2-based nanozyme for ECL glucose biosensing [reproduced from ref. 235 with permission from Elsevier, copyright 2024], (c) CoS_2/sulfur-doped Ti_3C_2-based nanozyme for the detection of CAP [reproduced from ref. 239 with permission from Elsevier, copyright 2023], and (d) synthesis and nanozyme activity of Nb_2CT_x-stabilized Au–Ag alloy NPs integrated into ZIF-8 frameworks for the detection of biomarkers [reproduced from ref. 224 with permission from Elsevier, copyright 2025].

of its good antibacterial action and affordable cost.[236] However, CAP residues in the environment would make their way into the human body *via* the food chain and cause major negative reactions and side effects, for example, aplastic anemia, gastric intolerance, and marrow suppression.[237,238] Thus, it is essential to create a straightforward, affordable, highly sensitive, and selective CAP monitoring approach. To detect CAP in real water samples, Zilian Zhang *et al.* discovered a novel ECL aptasensor for detecting CAP, utilizing a luminol-dissolved oxygen (DO) system enhanced with cobalt sulfide (CoS_2)/sulfur-doped Ti_3C_2-based MXzymes and micro-nano bubbles (MNBs).[239] The CoS_2/sulfur-doped Ti_3C_2-based MXzymes acted as a co-reaction accelerator, significantly improving the reduction efficacy of DO and generating ROS for enhanced ECL performance (Fig. 10c). The ECL signal was further amplified by the addition of MNBs, which raised the DO concentration and ROS generation. Notably, this tackle confirmed an 8.7-fold perfection in ECL signal intensity in contrast to orthodox luminol-DO systems, with a sensing range from 0.1 fM to 10 pM and an ultra-LOD of 105 fM. The aptasensor demonstrated outstanding selectivity, stability, and repeatability, and it was successfully used to analyze real-world samples such as milk, tap water, and pond water. However, this sensing protocol demonstrated the potential of CoS_2/sulfur-doped Ti_3C_2-based MXzymes and MNBs to alter ECL sensing by eliminating the need for H_2O_2, opening the door for more practical, biocompatible, and sensitive biosensors in the monitoring of food and environmental safety.

A rather uncommon and varied class of malignancies, neuroendocrine tumors (NETs) develop from specialized cells dispersed throughout the body. Despite being somewhat uncommon, they can be difficult to diagnose and treat properly.[240] The most adopted biological indicator in medical studies for NET identification is chromogranin A (CgA). Because of this, it is an asset for enhancing the knowledge and diagnosis of these intricate cancers.[241] To detect CgA in human serum and saliva, F. Kareem and his colleagues described a dual-mode immunosensor that practices Nb_2CT_x-stabilized Au–Ag bimetallic nanoparticles (BiMNPs) integrated into ZIF-8 frameworks.[13] This first study uses Nb-based MXzymes rather than Ti-based MXzymes in this part. Moreover, Nb_2CT_x has better

electrochemical stability than $Ti_3C_2T_x$, which results in enhanced electrochemical sensing capabilities.[242] Nb_2CT_x MXene acted as a reducing and stabilizing agent for synthesizing BiMNPs, which demonstrated excellent POD-like activity and enhanced ECL performance in the $Ru(bpy)_3^{2+}$/TPrA system.[224] The ECL signal was greatly enhanced, and colorimetric detection by TMB oxidation was made possible by the ZIF-8 framework's wide surface area and ease of biomolecule immobilization (Fig. 10d). The immunosensor exhibited a wide linear detection range (0.001–1000 pg mL^{-1} for ECL, 0.1–4000 ng mL^{-1} for colorimetry) and ultra-low detection limits (0.11 fg mL^{-1} for ECL, 100 pg mL^{-1} for colorimetry). Its remarkable recovery rates from the analysis of real-world human serum and saliva samples confirmed its great selectivity, repeatability, and stability. The work demonstrated the Nb_2CT_x MXene-stabilized BiMNPs@ZIF-8 nanohybrid's capacity for precise and sensitive biomarker identification, providing a viable platform for the diagnosis of neuroendocrine tumors and the monitoring of psychophysical stress (Fig. 10d). In all the systems, the catalytic generation of ROS, like hydroxyl radicals, is used to enhance ECL signals. The 2D stacked MXenes' thin nanosheets feature a lot of surface functional groups and surface area. This feature makes them extremely versatile for the quantification of a wide range of biomolecules by allowing conductivity tweaks and customized alterations aimed at biomolecules.[243] When combined with other nanostructured materials, MXene's unique capabilities work in concert with the unique qualities of the combined nanomaterials to produce often better performance than when the components are used alone.[217] The incorporation of MXene's high conductivity and nanostructured materials' catalytic features/electron transporters highlights the importance of catalytic efficiency and ROS generation in enhancing the detection process. These species played a pivotal role in CL or ECL reactions, amplifying the signal intensity for sensitive analyte detection.

5.6. MXzyme-based electrochemical sensors

Research on electrochemical sensors has been one of the most investigated analytical topics. Electrochemical sensors' ability to recognize specific target analytes of attention hangs deeply on the electrode's materials and/or receptors.[244,245] Most potential target analytes interacting with electrode-deposited materials and/or electrode receptors in electrochemical sensors can produce a response that is possibly deciphered into computable electrochemical signals that designate the analyte dosage level. The quick reaction time, combinatorial features, and potential of portable (even wearable) measurement devices are some of the benefits of electrochemical sensors over alternative sensing techniques.[246,247] They can also be made smaller and more affordable. By using biomarker-specific reactions, electrochemical biosensors use the principles of electrochemistry to convert biological processes into quantifiable electrical signals.[248,249] The targeted potentially specific biomarkers (*e.g.*, cancer biomarkers) might be detected precisely and quantitatively thanks to this electrochemical signal, which would be proportionate to their concentration.[249] Lightning-fast, immediate fashion, accurate, long-lasting, and inexpensive high-impact analyte detection is made possible by the incorporation of nanozymes into electrochemical sensors. When compared to natural enzymes, nanozymes offer several advantages, such as increased robustness and durability, cost-effectiveness, adaptable catalytic characteristics, and strong electrical conductivity.[73,250] Generally speaking, there are two approaches to disseminating the mechanisms of action of electrochemical sensors based on nanozymes. The first uses catalytic reactions mediated by nanozymes to generate or amplify electrochemical signals, while the second uses catalysis to produce or activate electroactive chemicals that are relevant to the target and employed as electrochemical signals.[250] Examples of electrochemical methods for biomarker detection include amperometry, electrochemiluminescence (ECL), photoelectrochemistry (PEC), impedometry (electrochemical impedance spectroscopy; EIS), and various voltammetry methods, such as square wave voltammetry (SWV), linear sweep voltammetry (LSV), differential pulse voltammetry (DPV), and stripping voltammetry (SV). In general, these electrochemical sensing techniques operate as follows:

(i) An antibody that resembles a tracer receptor is labeled with an electroactive species, like nanozymes.

(ii) The receptor becomes entrenched on the electrode's surface after binding with the analyte.

(iii) Applying a voltage and assessing the current, resistance, and luminescence that is induced at the electrode allows one to determine the amount of the desired analytes.

In essence, the labeled electroactive species undergo a redox reaction when the voltage is applied, producing an electrical signal that represents the amount of the receptor-bound analytes.[251] Furthermore, the coating of nanostructured materials enhanced the electrochemical catalytic performance. Because of their versatility, MXenes can be effectively customized by integrating metal, metal oxide, or carbon-based nanoparticles, which makes it possible to rationally build effective MXene composites. MXenes were often designed by carefully choosing the X and M components, as well as surface terminal groups, to improve their physio-chemical performances and attain desired properties. Given that MXenes excellently trap enzymes on their surface, enabling efficient electrical communication between the electrode and the protein backbone of enzymes, they were initially utilized as an immobilization matrix of natural enzymes. Thus, MXene has been identified as a substrate that facilitates rapid electron transfer, resulting in enhanced electron kinetics and greater susceptibility of electrochemical sensors based on enzymes.[250,252] It was recently found that MXenes can mimic

the catalytic activity of natural enzymes such as CAT, SOD, OD, and POD, usually by effectively relating with other catalytic nanostructured materials.[36,38] Based on this, the mimic features of MXene-supported composite materials have been applied in electrochemical sensors for the detection of potential analytes.

5.6.1. Heavy metal ions. It is commonly acknowledged that heavy metal pollution is a worldwide environmental issue brought on by a variety of industrial processes, including agricultural products, the electroplating process, mining, *etc.*[15] Because of their severe poisoning and biological accumulation impact, heavy metal ions are considered to be among the most harmful contaminants. The detrimental effects of mercury ions (Hg^{2+} ions) on living things are widely recognized.[253] The increase in the concentration of Hg^{2+} ions in the environment is an important issue, even with the efforts of many regulatory authorities.[254] This demands the fabrication of alternative and effective approaches for use in examinations, along with the quantification and identification of Hg^{2+} ions in the environmental matrix. For instance, Hg^{2+} ion-stimulated $Ti_3C_2T_x$ MXene nanoribbons in conjunction with Au nanozyme activity were used in the most recently published research to produce a highly sensitive homogeneous voltametric sensing method for Hg^{2+} ion detection in environmental samples with an excellent recovery rate.[255] The researchers synthesized the $Ti_3C_2T_x$ MXene@Au nanohybrid through a self-reduction process and investigated its nanozyme properties. The nanohybrid material was discovered to have mild POD-like activity, which was greatly increased when Hg^{2+} ions were present. This resulted in the effective oxidation of colorless substrates into colored products (Fig. 11a). The foundation of a unique homogeneous voltammetric sensing technique was the substantial reduction current shown by the oxidation product of OPD, which was linearly connected with the concentration of Hg^{2+} ions. In contrast to traditional DPV electrochemical techniques, this method achieved great sensitivity and quantification without requiring electrode change. This sensing investigation also optimized experimental conditions, achieving a low detection limit of 17.0 pM and a broad linear detection range of 0.4 nM to 2.0 μM. Additionally, this sensing strategy opened up a promising new door for heavy metal ion electrochemical detection using nanozymes, which could expand the range of environmental monitoring applications.

5.6.2. Emerging organic contaminants. Organic molecules derived from humans are employed daily in many different industries around the world, including food, medications,

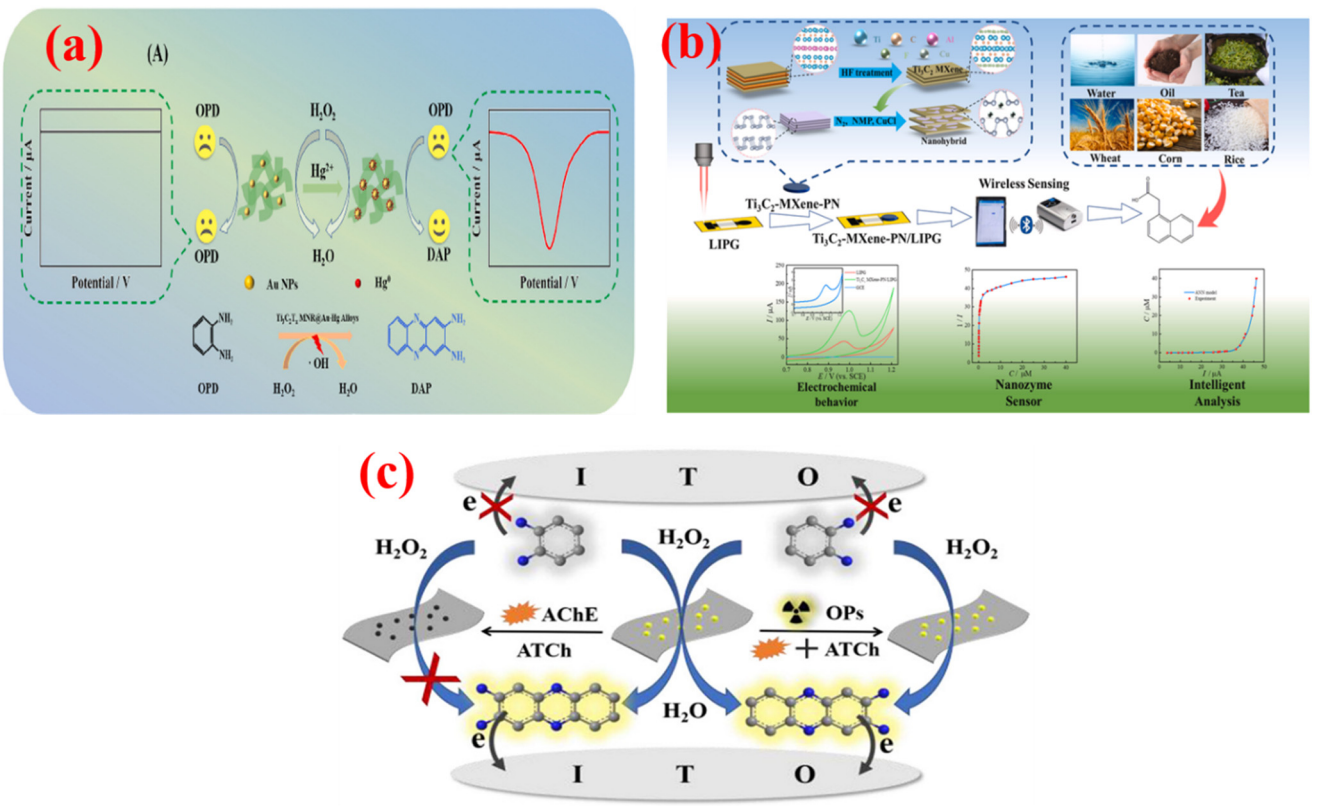

Fig. 11 MXzymes for electrochemical sensors for hazardous analytes. (a) $Ti_3C_2T_x$ MXene nanoribbons in conjunction with Au nanozyme activity-based DPV detection of Hg^{2+} ions [reproduced from ref. 255 with permission from Elsevier, copyright 2023], (b) a self-assembled phosphorene/$Ti_3C_2T_x$ MXene nanohybrid electrode based on nanozyme applied in the multimodal detection of NAA in agricultural/food samples [reproduced from ref. 265 with permission from Elsevier, copyright 2021], and (c) cobalt-doped 2D $Ti_3C_2T_x$ MXene nanosheets with POD-like characteristics as a novel homogeneous electrochemical sensing of OPs [reproduced from ref. 269 with permission from American Chemical Society, copyright 2022].

surfactants, insecticides, and agricultural chemicals. These substances are categorized as emerging organic contaminants (EOCs) when discovered in the environment in undesired or harmful concentrations.[256] These substances so contaminate the downstream surface water. Agricultural runoff and livestock farms can also quickly contaminate surface water. Our contemporary concerns about EOCs, however, are not limited to the ecosystem; they also include the deterioration of supplies of drinking water, which may eventually affect human health.[257] As a result, the EOCs' basic sensing strategy is extremely important.

Ochratoxins (OTs) are thermostable fungal secondary metabolites that damage kidneys, suppress immunity, and have mutagenic and carcinogenic effects. OT contamination can occur before or after harvesting, as well as during food processing, packing, distribution, and storage.[258] Among the different OTs, ochratoxin A (OTA) poses a serious risk to both human and animal health.[259] For the detection of OTA, a signal-on/off paper-based electrochemical aptasensor that combines Pt@NiCo-layered double hydroxide (LDH) nanozyme for signal amplification with MXene–Au as a sensing substrate was developed.[259] *In situ* reduction was used for generating the MXene–Au composite, which offers a robust and highly conductive platform for electrode fabrication. MXene–Au composite-supported Pt@NiCo-LDH nanozyme, possessing POD-like activity, catalyzed the oxidation of OPD in the presence of H_2O_2, producing a strong electrochemical signal in the "signal on" state. When OTA was introduced, the aptamer selectively attached itself to it, which caused the aptamer–cDNA complex to dissociate and release the Pt@NiCo-LDH nanozyme. This put the sensor in the "signal off" condition and reduced the DPV signal. The aptasensor outperformed traditional OTA detection techniques with a low detection limit of 8.9 fg mL^{-1} and a broad detection range of 20 fg mL^{-1} to 100 ng mL^{-1}. This study demonstrated the potential of MXene-based electrochemical aptasensors for quick, accurate, and economical OTA detection, providing a viable point-of-care testing (POCT) instrument for applications including food safety. Based on the POD-like activity of AgNPs, combined N-doped $Ti_3C_2T_x$ MXene was utilized for the detection of H_2O_2.[260] This work highlighted the challenges associated with AgNPs' agglomeration, which diminished their catalytic activity, and demonstrated that nitrogen doping improved the conductivity and catalytic efficiency of the $Ti_3C_2T_x$ MXene substrate. The findings of the study highlighted the importance of carrier modification for better nanozyme-based sensors by showing that the combined impacts of nitrogen-doped MXene and AgNPs increased electrochemical sensing performance.

Due to their harmful effects, phenolic compounds (PCs), which are abundant in both the natural environment and human life, represent a serious risk to human health.[261] Consequently, the development of robust, efficient, and trustworthy PC detection techniques is required. For example, strong adsorption between the hydroxyl group of PCs and oxygen atoms on the MXene surface allowed the researchers to establish the catalytic properties of $Ti_3C_2T_x$ MXzymes, proving their effectiveness in the oxidation of phenolic substances.[262] Through the integration of MXene with alkaline phosphatase for electrochemical signal improvement, a cascade catalytic amplification technique (1-naphthyl phosphate substrate) was created, allowing for the detection of the BCR/ABL fusion gene, a crucial biomarker for leukemia diagnosis, using an ultrasensitive biosensor. This sensor demonstrated excellent specificity, stability, and reproducibility, with a detection limit of 0.05 fM. The biosensor's clinical application was demonstrated when it successfully identified the fusion gene in human serum. Next, the development of a robust biosensing platform using $Ti_3C_2T_x$ MXzymes was applied for the ultrasensitive detection of phenol.[263] To build a mediator-free electrochemical biosensor, this sensing investigation used MXene as a matrix to immobilize tyrosinase, an enzyme that can catalyze phenol oxidation. The biosensor exhibited a broad linear detection range (0.05–15.5 μM), a low detection limit of 12 nM, and high sensitivity (414.4 mA M^{-1}). This sensor maintained high enzymatic activity throughout time and showed outstanding repeatability, reproducibility, and stability. Overall, these studies underscored the potential of $Ti_3C_2T_x$ MXene in electrochemical biosensing, organic synthesis, and environmental applications, paving the way for advanced nanozyme-based analytical tools.

A common phyto-regulator (plant growth regulator) made from naphthalene, α-naphthalene acetic acid (NAA), can be found in harvests to increase their protein and fat content. Nevertheless, NAA poses a risk to human health since it can remain in agricultural products by absorbing environmental contaminants; dishonest traders even use it to produce rootless soybean sprouting. Thus, it is essential to create a new, sensitive, quick, easy, and affordable technique to identify the trace level of NAA in agricultural land settings and agricultural commodities utilizing wireless intelligent portable devices for the fortification of nutriment and agro-product protection, as well as ecological contamination monitoring.[264] In this regard, a new method employing a portable wireless nanozyme sensor was developed to detect ultra-trace quantities of NAA, a plant growth regulator.[265] A self-assembled phosphorene/$Ti_3C_2T_x$ MXene nanohybrid electrode was designed in this sensing experiment on a flexible laser-induced porous graphene substrate, guaranteeing excellent ambient stability, effective electrochemical, colorimetric, and wireless responsiveness in real samples (Fig. 11b). This sensor achieved a low detection limit of 1.6 nM and a broad linear range (0.02–40 μM) through the use of LSV for NAA detection. Furthermore, a machine learning approach based on artificial neural networks was used for intelligent data interpretation, increasing dynamic range and accuracy. According to the results of the suggested sensing investigation, this highly sensitive, quick, and affordable sensor offered a viable platform for identifying hazardous materials in agriculture.

The main purpose of organophosphorus pesticides (OPs) is to keep insects away from farms. Since the utilization of OPs in many farming processes has increased significantly, it is now crucial to precisely track their concentration levels to safeguard ecosystems and the supply of food. Nonetheless, OPs are categorized as extremely harmful chemical substances by the WHO.[266–268] Given their ubiquitous use and toxicity, simple, fast, and highly sensitive procedures must be designed, for example, using cobalt-doped 2D $Ti_3C_2T_x$ MXene nanosheets with POD-like characteristics as a novel homogeneous electrochemical sensing technique for the detection of organophosphate pesticides (OPs).[269] A considerable reduction current is produced by stimulating the oxidation of OPD into an electrically active product, describing exactly how this sensor operates. By blocking acetylcholinesterase (AChE) activity, the system illustrated a distinct reaction to thiol chemicals, enabling selective OP detection, preventing thiol production, and reestablishing the POD-like action of cobalt-doped 2D $Ti_3C_2T_x$ MXene nanosheets (Fig. 11c). Electrochemical measurements confirmed the sensor's sensitivity, yielding a detection limit of 0.02 ng mL^{-1} with a broad linear range. This sensing protocol emphasized the potential of cobalt-doped 2D $Ti_3C_2T_x$ MXene nanosheet-based homogeneous electrochemical sensors for more precise, rapid, and cost-effective pesticide residue monitoring. Based on the same AChE activity, chitosan functionalized $Ti_3C_2T_x$ MXene nanocomposites were applied for detecting OPs, particularly malathion.[21] The researchers established that biosensors exhibited a linear detection range between 10 fM and 10 nM, with a LOD of 3 fM. The combination of chitosan boosted biocompatibility and enzyme stability, while the high conductivity and large surface area of $Ti_3C_2T_x$ MXene nanosheets enhanced electron transfer. Furthermore, using a similar concept like AChE action, self-reduced Au–Pd bimetallic nanoparticles on ultrathin $Ti_3C_2T_x$ MXene nanosheets were fabricated for the sensing of paraoxan.[270] Effective AChE immobilization on a screen-printed electrode (SPE) was completely attainable by the excellent conductivity, catalytic activity, and stability of the Au–Pd bimetallic nanoparticles. This sensor worked by identifying the paraoxon-induced suppression of AChE activity, which was measured using DPV. Under optimized experimental settings, the DPV sensor unveiled an extensive linear detection range (0.1–1000 μg L^{-1}) and an ultra-LOD of 1.75 ng L^{-1}. The promise of MXene-based nanocomposites as affordable, sensitive, and environmentally benign substrates for pesticide tracking in food and environmental samples was highlighted by these OP sensing investigations, opening up opportunities for more widespread uses in environmental analysis and biosensing.

5.6.3. Biomolecules. Demonstrating the significance of many biomolecules, including protein, uric acid, biomarkers, cholesterol, glucose, ascorbic acid, bacteria, fungus, and deoxyribose, DNA/RNA detection in human bodies is highly crucial. These molecules showed the illnesses brought on by excess or shortage of these biomolecules.[271] As an example, 2D $Ti_3C_2T_x$ MXene nanosheets have been utilized for the detection of *Mycobacterium tuberculosis* (*M. tuberculosis*) using a 16S rDNA biomarker.[272] In this sensor, the target 16S rDNA fragments were selectively hybridized with peptide nucleic acid (PNA) capture probes that were mounted on an AuNPs nanogap network electrode. By connecting with the target DNA's phosphate groups, zirconium-cross-linked 2D $Ti_3C_2T_x$ MXene nanosheets bridged the nanogap and produced a detectable change in conductance, improving signal transduction. This biosensing technique exhibited a LOD of 20 CFU mL^{-1} and a short detection time of 2 hours, making it extremely efficient for fast tuberculosis diagnosis. Additionally, the EIS signal completely validated this work and demonstrated outstanding stability, reproducibility, and great specificity, effectively differentiating *M. tuberculosis* from other bacterial species. The postulated biosensor presented its promise for use in healthcare by providing a straightforward, affordable, and extremely sensitive substitute for current diagnostic methods such as PCR, SPR, and ELISA in the initial identification of tuberculosis. Y. Chen's research group explored the development of a nanozyme-based electrochemical aptasensor for tuberculosis (TB) diagnosis, combining conductive AuNP self-assembled $Ti_3C_2T_x$ MXene@hemin with strong metal–support interactions.[273] Due to its improved charge transfer and catalytic characteristics, the AuNP self-assembled $Ti_3C_2T_x$ MXene@hemin composite has been reported to have elevated POD-like activity. Specialized *Mycobacterium tuberculosis* ESAT-6 antigen aptamers were used in this sandwich-format biosensing technique for amperometric detection. It achieved a detection range from 100 fg mL^{-1} to 50 ng mL^{-1}, with a LOD as low as 2.36 fg mL^{-1}, outstripping marketable ELISA test kits in specificity (100% *vs.* 20.59%) and investigative precision (AUC of 0.987 *vs.* 0.596). Clinical testing using serum samples from controls and TB patients validated the endurance, preference, and repeatability of the sensor. The aptasensor nanozyme amplification approach produced results that markedly increased sensitivity, providing a viable tool for clinical applications, including early and precise TB diagnosis.

Gliotoxin (GTX), the most famous example of an epidithiodioxopiperazine mycotoxin, has drawn a lot of attention during the past 20 years. The health of humans and animals is seriously threatened by it, as it has a wide variety of proapoptotic effects on different types of cells in diverse species, including humans, primates, rats, pigs, fish, and insects.[274] Consequently, a practical method for sensing GTX must be established to monitor safety and aid in the early recognition of fungal infections, particularly invasive aspergillosis. For instance, a label-free electrochemical biosensor for the specific detection of GTX by DNA nanostructure/$Ti_3C_2T_x$ MXene nano complexes was developed.[275] It explained how phosphate–titanium coordination was used to immobilize tetrahedral DNA nanostructures (TDNs) onto $Ti_3C_2T_x$ MXene nanosheets,

obviating the requirement for expensive DNA alterations. The high conductivity and huge surface area of the $Ti_3C_2T_x$ MXene nanosheets improved signal amplification and electron transport. This biosensor was successfully fabricated with the help of EIS and CV techniques, which exhibited a linear range from 5 pM to 10 nM, with a LOD of 5 pM. Reliable detection was ensured by the great selectivity of this GTX sensing technology against potential interferents, such as proteins and mycotoxins. Furthermore, this study found that combining MXene and TDNs allowed for a selective, ultrasensitive, and economical method of gliotoxin detection, underscoring its potential for wider uses in clinical diagnostics and mycotoxin monitoring. In addition, a summary of electrochemical MXene conjugated material based potential sensors for important analytes is given in Table 4. MXene-based nanohybrids boost nanozyme sensor performance in chemiluminescence, electrochemiluminescence, electrochemistry, and SERS, offering high sensitivity and a dynamic linear range for target analytes.

Table 4 Summary of MXene-coupled nanostructured materials for nanozyme-based chemiluminescent, electrochemiluminescent, electrochemical, and SERS sensors for important analytes

Material	Nanozyme activity/substrate	Role of MXene	Analyte	Linear range	LOD	Ref.
$Ti_3C_2T_x$ MXene–Nafion composite	OD/Luminol	Catalytic enhancer	H_2O_2	10 nM–1 mM	3.1 nM	207
PB/$Ti_3C_2T_x$ MXene nanocomposite	OD/Luminol	Reducing agent and carrier	Uric acid	0.2–30 μM	0.19 μM	208
Ag/MXene nanozymes	POD/Luminol	Catalytic supporter	GSH	50 nM–20 μM	0.83 nM	211
Ag/MXene nanozymes	POD/Luminol	Catalytic supporter	Uric acid	1–35 μM	0.37 μM	211
Nb_2CT_x-stabilized Au–Ag bimetallic nanoparticles	POD/$Ru(bpy)_3^{2+}$/ POD/TMB	Catalytic supporter	Chromogranin A	0.001–1000 pg mL^{-1}	0.11 fg mL^{-1}	224
Ti_3C_2 MXene@MNOFs	POD/Luminol	Signal amplifier	H_2O_2 from cancer cells	0.05–650 μM	0.45 nM	230
ZIF-67@Ti_3C_2 MXene	POD/Luminol	Catalytic enhancer	Prostate-specific antigen	—	0.91 pg mL^{-1}	231
$Ti_3C_2T_x$ MXene@TiO_2–MoS_2 hybrids	POD/Luminol	Electron mediator	Cytokeratin-19 fragment	0.1 pg mL^{-1}–100 ng mL^{-1}	0.046 pg mL^{-1}	234
Bromophenol blue with delaminated Ti_3C_2	POD/Luminol	Catalytic accelerator	Glucose	0.1–40 000 μM	0.02 μM	235
CoS_2/sulfur-doped Ti_3C_2 MXene	POD/Luminol	Conductive material	Chloramphenicol	0.1 fM–1. pM	105 fM	239
$Ti_3C_2T_x$ MXene@Au nanohybrid	OD/OPD	Catalytic enhancer	Hg^{2+}	0.4–2000 nM	17 pM	255
MXene–au composite-supported Pt@NiCo-LDH	POD/OPD	Catalytic supporter	Ochratoxin A	20 fg mL^{-1}–100 ngmL^{-1}	8.9 fg mL^{-1}	259
N-Doped $Ti_3C_2T_x$ MXene combined AgNPs	POD	Catalytic promoter	H_2O_2			260
$Ti_3C_2T_x$ MXzymes	POD/1-naphthyl phosphate	Catalyst	BCR/ABL fusion gene	0.2 fM–20 nM	0.05 fM	262
$Ti_3C_2T_x$ MXzymes	Catalase/tyrosinase	Electron carrier	Phenol	0.05–15.5 μM	12 nM	263
Phosphorene/$Ti_3C_2T_x$ MXene nanohybrid	OD	Catalyst stability enhancer	α-Naphthalene acetic acid	0.02–40 μM	1.6 nM	265
Cobalt-doped 2D $Ti_3C_2T_x$ MXene nanosheets	POD/OPD	Nanozyme catalyst	Paraoxon	0.05–50 ng mL^{-1}	0.02 ng mL^{-1}	268
Chitosan functionalized $Ti_3C_2T_x$ MXene nanocomposites	POD/acetylcholine	Catalytic supporter	Malathion	10 fM–10 nM	3 fM	21
Ultrathin $Ti_3C_2T_x$ nanosheets/Au–Pd BMNPs	POD/acetylcholine	Catalytic supporter	Paraoxon	0.1–1000 μg L^{-1}	1.75 ng L^{-1}	270
AuNP self-assembled $Ti_3C_2T_x$ MXene@hemin composite	POD/TMB	Catalytic supporter	Tuberculosis	100 fg mL^{-1}–50 ng mL^{-1}	2.36 fg mL^{-1}	273
DNA nanostructure/$Ti_3C_2T_x$ MXene nano complexes	OD	Catalyst booster	Gliotoxin	5–10 000 pM	5 pM	275
$Ti_3C_2T_x$ MXene nanosheets	POD/horseradish	Nanozyme catalyst	Prostate-specific antigen	0.1–50 ng mL^{-1}	0.031 ng mL^{-1}	276
$Ti_3C_2T_x$ MXene/Ag_2S combined with CDs decorated with Au@Ag core–shell nanozymes	POD	Catalytic supporter	MicroRNA-155, a cancer biomarker	1–10 000 fM	0.83 fM	277
$Ti_3C_2T_x$ MXene@AuNPs	OD/thionine	Catalytic supporter	Creatinine	0.4–5000 μg mL^{-1}	0.03 μg mL^{-1}	279
$Ti_3C_2T_x$ incorporated Fe atom-based single-atom nanozymes	POD/TMB	Catalytic support	Ascorbic acid Uric acid Melatonin GSH Tea polyphenols	10^{-8} to 10^{-3} M	—	288

5.6.4. Cancer biomarkers. One of the most urgent global health concerns is cancer, a diverse collection of diseases characterized by unregulated cell proliferation and development.[250] It has been shown that cancer biomarkers such as prostate-specific antigen (PSA), carcinoembryonic antigen (CEA), cancer antigen 125 (CA-125), and mucin1 (MUC1) are useful in the diagnosis of cancer. Crucially, cutting-edge technologies that provide great selectivity, sensitivity, and accessibility are needed for their precise and prompt detection.[248–250] As an example, $Ti_3C_2T_x$ MXene nanosheet-modified immune sensing electrode devices were utilized for the detection of PSA.[276] To increase detection sensitivity, this study used a tyramine-enzyme amplification technique in conjunction with an interdigitated micro-comb electrode. To fabricate the immunosensor, anti-PSA antibodies were immobilized on electrodes coated with $Ti_3C_2T_x$ MXene nanosheets. AuNPs functionalized with HRP and secondary antibodies served as signal transducers. 4-Chloro-1-naphthol was extracted by enzymatic biocatalysis, which produced an insulating layer that changed the local capacitance and increased detection precision. This PSA detection tactic established a detection range of 0.1–50 ng mL^{-1} and a LOD of 0.031 ng mL^{-1}, showing strong specificity and reproducibility. Additionally, there was a strong correlation between the sensor's performance in human serum samples and marketed PSA ELISA kits. Additionally,[277] it was reported that 2D $Ti_3C_2T_x$ MXene/Ag_2S composites combined with carbon dots decorated with Au@Ag core–shell nanozymes exhibited significant levels of POD-like activity. These composites were utilized for the electrochemical PEC-based detection of microRNA-155, a cancer biomarker. Target microRNA-associated bipedal DNA enabled the opening of a

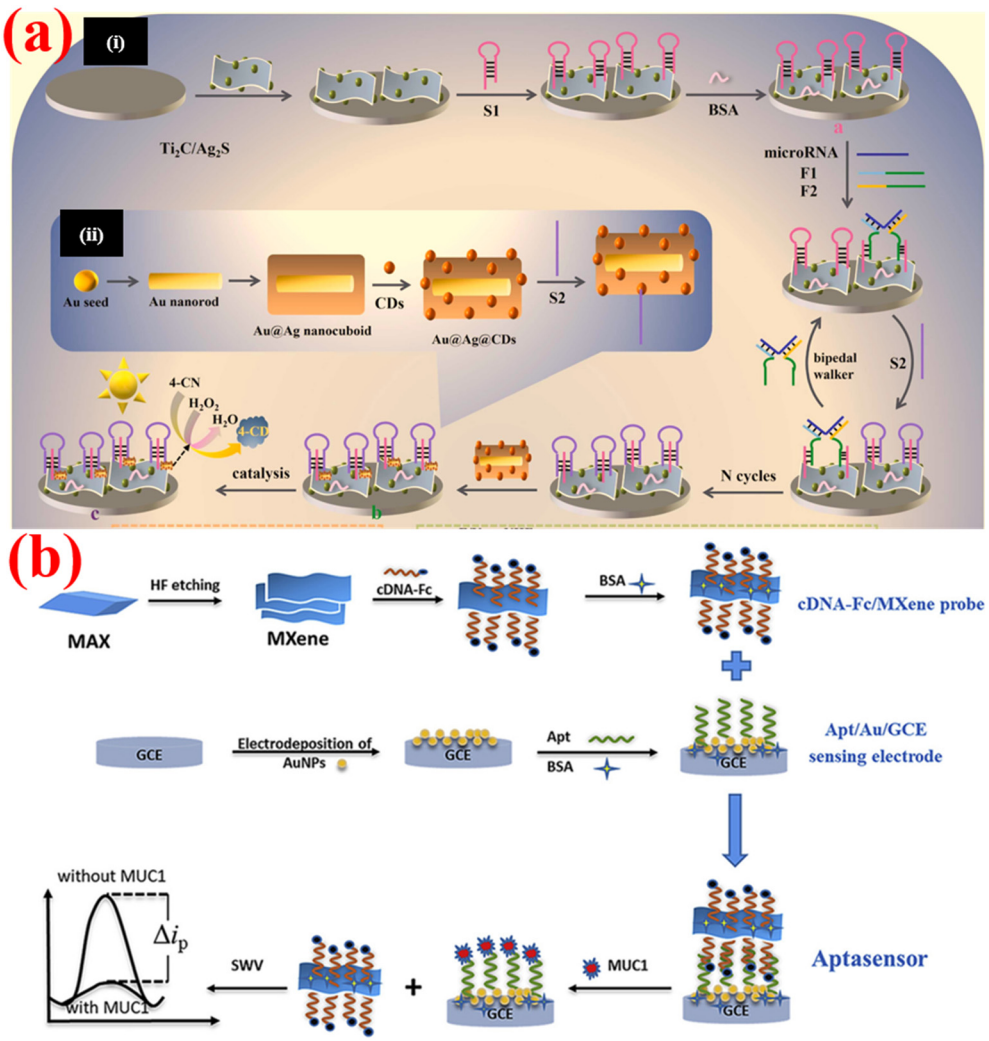

Fig. 12 MXene composite material-based nanozyme sensors for cancer biomarkers. (a) PEC-based sensors for microRNA. In (i) and (ii), preparation methods for hairpin probe (S1)-conjugated Au@Ag@CDs and multifunctional signal amplification strategies, based on 2D $Ti_3C_2T_x$ MXene/Ag_2S composites, Ag@Ag@CDs, and target microRNA-induced formation of triple helix molecules on the electrode, were exemplified, respectively [reproduced from ref. 277 with permission from Elsevier, copyright 2022]. (b) Synthetic protocol of the cDNA-Fc/$Ti_3C_2T_x$ MXene probe and the formation of the cDNA-Fc/$Ti_3C_2T_x$ MXene/Apt/Au/GCE aptasensor for MUC1 detection [reproduced from ref. 278 with permission from Elsevier, copyright 2020].

hairpin probe (S1) to produce triple helix molecules by immobilizing S1 onto the 2D $Ti_3C_2T_x$ MXene/Ag_2S surface. Following this, the carbon dots decorated with Au@Ag core–shell NPs coupled with the S2 probe were added to the biosensing platform, acting as a POD-like nanozyme and multipurpose signal amplifier (Fig. 12a). Using the 2D $Ti_3C_2T_x$ MXene/Ag_2S nanozyme-based approach, target microRNA-155 was linearly identified with a LOD of 0.83 fM over a wide range of 1–10 000 fM. F. Zhang's research team reported a competitive electrochemical aptasensor based on a cDNA-ferrocene/$Ti_3C_2T_x$ MXene probe for detecting the breast cancer biomarker mucin1 (MUC1).[278] Notable for their excellent electrical conductivity and extensive surface area, $Ti_3C_2T_x$ MXene nanosheets were employed as transporters for the cDNA-ferrocene (cDNA-Fc) probe. The aptasensor was fabricated by immobilizing an MUC1 aptamer on an AuNP-modified glassy carbon electrode (Au/GCE) *via* Au–S bonding, forming Apt/Au/GCE. The complementary cDNA-Fc probe was then attached to the $Ti_3C_2T_x$ MXene surface, creating the cDNA-Fc/$Ti_3C_2T_x$ MXene probe, which hybridized with the aptamer to form the final cDNA-Fc/$Ti_3C_2T_x$ MXene/Apt/Au/GCE aptasensor. This reaction scheme is displayed in Fig. 12b. The cDNA-Fc/$Ti_3C_2T_x$ MXene probe was removed from the electrode *via* a competitive recognition process upon the introduction of MUC1, lowering the electrical signal that was linked with the concentration of MUC1. This aptasensor was monitored by SWV and EIS. This sensor exhibited a wide linear detection range (1 pM to 10 mM) and a low detection limit (0.33 pM), demonstrating high sensitivity. The findings demonstrated the MXene-based aptasensor's potential for clinical diagnostic applications by showing that it offered an early breast cancer detection method that was sensitive, selective, and economical. In addition, molecularly imprinted polymer (MIP) and a biomimic nanozyme using $Ti_3C_2T_x$ MXene@AuNPs have been applied for the detection of creatinine.[279] To refine its synthesis and surface functions, clarify the catalytic mechanisms, and realize its applications, more research studies are needed. The development of MXene and its composite-based nanozymes is still in its early stages. Superactive MXzymes would need to be carefully designed and developed, and their successful integration with simple detection methods would be necessary for their broad use. MXzyme may develop into a strong contender for electrochemical biosensing of cancer biomarkers as a result of these initiatives.

5.7. MXzyme-based SERS sensors

The ongoing development of sensor technology is necessary to meet the growing requirement for a secure and dependable approach in metabolic sensing. Surface-enhanced Raman spectroscopy (SERS) has become one of its most anticipated tools for sensitivity and identification or detection in biomedical and agri-food applications in the past 20 years. SERS is distinct and adaptable among spectroscopy methods because it circumvents the intrinsic sensitivity limit of Raman spectroscopy, which produces vibrational "fingerprint" spectra of molecules.[280–283] The pyridine Raman spectra on polished Ag were originally observed in 1974, although the investigators were unaware that these spectra were the result of any novel, increased, or unexpected events at the time.[284] SERS is, at its most basic, a method of greatly boosting the signal from the weak but substantially enriched Raman scattering technique.[282] Although scientists have used several techniques, such as electronic resonance intensification and triggered Raman processes, to improve the effectiveness of Raman scattering, SERS provides the most notable amplification of the Raman signal.[285,286] Because of the significant improvement, single molecules are now frequently detected at their most complicated level.[282] Furthermore, SERS is a superb method for characterizing a limited number of molecules that are attached to or close to nanostructured material surfaces.[280]

Biologically important compounds, such as melatonin (ME), AA, UA, GSH, and tea polyphenols (TP), are five antioxidants that are directly linked to human disorders. Free radicals can be captured and neutralized by these antioxidants in the human body. An excess of these antioxidants will result in oxidative stress and many diseases.[287] Thus, it is very desirable to develop appropriate sensing techniques for these antioxidants. P. Yin's research group investigated the development of $Ti_3C_2T_x$ incorporated Fe atom-based single-atom nanozymes (Fe-SA/$Ti_3C_2T_x$) as efficient alternatives to natural enzymes for the detection of five different antioxidants by the SERS method.[288] By stimulating the oxidation of TMB by colorimetric reactions, these materials showed inherent POD-like activity. By stimulating the oxidation of TMB by colorimetric reactions, the Fe-SA/$Ti_3C_2T_x$ material showed inherent POD-like activity. Density functional theory (DFT) simulations verified the spontaneous dissociation of H_2O_2 and the generation of hydroxyl radicals, whereas X-ray absorption fine structure (XAFS) studies verified electron transport between Fe and $Ti_3C_2T_x$ *via* Fe–O–Ti ligands. Furthermore, Fe-SA/$Ti_3C_2T_x$-based nanozyme was utilized as a SERS substrate for sensing oxidized TMB (TMB^+), accomplishing noteworthy indicator magnification. This method made it easier to distinguish between five antioxidants, including AA, UA, GSH, ME, and TP, depending on the degree to which they inhibit free radical reactions. Furthermore, all five antioxidants were found to have a broad detection range of 10^{-8} to 10^{-3} M. This sensing analysis opened the door for the use of Fe-SA/$Ti_3C_2T_x$ in biochemical sensing by demonstrating its potential as an efficient and discriminating platform for antioxidant detection (Table 4). In the Fe-SA/$Ti_3C_2T_x$-based nanozyme, $Ti_3C_2T_x$ MXene played a crucial role as a support material for Fe single-atom nanozymes. Through the use of Fe–O–Ti ligands, electron transport between Fe atoms and the substrate was made easier by the highly conductive and chemically robust

platform that the MXene matrix offered. Additionally, $Ti_3C_2T_x$ subsidized the POD-like catalytic activity of Fe-SA/$Ti_3C_2T_x$-based nanozyme by boosting the impulsive dissociation of H_2O_2 and helping the production of hydroxyl radicals. Furthermore, $Ti_3C_2T_x$ enhanced the SERS signal response, permitting the specific sensing of antioxidants by magnifying the signals of oxidized TMB (TMB^+). As a result, $Ti_3C_2T_x$ MXene greatly improved the activity of Fe-SA nanozymes in antioxidant sensing applications by acting as a structural, electrical, and catalytic booster.

6. Conclusions

Undoubtedly, nanozymes have been increasingly popular in recent years due to their enzyme-mimicking ability, chemical stability, and low fabrication cost. Particularly, MXzymes have been recognized as one of the representative nanozymes that have yet to be developed from a material point of view. In this review, we first briefly summarize the synthesis of MXenes and their unique characteristics. The enzyme-like capabilities of MXene materials with their flexible physicochemical features have found applications that include environmental engineering and catalytic synthesis. In particular, it is indisputable that MXzymes can lend themselves to sensing technologies. In addition, MXzymes manifested as POD, ODs, CAT, and SOD agents, and function in multi-enzyme mimic reactions. Different types of nanozymes incorporated into 2D MXene nanocomposites, the sensing mechanisms of MXzyme-based sensors, and the factors affecting nanozyme activity were discussed. Multiple investigations have shown that MXzymes can serve as core building blocks for biosensors that detect high-impact analytes due to their superior enzyme-mimicking ability, high electrical conductivity, high surface area, and customizable surface chemistry. MXzymes have been exploited for the analysis of a wide range of chemical and biological analytes in various sensing platforms such as colorimetric, smartphone-assisted, fluorescent, chemiluminescent, electrochemiluminescent, electrochemical, and SERS. Dealing with comprehensive details of the MXzymes, this review aims to provide insights into a strong basis for future research and pathways to solutions to challenges encountered in sensing applications.

Future perspectives

Although research into design, synthesis, and performance has significantly advanced over the past decade, the use of MXzymes for biochemical sensing and monitoring is still at a relatively early-stage. Their future development in this area depends on several key factors. Creating MXene-based nanomaterials with precise sizes, uniform thickness, and high durability remains difficult. Additionally, it is crucial to develop effective techniques for scalable production using environmentally friendly chemicals. Future research on MXene-based catalysts should focus on improving their catalytic efficiency and addressing current deployment challenges. Potential strategies include designing hybrid MXene composites with metals, carbon materials, or polymers for better stability and conductivity, as well as surface modifications through heteroatom doping or defect engineering to enhance activity and selectivity. Progress in their practical application will also require more cost-effective and scalable manufacturing methods, improved oxidation resistance, and deeper mechanistic understanding *via in situ* characterization. They must also possess excellent dispersibility for various uses.

The effects of MXenes on the environment and human health must be carefully considered as they advance toward practical biosensing applications. By reducing negative effects, surface functionalization with polymers or biocompatible ligands like antioxidants may enhance safety profiles. It is also crucial to comprehend their ecological fate, which includes persistence, bioaccumulation, and environmental modification. The implementation of MXene-based biosensors will be safer and more sustainable with the development of green synthesis techniques and regulatory norms.

Future studies will focus on elucidating the environmental stability, biodegradation, and biocompatibility of MXene-based nanomaterials, as these characteristics are currently mostly unknown. According to recent research, harmful effects like oxidative stress and inflammatory reactions may be brought on by the surface chemistry and possible metal ion release of V-, Mo-, and Nb-based MXenes. These results highlight how crucial it is to conduct thorough toxicological analyses to guarantee safe use.[289,290] However, the great catalytic potential of V-, Mo-, and Nb-based MXenes beyond the comparatively safer Ti_3C_2 MXene could be utilized for novel applications if these toxicity issues are properly addressed. The availability of diverse surface chemistries and electrical properties of these alternative MXenes may benefit high sensitivity and binding flexibility for sensing applications. Beyond Ti-based MXzymes, this exploration may transform sensing strategies and open the way for next-generation, rapid, economical, and extremely effective detection systems in the biological and environmental domains.

While the majority of the current MXene-based nanozymes catalyze redox reactions, it is worthwhile to discover new types of catalytic activities due to their enzyme-mimicking ability and structural versatility. Further developments may enable MXenes to replicate their structures as well as functions towards multifunctional designs with the aid of advanced molecular engineering and nanotechnology. These developments would increase the potential of MXzymes in a variety of disciplines, including biochemical detection.

The inherent chemical stability of MXzymes that allows sensing techniques to be realized in a portable scheme, even

in challenging circumstances, can be further optimized for smartphone-assisted MXene-based biosensors. This smartphone-assisted platform may revolutionize the real-time monitoring format that enables multi-target sensing, IoT integration, and artificial intelligence-powered analyses as the next-generation sensors for health care and environmental monitoring.

The commercialization of nanozyme-based sensors for potential analytes remains slow due to challenges in translating lab research into practical technologies. Achieving high sensitivity and specificity in complex biological and environmental matrices is crucial for quantifiable relevance. Nanozymes have promising real-world applications due to their remarkable stability, affordability, and adjustable features. Still, large-scale manufacture and severe clinical validation are vital for biomarkers. Cost-effective manufacturing and close multidisciplinary cooperation between scientists, business executives, and legislators will be necessary for future developments. By integrating advanced approaches, these sensors can revolutionize health care and environmental monitoring. As the investigation intensifies, nanozyme-based sensing technology will become a vital tool for early disease detection, enhancing healthcare, and precision environmental monitoring. Breakthrough developments in healthcare and other fields will be made possible by minimizing the gap between proof-of-concept and commercial reality. We strongly believe that this comprehensive review will be a good starting point for future research into MXzyme sensors for high-impact analytes.

Conflicts of interest

There are no conflicts to declare.

Data availability

No new primary data were generated for this review. The analysis of the methodologies presented herein is based entirely on data extracted from previously published studies, all of which are appropriately cited within the manuscript.

Acknowledgements

This work was supported by the National Research Foundation of Korea (NRF) grants funded by the Korean government (MSIT) (No. NRF-2021M3H4A3A02086939 and No. RS-2023-00279149).

References

1 Y. Huang, J. Ren and X. Qu, Nanozymes: classification, catalytic mechanisms, activity regulation, and applications, *Chem. Rev.*, 2019, **119**(6), 4357–4412.
2 S. Ahmadi, K. Rahimizadeh, A. Shafiee, N. Rabiee and S. Iravani, Nanozymes and their emerging applications in biomedicine, *Process Biochem.*, 2023, **131**, 154–174.
3 H. L. Anderson and J. K. Sanders, Enzyme mimics based on cyclic porphyrin oligomers: strategy, design, and exploratory synthesis. Journal of the Chemical Society, *Perkin Trans. 1*, 1995, **18**, 2223–2229.
4 S. J. Hong, H. Chun, M. Hong and B. Han, N-and B-doped fullerene as peroxidase-and catalase-like metal-free nanozymes with pH-switchable catalytic activity: a first-principles approach, *Appl. Surf. Sci.*, 2022, **598**, 153715.
5 D. Zhu, M. Zhang, L. Pu, P. Gai and F. Li, Nitrogen-enriched conjugated polymer enabled metal-free carbon nanozymes with efficient oxidase-like activity, *Small*, 2022, **18**(3), 2104993.
6 E. Cheng, B. Li and Q. Zou, Porphyrin-based nanozymes for biomedical applications, *Adv. Ther.*, 2024, **7**(4), 2300329.
7 L. J. Zhi and A. L. Sun, Platinum nanozyme-encapsulated poly (amidoamine) dendrimer for voltammetric immunoassay of pro-gastrin-releasing peptide, *Anal. Chim. Acta*, 2020, **1134**, 106–114.
8 R. Yu, R. Wang, Z. Wang, Q. Zhu and Z. Dai, Applications of DNA-nanozyme-based sensors, *Analyst*, 2021, **146**(4), 1127–1141.
9 D. Wang, D. Jana and Y. Zhao, Metal–organic framework derived nanozymes in biomedicine, *Acc. Chem. Res.*, 2020, **53**(7), 1389–1400.
10 L. Gao, J. Zhuang, L. Nie, J. Zhang, Y. Zhang, N. Gu and X. Yan, Intrinsic peroxidase-like activity of ferromagnetic nanoparticles, *Nat. Nanotechnol.*, 2007, **2**(9), 577–583.
11 M. K. Sarangi, G. Rath and D. K. Yi, Metal-organic framework-based nanozymes explored with their environmental pollution control strategies, *Inorg. Chem. Commun.*, 2024, 113334.
12 R. Liang, Y. Li, M. Huo, H. Lin and Y. Chen, Triggering sequential catalytic fenton reaction on 2D MXenes for hyperthermia-augmented synergistic nanocatalytic cancer therapy, *ACS Appl. Mater. Interfaces*, 2019, **11**(46), 42917–42931.
13 L. Zhang, X. Bi, X. Liu, Y. He, L. Li and T. You, Advances in the application of metal–organic framework nanozymes in colorimetric sensing of heavy metal ions, *Nanoscale*, 2023, **15**(31), 12853–12867.
14 X. Wang, H. Wang and S. Zhou, Progress and perspective on carbon-based nanozymes for peroxidase-like applications, *J. Phys. Chem. Lett.*, 2021, **12**(48), 11751–11760.
15 B. Unnikrishnan, C. W. Lien, H. W. Chu and C. C. Huang, A review on metal nanozyme-based sensing of heavy metal ions: Challenges and future perspectives, *J. Hazard. Mater.*, 2021, **401**, 123397.
16 M. Xu, S. Zhao, W. Zhang, D. Li, Y. Peng, M. Tanemura and Y. Yang, Wheatgrass-inspired $MoSe_2$@ Pt heterojunctions with enhanced catalytic and photothermal functionalities for highly sensitive pathogen diagnosis based on machine learning, *Sens. Actuators, B*, 2025, **426**, 137020.
17 J. Zhao, Z. Shi, M. Chen and F. Xi, Highly active nanozyme based on nitrogen-doped graphene quantum dots and iron

ion nanocomposite for selective colorimetric detection of hydroquinone, *Talanta*, 2025, **281**, 126817.
18 X. Kang, Y. Li, Z. Duan, X. Shen, R. Fu and D. Fan, A Mxene@ TA/Fe dual-nanozyme composited antifouling hydrogel for burn wound repair, *Chem. Eng. J.*, 2023, **476**, 146420.
19 M. Naguib, M. Kurtoglu, V. Presser, J. Lu, J. Niu, M. Heon, L. Hultman, Y. Gogotsi and M. W. Barsoum, Two-dimensional nanocrystals produced by exfoliation of Ti_3AlC_2, *Adv. Mater.*, 2011, **23**, 4248e4253.
20 A. M. Patil, A. A. Jadhav, N. R. Chodankar, A. T. Avatare, J. Hong, S. D. Dhas and S. C. Jun, Recent progress of MXene synthesis, properties, microelectrode fabrication techniques for micro supercapacitors and microbatteries energy storage devices and integration: A comprehensive review, *Coord. Chem. Rev.*, 2024, **517**, 216020.
21 L. Zhou, X. Zhang, L. Ma, J. Gao and Y. Jiang, Acetylcholinesterase/chitosan-transition metal carbides nanocomposites-based biosensor for the organophosphate pesticides detection, *Biochem. Eng. J.*, 2017, **128**, 243–249.
22 R. Rajamanikandan, K. Sasikumar and H. Ju, Ti_3C_2 MXene quantum dots as an efficient fluorescent probe for bioflavonoid quercetin quantification in food samples, *Anal. Chim. Acta*, 2024, **1322**, 343069.
23 P. K. Kalambate, N. S. Gadhari, X. Li, Z. Rao, S. T. Navale, Y. Shen and Y. Huang, Recent advances in MXene–based electrochemical sensors and biosensors, *TrAC, Trends Anal. Chem.*, 2019, **120**, 115643.
24 A. Rhouati, M. Berkani, Y. Vasseghian and N. Golzadeh, MXene-based electrochemical sensors for detection of environmental pollutants: A comprehensive review, *Chemosphere*, 2022, **291**, 132921.
25 B. Muthukutty, P. S. Kumar, A. K. Vivekanandan, M. Sivakumar, S. Lee and D. Lee, Progress and Perspective in harnessing MXene–carbon-based composites (0–3D): synthesis, performance, and applications, *Chemosphere*, 2024, 141838.
26 R. Mangiri, T. Ramachandran, Y. A. Kumar, A. Ghosh, A. G. Al-Sehemi, A. K. Yadav and D. Mani, Surface engineering of M_5X_4 MXenes for next-gen energy solutions, *Mater. Today Chem.*, 2025, **48**, 102864.
27 B. Lu, Z. Zhu, B. Ma, W. Wang, R. Zhu and J. Zhang, 2D MXene nanomaterials for versatile biomedical applications: current trends and future prospects, *Small*, 2021, **17**(46), 2100946.
28 K. Enoch, A. Sundaram, S. S. Ponraj, S. Palaniyappan, S. D. B. George and R. K. Manavalan, Enhancement of MXene optical properties towards medical applications via metal oxide incorporation, *Nanoscale*, 2023, **15**(42), 16874–16889.
29 X. Wu, T. Chen, Y. Chen and G. Yang, Modified Ti_3C_2 nanosheets as peroxidase mimetics for use in colorimetric detection and immunoassays, *J. Mater. Chem. B*, 2020, **8**(13), 2650–2659.
30 A. Sreedhar, M. R. Pallavolu and J. S. Noh, Progress in surface and interlayer distance modulated 2D Ti_3C_2 MXenes for potential flexible supercapacitors: a review, *Appl. Mater. Today*, 2023, **35**, 101942.
31 S. Vallem, S. Venkateswarlu, S. Song, J. Kim, Y. Li and J. Bae, Flexible MXene-conjugated polymer nanoarchitectures: Current developments and future frontiers in battery technology, *Coord. Chem. Rev.*, 2024, **510**, 215778.
32 A. Sreedhar, Q. T. H. Ta and J. S. Noh, Advancements in the photocatalytic activity of various bismuth-based semiconductor/Ti_3C_2 MXene interfaces for sustainable environmental management: A review, *J. Ind. Eng. Chem.*, 2022, **115**, 26–47.
33 A. Sreedhar, Q. T. H. Ta and J. S. Noh, Versatile role of 2D Ti_3C_2 MXenes for advancements in the photodetector performance: A review, *J. Ind. Eng. Chem.*, 2023, **127**, 1–17.
34 S. Y. Pang, W. F. Io, F. Guo, Y. Zhao and J. Hao, Two-dimensional MXene-based devices for information technology, *Mater. Sci. Eng., R*, 2025, **163**, 100894.
35 S. Wang, H. Ma, S. Ge, M. Rezakazemi and J. Han, Advanced design strategies and multifunctional applications of Nanocellulose/MXene composites: A comprehensive review, *Mater. Sci. Eng., R*, 2025, **163**, 100925.
36 R. Yang, S. Wen, S. Cai, W. Zhang, T. Wu and Y. Xiong, MXene-based nanomaterials with enzyme-like properties for biomedical applications, *Nanoscale Horiz.*, 2023, **8**(10), 1333–1344.
37 S. Iravani and R. S. Varma, MXene-based composites as nanozymes in biomedicine: a perspective, *Nano-Micro Lett.*, 2022, **14**(1), 213.
38 C. Y. Hsu, N. M. Alshik, I. Ahmad, S. Uthirapathy, S. Ballal, A. Singh and K. K. Joshi, Recent advances in MXene nanozymes-based optical and electrochemical biosensors for food safety analysis, *Nanoscale*, 2025, **17**, 7697–7712.
39 P. F. Huang and W. Q. Han, Recent advances and perspectives of lewis acidic etching route: an emerging preparation strategy for MXenes, *Nano-Micro Lett.*, 2023, **15**, 68.
40 M. Naguib, M. Kurtoglu, V. Presser, J. Lu, J. Niu, M. Heon, L. Hultman, Y. Gogotsi and M. W. Barsoum, Two-dimensional nanocrystals produced by exfoliation of Ti3AlC2, *Adv. Mater.*, 2011, **23**(37), 4248–4253.
41 V. Natu and M. W. Barsoum, MXene surface terminations: a perspective, *J. Phys. Chem. C*, 2023, **127**(41), 20197–20206.
42 M. Alhabeb, K. Maleski, T. S. Mathis, A. Sarycheva, C. B. Hatter, S. Uzun, A. Levitt and Y. Gogotsi, Selective Etching of Silicon from Ti_3SiC_2 (MAX) to Obtain 2D Titanium Carbide (MXene), *Angew. Chem., Int. Ed.*, 2018, **57**(19), 5444–5448.
43 G. Deysher, C. E. Shuck, K. Hantanasirisakul, N. C. Frey, A. C. Foucher, K. Maleski, A. Sarycheva, V. B. Shenoy, E. A. Stach, B. Anasori and Y. Gogotsi, Synthesis of Mo_4VAlC_4 MAX phase and two-dimensional Mo_4VC_4 MXene with five atomic layers of transition metals, *ACS Nano*, 2019, **14**(1), 204–217.
44 A. VahidMohammadi, A. Hadjikhani, S. Shahbazmohamadi and M. Beidaghi, Two-dimensional vanadium carbide

(MXene) as a high-capacity cathode material for rechargeable aluminum batteries, *ACS Nano*, 2017, **11**(11), 11135–11144.

45 P. Lakhe, E. M. Prehn, T. Habib, J. L. Lutkenhaus, M. Radovic, M. S. Mannan and M. J. Green, Process safety analysis for $Ti_3C_2T_x$ MXene synthesis and processing, *Ind. Eng. Chem. Res.*, 2019, **58**(4), 1570–1579.

46 Y. An, Y. Tian, H. Shen, Q. Man, S. Xiong and J. Feng, Two-dimensional MXenes for flexible energy storage devices, *Energy Environ. Sci.*, 2023, **16**(10), 4191–4250.

47 M. Ghidiu, M. R. Lukatskaya, M. Q. Zhao, Y. Gogotsi and M. W. Barsoum, Conductive two-dimensional titanium carbide 'clay' with high volumetric capacitance, *Nature*, 2014, **516**(7529), 78–81.

48 X. Wang, C. Garnero, G. Rochard, D. Magne, S. Morisset, S. Hurand, P. Chartier, J. Rousseau, T. Cabioc'h, C. Coutanceau and V. Mauchamp, A new etching environment (FeF_3/HCl) for the synthesis of two-dimensional titanium carbide MXenes: a route towards selective reactivity vs. water, *J. Mater. Chem. A*, 2017, **5**(41), 22012–22023.

49 F. Liu, A. Zhou, J. Chen, J. Jia, W. Zhou, L. Wang and Q. Hu, Preparation of Ti_3C_2 and Ti_2C MXenes by fluoride salts etching and methane adsorptive properties, *Appl. Surf. Sci.*, 2017, **416**, 781–789.

50 A. Feng, Y. Yu, Y. Wang, F. Jiang, Y. Yu, L. Mi and L. Song, Two-dimensional MXene Ti_3C_2 produced by exfoliation of Ti3AlC2, *Mater. Des.*, 2017, **114**, 161–166.

51 J. Halim, M. R. Lukatskaya, K. M. Cook, J. Lu, C. R. Smith, L. Å. Näslund, S. J. May, L. Hultman, Y. Gogotsi, P. Eklund and M. W. Barsoum, Transparent conductive two-dimensional titanium carbide epitaxial thin films, *Chem. Mater.*, 2014, **26**(7), 2374–2381.

52 M. Alhabeb, K. Maleski, B. Anasori, P. Lelyukh, L. Clark, S. Sin and Y. Gogotsi, Guidelines for synthesis and processing of two-dimensional titanium carbide ($Ti_3C_2T_x$ MXene), *Chem. Mater.*, 2017, **29**(18), 7633–7644.

53 S. Zhou, Y. Guan, L. Tan, X. Li, H. Zhu, Q. Zhang, Z. Dong, N. Yang and Y. Cong, Recent advances in multiple transition metal MXenes: Synthesis, properties, and applications in energy storage, *J. Energy Storage*, 2025, **120**, 116419.

54 L. Wang, H. Zhang, B. Wang, C. Shen, C. Zhang, Q. Hu, A. Zhou and B. Liu, Synthesis and electrochemical performance of $Ti_3C_2T_x$ with hydrothermal process, *Electron. Mater. Lett.*, 2016, **12**, 702–710.

55 Y. Guo, S. Jin, L. Wang, P. He, Q. Hu, L. Z. Fan and A. Zhou, Synthesis of two-dimensional carbide Mo_2CT_x MXene by hydrothermal etching with fluorides and its thermal stability, *Ceram. Int.*, 2020, **46**(11), 19550–19556.

56 C. Peng, P. Wei, X. Chen, Y. Zhang, F. Zhu, Y. Cao, H. Wang, H. Yu and F. Peng, A hydrothermal etching route to synthesis of 2D MXene (Ti_3C_2, Nb_2C): Enhanced exfoliation and improved adsorption performance, *Ceram. Int.*, 2018, **44**(15), 18886–18893.

57 S. Siddique, A. Waheed, M. Iftikhar, M. T. Mehran, M. Z. Zarif, H. A. Arafat and F. Shahzad, Fluorine-free MXenes via molten salt Lewis acidic etching: applications, challenges, and future outlook, *Prog. Mater. Sci.*, 2021, **139**, 101183.

58 C. Wang, H. Shou, S. Chen, S. Wei, Y. Lin, P. Zhang, Z. Liu, K. Zhu, X. Guo, X. Wu and P. M. Ajayan, HCl-based hydrothermal etching strategy toward fluoride-free MXenes, *Adv. Mater.*, 2021, **33**(27), 2101015.

59 P. Urbankowski, B. Anasori, T. Makaryan, D. Er, S. Kota, P. L. Walsh, M. Zhao, V. B. Shenoy, M. W. Barsoum and Y. Gogotsi, Synthesis of two-dimensional titanium nitride Ti_4N_3 (MXene), *Nanoscale*, 2016, **8**(22), 11385–11391.

60 I. R. Shein and A. L. Ivanovskii, Graphene-like titanium carbides and nitrides $Ti_{n+1}C_n$, Ti_n+ $1N_n$ (n= 1, 2, and 3) from de-intercalated MAX phases: First-principles probing of their structural, electronic properties and relative stability, *Comput. Mater. Sci.*, 2012, **65**, 104–114.

61 M. Li, J. Lu, K. Luo, Y. Li, K. Chang, K. Chen, J. Zhou, J. Rosen, L. Hultman, P. Eklund and P. O. Persson, Element replacement approach by reaction with Lewis acidic molten salts to synthesize nanolaminated MAX phases and MXenes, *J. Am. Chem. Soc.*, 2019, **141**(11), 4730–4737.

62 V. Kamysbayev, A. S. Filatov, H. Hu, X. Rui, F. Lagunas, D. Wang, R. F. Klie and D. V. Talapin, Covalent surface modifications and superconductivity of two-dimensional metal carbide MXenes, *Science*, 2020, **369**(6506), 979–983.

63 K. Xie, J. Wang, K. Xu, Z. Wei, M. Zhang and J. Zhang, In-situ synthesis of fluorine-free MXene/TiO_2 composite for high-performance supercapacitor, *Arabian J. Chem.*, 2024, **17**(2), 105551.

64 B. Zhang, J. Zhu, P. Shi, W. Wu and F. Wang, Fluoride-free synthesis and microstructure evolution of novel two-dimensional $Ti_3C_2(OH)_2$ nanoribbons as high-performance anode materials for lithium-ion batteries, *Ceram. Int.*, 2019, **45**(7), 8395–8405.

65 T. Li, L. Yao, Q. Liu, J. Gu, R. Luo, J. Li, X. Yan, W. Wang, P. Liu, B. Chen and W. Zhang, Fluorine-free synthesis of high-purity $Ti_3C_2T_x$ (T= OH, O) via alkali treatment, *Angew. Chem., Int. Ed.*, 2018, **57**(21), 6115–6119.

66 W. Sun, S. A. Shah, Y. Chen, Z. Tan, H. Gao, T. Habib, M. Radovic and M. J. Green, Electrochemical etching of Ti_2AlC to Ti_2CT_x (MXene) in low-concentration hydrochloric acid solution, *J. Mater. Chem. A*, 2017, **5**(41), 21663–21668.

67 S. Yang, P. Zhang, F. Wang, A. G. Ricciardulli, M. R. Lohe, P. W. Blom and X. Feng, Fluoride-free synthesis of two-dimensional titanium carbide (MXene) using a binary aqueous system, *Angew. Chem., Int. Ed.*, 2018, **57**(47), 15491–15495.

68 H. Shi, P. Zhang, Z. Liu, S. Park, M. R. Lohe, Y. Wu, A. Shaygan Nia, S. Yang and X. Feng, Ambient-stable two-dimensional titanium carbide (MXene) enabled by iodine etching, *Angew. Chem., Int. Ed.*, 2021, **60**(16), 8689–8693.

69 C. Xu, L. Wang, Z. Liu, L. Chen, J. Guo, N. Kang, X. L. Ma, H. M. Cheng and W. Ren, Large-area high-quality 2D ultrathin Mo_2C superconducting crystals, *Nat. Mater.*, 2015, **14**(11), 1135–1141.

70 J. Vacík, P. Horák, S. Bakardjieva, V. Bejsovec, G. Ceccio, A. Cannavo, A. Torrisi, V. Lavrentiev and R. Klie, Ion

sputtering for preparation of thin MAX and MXene phases, *Radiat. Eff. Defects Solids*, 2020, **175**(1–2), 177–189.

71 D. L. Druffel, M. G. Lanetti, J. D. Sundberg, J. T. Pawlik, M. S. Stark, C. L. Donley, L. M. McRae, K. M. Scott and S. C. Warren, Synthesis and electronic structure of a 3D crystalline stack of MXene-like sheets, *Chem. Mater.*, 2019, **31**(23), 9788–9796.

72 M. Zandieh and J. Liu, Nanozymes: definition, activity, and mechanisms, *Adv. Mater.*, 2024, **36**(10), 2211041.

73 X. Zhang, X. Chen and Y. Zhao, Nanozymes: versatile platforms for cancer diagnosis and therapy, *Nano-Micro Lett.*, 2022, **14**(1), 95.

74 A. Deisseroth and A. L. Dounce, Catalase: Physical and chemical properties, mechanism of catalysis, and physiological role, *Physiol. Rev.*, 1970, **50**(3), 319–375.

75 Y. Chen, B. Li, K. Li and Y. Lin, Superoxide dismutase nanozymes: current status and future perspectives on brain disease treatment and diagnosis, *Chem. Commun.*, 2024, **60**(31), 4140–4147.

76 C. Ding, J. Liang, Z. Zhou, Y. Li, W. Peng, G. Zhang and X. Fan, Photothermal enhanced enzymatic activity of lipase covalently immobilized on functionalized $Ti_3C_2T_X$ nanosheets, *Chem. Eng. J.*, 2019, **378**, 122205.

77 J. Wang, X. Wei, X. Wang, W. Song, W. Zhong, M. Wang and Y. Tang, Plasmonic Au nanoparticle@ $Ti_3C_2T_x$ heterostructures for improved oxygen evolution performance, *Inorg. Chem.*, 2021, **60**(8), 5890–5897.

78 S. Wen, Y. Xiong, S. Cai, H. Li, X. Zhang, Q. Sun and R. Yang, Plasmon-enhanced photothermal properties of Au@ $Ti_3C_2T_x$ nanosheets for antibacterial applications, *Nanoscale*, 2022, **14**(44), 16572–16580.

79 Z. Jin, G. Xu, Y. Niu, X. Ding, Y. Han, W. Kong and Y. Xu, $Ti_3C_2T_x$ MXene-derived TiO2/C-QDs as oxidase mimics for the efficient diagnosis of glutathione in human serum, *J. Mater. Chem. B*, 2020, **8**(16), 3513–3518.

80 H. Hu, H. Huang, L. Xia, X. Qian, W. Feng, Y. Chen and Y. Li, Engineering vanadium carbide MXene as multienzyme mimetics for efficient in vivo ischemic stroke treatment, *Chem. Eng. J.*, 2022, **440**, 135810.

81 D. Zhang, L. Jiang, L. Li, X. Li, W. Zheng, L. Gui and M. Gong, Integrated metabolomics revealed the fibromyalgia-alleviation effect of Mo_2C nanozyme through regulated homeostasis of oxidative stress and energy metabolism, *Biomaterials*, 2022, **287**, 121678.

82 X. Ren, M. Huo, M. Wang, H. Lin, X. Zhang, J. Yin and H. Chen, Highly catalytic niobium carbide (MXene) promotes hematopoietic recovery after radiation by free radical scavenging, *ACS Nano*, 2019, **13**(6), 6438–6454.

83 X. Zhao, Y. Chen, R. Niu, Y. Tang, Y. Chen, H. Su and L. Meng, NIR plasmonic nanozymes: synergistic enhancement mechanism and multi-modal anti-infection applications of MXene/MOFs, *Adv. Mater.*, 2024, **36**(8), 2307839.

84 X. Kang, Y. Li, Z. Duan, X. Shen, R. Fu and D. Fan, A Mxene@ TA/Fe dual-nanozyme composited antifouling hydrogel for burn wound repair, *Chem. Eng. J.*, 2023, **476**, 146420.

85 H. Wang, C. Liu, Y. Zhao, X. Luo, P. Yin, F. Du and G. Zeng, Facile preparation of $V_2C@VO_x$ nanosheets with excellent multi-enzyme activity and their colorimetric sensing application, *New J. Chem.*, 2024, **48**(11), 4886–4895.

86 W. Feng, X. Han, H. Hu, M. Chang, L. Ding, H. Xiang and Y. Li, 2D vanadium carbide MXenzyme to alleviate ROS-mediated inflammatory and neurodegenerative diseases, *Nat. Commun.*, 2021, **12**(1), 2203.

87 T. Sahare, N. Singh, B. N. Sahoo and A. Joshi, Smartphone-enhanced nanozyme sensors: Colorimetric and fluorescence sensing techniques, *Biosens. Bioelectron.:X*, 2024, 100544.

88 N. N. Phuong Truong, R. Rajamanikandan, K. Sasikumar and H. Ju, Smartphone-Assisted Plasmonic Nanosensor for Visual and Specific Sensing of Toxic Cyanide Ions by β–Cyclodextrin Templated Gold-Rich/Silver Bimetallic Alloy Nanoparticles, *Materials*, 2025, **18**(7), 1604.

89 B. Liu, J. Zhuang and G. Wei, Recent advances in the design of colorimetric sensors for environmental monitoring, *Environ. Sci.: Nano*, 2020, **7**(8), 2195–2213.

90 R. Rajamanikandan, K. Sasikumar and H. Ju, β-Cyclodextrin Functionalized Au@Ag Core-Shell Nanoparticles: Plasmonic Sensors for Cysteamine and Efficient Nanocatalysts for Nitrobenzene-to-Aniline Conversion, *Biosensors*, 2024, **14**(11), 544.

91 R. Rajamanikandan and M. Ilanchelian, Simple smartphone-merged rapid colorimetric platform for the environmental monitoring of toxic sulfide ions by cysteine functionalized silver nanoparticles, *Microchem. J.*, 2022, **174**, 107071.

92 (*a*) S. Kaushal, S. S. Nanda, D. K. Yi and H. Ju, Effects of aspect ratio heterogeneity of an assembly of gold nanorods on localized surface plasmon resonance, *J. Phys. Chem. Lett.*, 2020, **11**(15), 5972–5979; (*b*) N. T. T. Phuong, V. Q. Dang, T. N. Bach, B. X. Khuyen, H. K. T. Ta, H. Ju and N. H. T. Tran, Functionalized silver nanoparticles for SERS amplification with enhanced reproducibility and for ultrasensitive optical fiber sensing in environmental and biochemical assays, *RSC Adv.*, 2022, **12**(48), 31352–31362.

93 K. Sasikumar, R. Rajamanikandan and H. Ju, Fluorescent carbon dots for highly sensitive bilirubin sensing with excellent selectivity, *J. Sci.:Adv. Mater. Devices*, 2023, **8**(3), 100599.

94 A. S. Sharma and N. Y. Lee, Advancements in visualizing loop-mediated isothermal amplification (LAMP) reactions: a comprehensive review of colorimetric and fluorometric detection strategies for precise diagnosis of infectious diseases, *Coord. Chem. Rev.*, 2024, **509**, 215769.

95 L. Yang, X. Xu, Y. Song, J. Huang and H. Xu, Research progress of nanozymes in colorimetric biosensing: Classification, activity, and application, *Chem. Eng. J.*, 2024, 150612.

96 V. G. Panferov and J. Liu, Optical and catalytic properties of nanozymes for colorimetric biosensors: Advantages, limitations, and perspectives, *Adv. Opt. Mater.*, 2024, **12**(30), 2401318.

97 Z. Lyu, J. Zhou, S. Ding, D. Du, J. Wang, Y. Liu and Y. Lin, Recent advances in single-atom nanozymes for colorimetric biosensing, *TrAC, Trends Anal. Chem.*, 2023, **168**, 117280.
98 S. Mansouri, Detection of pathogenic bacteria with nanozymes-based colorimetric biosensors: Advances, challenges and future prospects, *Microchem. J.*, 2024, 111392.
99 C. P. Kurup and M. U. Ahmed, Nanozymes towards personalized diagnostics: a recent progress in biosensing, *Biosensors*, 2023, **13**(4), 461.
100 X. Niu, X. Li, Z. Lyu, J. Pan, S. Ding, X. Ruan and Y. Lin, Metal–organic framework based nanozymes: promising materials for biochemical analysis, *Chem. Commun.*, 2020, **56**(77), 11338–11353.
101 G. Zhu, J. Hou, J. Xu, J. Li, C. Wang and Y. Yi, Enhanced peroxidase-like activity based on electron transfer between platinum nanoparticles and $Ti_3C_2T_X$ MXene nanoribbons coupled smartphone-assisted hydrogel platform for detecting mercury ions, *Anal. Chim. Acta*, 2024, **1329**, 343250.
102 Y. Shi, Z. Liu, R. Liu, R. Wu and J. Zhang, DNA-encoded MXene-Pt nanozyme for enhanced colorimetric sensing of mercury ions, *Chem. Eng. J.*, 2022, **442**, 136072.
103 X. Zhou, J. Zhang, D. Liao, K. Wu, H. Liu, G. Zhu and Y. Yi, Self-reduce gold nanoparticles on $Ti_3C_2T_x$ MXene nanoribbons to highly sensitive colorimetric determination of mercury ion and cysteine based on the mercury-motivated peroxidase mimetic activity, *Sens. Actuators, B*, 2023, **379**, 133271.
104 Y. Cheng, P. Shen, X. Li, X. Li, K. Chu and Y. Guo, Synergistically enhanced peroxidase-like activity of Fe_3O_4/Ti_3C_2 MXene quantum dots and its application in colorimetric determination of Cr (VI), *Sens. Actuators, B*, 2023, **376**, 132979.
105 Z. G. Khan and P. O. Patil, A comprehensive review on carbon dots and graphene quantum dots based fluorescent sensor for biothiols, *Microchem. J.*, 2020, **157**, 105011.
106 J. Huang, P. Wu, Y. Qin, J. Zhang, W. Wang, X. Yi and Z. Chen, Tailoring the peroxidase-like properties of Mo atom nanoclusters/N-MXene nanozymes for sensitive colorimetric detection of glutathione, *Talanta*, 2024, **278**, 126485.
107 X. Lu, J. Jia, Z. Wang and W. Wang, MXene/Carbon Dots Nanozyme Composites for Glutathione Detection and Tumor Therapy, *Nanomaterials*, 2024, **14**(13), 1090.
108 J. Wang, W. Xu, L. Zhou, T. Zhang, N. Yang, M. Wang and W. Ge, Sensitive colorimetric sensing of glutathione and H_2O_2 based on enhanced peroxidase mimetic activity of MXene@ Fe_3O_4, *Microchim. Acta*, 2022, **189**(12), 452.
109 H. Geng, Z. Li, Q. Liu, Q. Yang, H. Jia, Q. Chen and W. He, Boosting the peroxidase-like activity of Pt nanozymes by a synergistic effect of Ti_3C_2 nanosheets for dual mechanism detection, *Dalton Trans.*, 2022, **51**(31), 11693–11702.
110 X. Xi, J. Wang, Y. Wang, H. Xiong, M. Chen, Z. Wu and W. Wen, Preparation of Au/Pt/$Ti_3C_2Cl_2$ nanoflakes with self-reducing method for colorimetric detection of glutathione and intracellular sensing of hydrogen peroxide, *Carbon*, 2022, **197**, 476–484.
111 Z. Lei, J. Guo, J. Zou and Z. Wang, Colorimetric determination of biothiols based on peroxidase-mimicking Ag nanoparticles decorated Ti_3C_2 nanosheets, *Microchim. Acta*, 2022, **189**(10), 369.
112 M. Lian, Y. Zhao, J. Zhao, W. Zhang, H. Zhang and D. Chen, Oxidase-like V_2C MXene nanozyme with inherent antibacterial properties for colorimetric sensing, *Talanta*, 2023, **265**, 124872.
113 S. Siva, G. A. Bodkhe, C. Cong, S. H. Kim and M. Kim, Heterostructured Au@ Pt/Nb_2C-MXene nanocomposite as a colorimetric sensor with peroxidase-like activity for reactive oxygen species of H_2O_2, *J. Ind. Eng. Chem.*, 2023, **124**, 523–531.
114 C. Ma, N. Jiang, X. Sun, L. Kong, T. Liang, X. Wei and P. Wang, Progress in optical sensors-based uric acid detection, *Biosens. Bioelectron.*, 2023, **237**, 115495.
115 M. Liu, Y. He, J. Zhou, Y. Ge, J. Zhou and G. Song, A "naked-eye"colorimetric and ratiometric fluorescence probe for uric acid based on Ti_3C_2 MXene quantum dots, *Anal. Chim. Acta*, 2020, **1103**, 134–142.
116 D. Chen, S. Shao, W. Zhang, J. Zhao and M. Lian, Nitrogen and sulfur co-doping strategy to trigger the peroxidase-like and electrochemical activity of Ti_3C_2 nanosheets for sensitive uric acid detection, *Anal. Chim. Acta*, 2022, **1197**, 339520.
117 M. H. Facure, L. A. Mercante, Y. Gogotsi and D. S. Correa, ZnO–Co_3O_4 Nanofibers/MXene Composite with Peroxidase-Like Activity for Ascorbic Acid Detection, *ACS Appl. Nano Mater.*, 2025, **8**, 4291–4299.
118 Q. Huang, J. Chen, Y. Zhao, J. Huang and H. Liu, Advancements in electrochemical glucose sensors, *Talanta*, 2025, **281**, 126897.
119 J. Huang, H. Gu, X. Feng, G. Wang and Z. Chen, Copper Nanoparticle/N-Doped $Ti_3C_2T_x$ MXene Hybrids with Enhanced Peroxidase-like Activity for Colorimetric Glucose Sensing, *ACS Appl. Nano Mater.*, 2022, **5**(10), 15531–15538.
120 Z. Li, T. Lei, T. Pei, K. Chen, Z. Zhao, M. Wang and Y. He, Facile synthesis of MXene-Ti_3C_2/Co nanosheet hydrogel sensor with the assistance of a smartphone for on-site monitoring of glucose in beverages, *Molecules*, 2023, **28**(13), 5075.
121 M. A. Sha, P. C. Meenu, H. Haspel and Z. Kónya, Metal-based non-enzymatic systems for cholesterol detection: mechanisms, features, and performance, *RSC Adv.*, 2024, **14**(34), 24561–24573.
122 Y. Chen, C. Rong, W. Gao, S. Luo, Y. Guo, Y. Gu and L. L. Qu, Ag-MXene as peroxidase-mimicking nanozyme for enhanced bacteriocide and cholesterol sensing, *J. Colloid Interface Sci.*, 2024, **653**, 540–550.
123 Y. Li, Z. Kang, L. Kong, H. Shi, Y. Zhang, M. Cui and D. P. Yang, MXene-Ti_3C_2/CuS nanocomposites: Enhanced peroxidase-like activity and sensitive colorimetric cholesterol detection, *Mater. Sci. Eng., C*, 2019, **104**, 110000.

124 V. K. Sharma, N. Johnson, L. Cizmas, T. J. McDonald and H. Kim, A review of the influence of treatment strategies on antibiotic resistant bacteria and antibiotic resistance genes, *Chemosphere*, 2016, **150**, 702–714.
125 W. Wang and S. Gunasekaran, MXene/Gold nanoparticles heterostructure as catalase mimic for colorimetric detection of penicillin G, *Chem. Eng. J.*, 2024, **482**, 148693.
126 S. Zhang, Q. Peng, N. Jiang, C. Qiao, S. Li and W. Yue, Peroxidase-like activity and mechanism of gold nanoparticle-modified Ti_3C_2 MXenes for the construction of H_2O_2 and ampicillin colorimetric sensors, *Microchim. Acta*, 2024, **191**(4), 195.
127 W. Wang, Y. Yin and S. Gunasekaran, Oxygen-terminated few-layered $Ti_3C_2T_x$ MXene nanosheets as peroxidase-mimic nanozyme for colorimetric detection of kanamycin, *Biosens. Bioelectron.*, 2022, **218**, 114774.
128 L. Yang, H. Guo, T. Hou, J. Zhang and F. Li, Metal-mediated Fe_3O_4@ polydopamine-aptamer capture nanoprobe coupling multifunctional MXene@ Au@ Pt nanozyme for direct and portable photothermal analysis of circulating breast cancer cells, *Biosens. Bioelectron.*, 2023, **234**, 115346.
129 Y. Tao, K. Yi, H. Wang, H. W. Kim, K. Li, X. Zhu and M. Li, CRISPR-Cas12a-regulated DNA adsorption and metallization on MXenes as enhanced enzyme mimics for sensitive colorimetric detection of hepatitis B virus DNA, *J. Colloid Interface Sci.*, 2022, **613**, 406–414.
130 W. Wang, S. Xiao, Z. Jia, H. Xie, T. Li, Q. Wang and N. Gan, A dual-mode aptasensor for foodborne pathogens detection using Pt, phenylboric acid and ferrocene modified Ti_3C_2 MXenes nanoprobe, *Sens. Actuators, B*, 2022, **351**, 130839.
131 X. Xu, W. Zhang, J. Huang and H. Xu, Colorimetric sensors for detection of organophosphorus pesticides in food: From sensing strategies to chemometrics-driven discrimination, *Trends Food Sci. Technol.*, 2024, 104683.
132 Y. He, X. Zhou, L. Zhou, X. Zhang, L. Ma, Y. Jiang and J. Gao, Self-Reducing Prussian Blue on $Ti_3C_2T_x$ MXene Nanosheets as a Dual-Functional Nanohybrid for Hydrogen Peroxide and Pesticide Sensing, *Ind. Eng. Chem. Res.*, 2020, **59**(35), 15556–15564.
133 Y. Guo, X. Li, P. Shen, X. Li, Y. Cheng and K. Chu, Dendritic-like MXene quantum dots@ CuNi as an efficient peroxidase candidate for colorimetric determination of glyphosate, *J. Colloid Interface Sci.*, 2024, **661**, 533–543.
134 Y. Yi, J. Li, X. Bi, L. Zhang, Y. Ren, L. Li and T. You, Highly active $Ti_3C_2T_x$ MXene nanoribbons@ AuPt bimetallic nanozyme constructed in a "two birds with one stone" manner for colorimetric sensing of dipterex, *Talanta*, 2025, **281**, 126881.
135 H. Gu, H. Li, G. Wang, J. Huang, B. Peng, J. Pei and H. Zhai, Electronic Metal–Support Interactions between Copper Nanoparticles and Nitrogen-Doped $Ti_3C_2T_x$ MXene to Boost Peroxidase-like Activity for Detecting Astaxanthin, *ACS Appl. Mater. Interfaces*, 2023, **15**(22), 26363–26372.
136 Y. Shi, Z. Niu, S. Chen, S. Wang, L. Yang and Y. Wang, Sensitive Detection of Umami Substances in Meat with Synthesized Electrochemical Sensor Enhanced by MXene Surface-Doped Peroxidase-Mimic Nanoenzymes (Fe_3O_4), *Food Bioprocess Technol.*, 2025, **18**(1), 807–817.
137 R. Rajamanikandan and M. Ilanchelian, β-Cyclodextrin protected gold nanoparticle based cotton swabs as an effective candidate for specific sensing of trace levels of cyanide, *Anal. Methods*, 2019, **11**(1), 97–104.
138 B. Kaur, N. Kaur and S. Kumar, Colorimetric metal ion sensors–A comprehensive review of the years 2011–2016, *Coord. Chem. Rev.*, 2018, **358**, 13–69.
139 K. Kaviya, R. Rajamanikandan, M. Santhamoorthy, M. A. Farah and K. S. Mani, A rhodamine-conjugated fluorescent and colorimetric receptor for the detection of Cu^{2+} ions: environmental utility and smartphone integration, *Anal. Methods*, 2025, **17**(6), 1389–1400.
140 D. S. Ali, R. O. Hassan, H. O. Othman, H. T. Taha, A. M. Khaneghah and S. Smaoui, Revolutionizing detection: Smartphone-powered colorimetry for the drugs and food analysis, *Microchem. J.*, 2024, **205**, 111228.
141 S. Kanchi, M. I. Sabela, P. S. Mdluli and K. Bisetty, Smartphone based bioanalytical and diagnosis applications: A review, *Biosens. Bioelectron.*, 2018, **102**, 136–149.
142 R. Rajamanikandan, M. Ilanchelian and H. Ju, Smartphone-enabled colorimetric visual quantification of highly hazardous trivalent chromium ions in environmental waters and catalytic reduction of p-nitroaniline by thiol-functionalized gold nanoparticles, *Chemosphere*, 2023, **340**, 139838.
143 R. Rajamanikandan, K. Shanmugaraj, M. Ilanchelian and H. Ju, Cysteamine-decorated gold nanoparticles for plasmon-based colorimetric on-site sensors for detecting cyanide ions using the smart-phone color ratio and for catalytic reduction of 4-nitrophenol, *Chemosphere*, 2023, **316**, 137836.
144 A. Zhou, J. Chen, X. Dong, P. Bai, Q. Zhu, H. M. Meng and Z. Li, Bimetallic CuRu nanozymes for colorimetric and smartphone-assisted rapid visual hypoxanthine biosensing in serum samples, *Microchim. Acta*, 2025, **192**(3), 159.
145 Q. Yang, X. Cui, Y. Qin, T. Lei, Y. He and G. Song, Cu nanoclusters decorated Ti_3C_2 nanosheets composite with tetraenzyme mimic activities and the application for smartphone-assisted detection of hypoxanthine, *Anal. Chim. Acta*, 2022, **1232**, 340494.
146 Q. Yang, Y. Qin, T. Lei, Y. Zhong, X. Cui, Y. He and G. Song, $Co(OH)_2$/MXene-Ti_3C_2 nanocomposites with triple-enzyme mimic activities as hydrogel sensing platform for on-site detection of hypoxanthine, *Microchim. Acta*, 2022, **189**(12), 481.
147 J. Fei, W. Yang, Y. Dai, W. Xu, H. Fan, Y. Zheng and X. Zhou, A biosensor based on Fe_3O_4@ MXene-Au nanocomposites with high peroxidase-like activity for colorimetric and smartphone-based detection of glucose, *Microchim. Acta*, 2023, **190**(8), 336.
148 S. E. Ekerim, N. Taşci and M. F. Demirkan, Determination of glyphosate with a novel optic membrane sensor, *Food Chem.*, 2025, 143361.

149 D. Liao, Y. Zhao, Y. Zhou, Y. Yi, W. Weng and G. Zhu, Colorimetric detection of organophosphorus pesticides based on Nb_2CT_x MXene self-reducing PdPt nanozyme integrated with hydrogel and smartphone, *J. Food Meas. Charact.*, 2024, **18**(11), 9223–9232.
150 M. Lin, Z. Gao, Z. Qian, Y. Deng, Y. Chen, Y. Wang and X. Li, Ultrasensitive $Ti_3C_2T_x$@ Pt-Based Immunochromatography with Catalytic Amplification and a Dual Signal for the Detection of Chloramphenicol in Animal-Derived Foods, *Foods*, 2024, **13**(9), 1416.
151 L. Zhang, A. Li, M. Shen, Z. Zhang, R. Wufuer and D. Wang, Palladium–platinum bimetallic modified MXene nanozyme for highly sensitive detection of active substances with acetylcholinesterase inhibitory effect, *Talanta*, 2025, **282**, 127020.
152 K. Chen, S. Fu, C. Jin, F. Guo, Y. He, Q. Ren and X. Wang, Smartphone-Enabled Fluorescence and Colorimetric Platform for the On-Site Detection of Hg^{2+} and Cl^- Based on the Au/Cu/Ti_3C_2 Nanosheets, *Molecules*, 2023, **28**(14), 5355.
153 H. Li, S. Zhao, Z. Wang and F. Li, Engineering a two-dimensional metal-carbon nanozyme-based portable paper-based colorimetric chip for onsite and visual analysis of pyrophosphate, *Talanta*, 2024, **278**, 126490.
154 T. Jiang, P. Ju, F. Bi, J. Chi, S. Wen, F. Jiang and Z. Chi, Target-induced enzymatic cleavage cycle amplification reaction-gated organic photoelectrochemical transistor biosensor for rapid detection of okadaic acid, *Biosens. Bioelectron.*, 2025, **267**, 116745.
155 J. Chi, P. Ju, F. Bi, S. Wen, Z. Xiang, J. Chen and M. Qiu, A smartphone-assisted ultrasensitive colorimetric aptasensor based on DNA-encoded porous MXene nanozyme for visual detection of okadaic acid, *Food Chem.*, 2025, **464**, 141776.
156 D. K. Mal, H. Pal and G. Chakraborty, A comprehensive review on recent advances in fluorescence-based bio-analytes sensing, *TrAC, Trends Anal. Chem.*, 2024, **171**, 117493.
157 D. Wu, A. C. Sedgwick, T. Gunnlaugsson, E. U. Akkaya, J. Yoon and T. D. James, Fluorescent chemosensors: the past, present and future, *Chem. Soc. Rev.*, 2017, **46**(23), 7105–7123.
158 R. Rajamanikandan and M. Ilanchelian, Highly selective and sensitive biosensing of dopamine based on glutathione coated silver nanoclusters enhanced fluorescence, *New J. Chem.*, 2017, **41**(24), 15244–15250.
159 D. S. Chumakov, S. S. Evstigneeva and O. I. Guliy, Luminescent Nanozyme-Based Sensors for Bacteria Detection, *Appl. Biochem. Microbiol.*, 2024, **60**(6), 1022–1034.
160 J. Zhang and J. Liu, Nanozyme-based luminescence detection, *Luminescence*, 2020, **35**(8), 1185–1194.
161 M. Zhou, Z. Diwu, N. Panchuk-Voloshina and R. P. Haugland, A stable nonfluorescent derivative of resorufin for the fluorometric determination of trace hydrogen peroxide: applications in detecting the activity of phagocyte NADPH oxidase and other oxidases, *Anal. Biochem.*, 1997, **253**(2), 162–168.
162 X. Yang and E. Wang, A nanoparticle autocatalytic sensor for Ag^+ and Cu^{2+} ions in aqueous solution with high sensitivity and selectivity and its application in test paper, *Anal. Chem.*, 2011, **83**(12), 5005–5011.
163 J. Sun, B. Wang, X. Zhao, Z. J. Li and X. Yang, Fluorescent and colorimetric dual-readout assay for inorganic pyrophosphatase with Cu^{2+}-triggered oxidation of o-phenylenediamine, *Anal. Chem.*, 2016, **88**(2), 1355–1361.
164 T. Lin, Y. Qin, Y. Huang, R. Yang, L. Hou, F. Ye and S. Zhao, A label-free fluorescence assay for hydrogen peroxide and glucose based on the bifunctional MIL-53 (Fe) nanozyme, *Chem. Commun.*, 2018, **54**(14), 1762–1765.
165 S. Chen, Z. Li, Z. Huang and Q. Jia, Investigation of efficient synergistic and protective effects of chitosan on copper nanoclusters: Construction of highly active and stable nanozyme for colorimetric and fluorometric dual-signal biosensing, *Sens. Actuators, B*, 2021, **332**, 129522.
166 D. Li, S. L. Garisto, P. J. J. Huang, J. Yang, B. Liu and J. Liu, Fluorescent detection of fluoride by CeO_2 nanozyme oxidation of Amplex red, *Inorg. Chem. Commun.*, 2019, **106**, 38–42.
167 C. Song, W. Zhao, H. Liu, W. Ding, L. Zhang, J. Wang and C. Yao, Two-dimensional FeP@ C nanosheets as a robust oxidase mimic for fluorescence detection of cysteine and Cu 2+, *J. Mater. Chem. B*, 2020, **8**(33), 7494–7500.
168 X. Xu, X. Zou, S. Wu, L. Wang, X. Niu, X. Li and M. Lan, In situ formation of fluorescent polydopamine catalyzed by peroxidase-mimicking FeCo-LDH for pyrophosphate ion and pyrophosphatase activity detection, *Anal. Chim. Acta*, 2019, **1053**, 89–97.
169 R. Govindaraju and J. Kim, MXene-enabled fluorescent sensing systems: recent advances in biomolecule detection, *Microchem. J.*, 2025, **218**, 115082.
170 W. Song, B. Zhao, C. Wang, Y. Ozaki and X. Lu, Functional nanomaterials with unique enzyme-like characteristics for sensing applications, *J. Mater. Chem. B*, 2019, **7**(6), 850–875.
171 L. Han, H. Zhang, D. Chen and F. Li, Protein-directed metal oxide nanoflakes with tandem enzyme-like characteristics: colorimetric glucose sensing based on one-pot enzyme-free cascade catalysis, *Adv. Funct. Mater.*, 2018, **28**(17), 1800018.
172 D. Wang, D. Jana and Y. Zhao, Metal-organic framework derived nanozymes in biomedicine, *Acc. Chem. Res.*, 2020, **53**(7), 1389–1400.
173 J. Chi, P. Ju, F. Bi, S. Wang, T. Jiang, S. Wen and M. Qiu, MXene@ $MnIn_2S_4$-Gated Organic Photoelectrochemical Transistors with Nanozyme-Mediated Multiple Quenching Effects for Ultrasensitive Detection of Okadaic Acid, *Adv. Funct. Mater.*, 2024, **34**(45), 2407201.
174 U. Amara, I. Hussain, M. Ahmad, K. Mahmood and K. Zhang, 2D MXene-based biosensing: a review, *Small*, 2023, **19**(2), 2205249.
175 K. Dhara and R. M. Debiprosad, Review on nanomaterials-enabled electrochemical sensors for ascorbic acid detection, *Anal. Biochem.*, 2019, **586**, 113415.
176 J. Huang, C. Shen, H. Gu, G. Wang, P. Zhou, X. Liu and Z. Chen, Cu Nanoparticles/N-Doped $Ti_3C_2T_x$-Based

Fluorescence Sensor for Detecting Ascorbic Acid, *ACS Sustainable Chem. Eng.*, 2023, **11**(49), 17472–17481.
177 A. Rohde, J. A. Hammerl, I. Boone, W. Jansen, S. Fohler, G. Klein and S. Al Dahouk, Overview of validated alternative methods for the detection of foodborne bacterial pathogens, *Trends Food Sci. Technol.*, 2017, **62**, 113–118.
178 S. Wang, J. Hu, S. Xiao, M. Wang, J. Yu, Z. Jia and N. Gan, Fluorescent/electrochemical dual-signal response biosensing strategy mediated by DNAzyme-ferrocene-triggered click chemistry for simultaneous rapid screening and quantitative detection of Vibrio parahaemolyticus, *Sens. Actuators, B*, 2023, **380**, 133393.
179 B. A. Al-Jaal, M. Jaganjac, A. Barcaru, P. Horvatovich and A. Latiff, Aflatoxin, fumonisin, ochratoxin, zearalenone and deoxynivalenol biomarkers in human biological fluids: A systematic literature review, 2001–2018, *Food Chem. Toxicol.*, 2019, **129**, 211–228.
180 H. F. Hassan, R. Kordahi, H. Dimassi, A. El Khoury, R. Daou, N. Alwan and L. Karam, Aflatoxin B1 in Rice: Effects of storage duration, grain type and size, production site, and season, *J. Food Prot.*, 2022, **85**(6), 938–944.
181 Y. Kong, Y. Zhu, J. Song, Q. Liu, L. Song, X. Fei and X. Li, A novel multimode biosensor for sensitive detection of AFB1 in food based on Mxenes nano enzymes, *Food Chem.*, 2023, **426**, 136645.
182 Y. Kong, Z. Li, Q. Liu, J. Song, Y. Zhu, J. Lin and X. Li, Artificial neural network-facilitated V_2C MNs-based colorimetric/fluorescence dual-channel biosensor for highly sensitive detection of AFB1 in peanut, *Talanta*, 2024, **266**, 125056.
183 N. Wang, L. Xu, S. Liu, M. He and L. Wang, An interferometric optical fiber sensor based on ion-imprinted sodium alginate for Pb(II) detection, *Opt. Fiber Technol.*, 2025, **90**, 104053.
184 F. Farahmandzadeh, K. Kermanshahian, E. Molahosseini, M. Molaei and M. Karimipour, Highly fluorescent CdTe/ZnSe quantum dot-based "turn-off" sensor for the on-site rapid detection of Lead ions in aqueous medium, *Spectrochim. Acta, Part A*, 2025, **324**, 124914.
185 Z. Suo, L. Zhang, Z. Zhang, R. Liang, H. Shen, X. Chen and H. Jin, A bifunctional MXene@ PtPd NPs cascade DNAzyme-mediated fluorescence/colorimetric dual-mode biosensor for Pb^{2+} determination, *Food Chem.*, 2025, **464**, 141845.
186 D. Liu, W. Chen, J. Wei, X. Li, Z. Wang and X. Jiang, A highly sensitive, dual-readout assay based on gold nanoparticles for organophosphorus and carbamate pesticides, *Anal. Chem.*, 2012, **84**(9), 4185–4191.
187 S. Dai, M. Hu, W. Zhang and Z. Lei, Selective colorimetric detection of carbosulfan based on its hydrolysis behavior and Ti_3C_2/AuPt nanozyme, *Anal. Chim. Acta*, 2025, **1336**, 343519.
188 Z. Lei, P. Lei, J. Guo and Z. Wang, Recent advances in nanomaterials-based optical and electrochemical aptasensors for detection of cyanotoxins, *Talanta*, 2022, **248**, 123607.
189 O. D. Hendrickson, E. A. Zvereva, A. V. Zherdev and B. B. Dzantiev, Ultrasensitive lateral flow immunoassay of phycotoxin microcystin-LR in seafood based on magnetic particles and peroxidase signal amplification, *Food Control*, 2022, **133**, 108655.
190 J. Guo, G. Wang, J. Zou and Z. Lei, DNA controllable peroxidase-like activity of Ti_3C_2 nanosheets for colorimetric detection of microcystin-LR, *Anal. Bioanal. Chem.*, 2023, **415**(17), 3559–3569.
191 R. Eivazzadeh-Keihan, Z. Saadatidizaji, A. Maleki, M. D. L. Guardia, M. Mahdavi, S. Barzegar and S. Ahadian, Recent progresses in development of biosensors for thrombin detection, *Biosensors*, 2022, **12**(9), 767.
192 A. Bini, M. Minunni, S. Tombelli, S. Centi and M. Mascini, Analytical performances of aptamer-based sensing for thrombin detection, *Anal. Chem.*, 2007, **79**(7), 3016–3019.
193 M. Li, X. Peng, Y. Han, L. Fan, Z. Liu and Y. Guo, Ti_3C_2 MXenes with intrinsic peroxidase-like activity for label-free and colorimetric sensing of proteins, *Microchem. J.*, 2021, **166**, 106238.
194 L. Zhao, J. Xu, L. Xiong, S. Wang, C. Yu, J. Lv and J. M. Lin, Recent development of chemiluminescence for bioanalysis, *TrAC, Trends Anal. Chem.*, 2023, 117213.
195 H. Zhu, X. Huang, Y. Deng, H. Chen, M. Fan and Z. Gong, Applications of nanomaterial-based chemiluminescence sensors in environmental analysis, *TrAC, Trends Anal. Chem.*, 2023, **158**, 116879.
196 Z. Zhang, S. Zhang and X. Zhang, Recent developments and applications of chemiluminescence sensors, *Anal. Chim. Acta*, 2005, **541**(1–2), 37–46.
197 K. Deshpande and L. Kanungo, Chemiluminescence and Fluorescence Biosensors for food application: A Review, *Sens Actuators Rep.*, 2023, **5**, 100137.
198 H. Y. Li, S. Q. Zhang, M. L. Chen and J. H. Wang, Lumi-HOF@ Tb as probes for multiple ratiometric fluorescence and chemiluminescence sensing of α-glucosidase, *Anal. Chem.*, 2022, **94**(44), 15448–15455.
199 B. R. Radziszewski, Untersuchungen über hydrobenzamid, amarin und lophin, *Ber. Dtsch. Chem. Ges.*, 1877, **10**(1), 70–75.
200 H. O. Albrecht, Über die chemiluminescenz des aminophthalsäurehydrazids, *Z. Phys. Chem.*, 1928, **136**(1), 321–330.
201 K. Gleu and W. Petsch, Die chemiluminescent der dimethyl-diacridyliumsalze, *Angew. Chem., Int. Ed.*, 1935, **48**(3), 57–59.
202 W. Adam, D. V. Kazakov and V. P. Kazakov, Singlet-oxygen chemiluminescence in peroxide reactions, *Chem. Rev.*, 2005, **105**(9), 3371–3387.
203 M. Yang, J. Huang, J. Fan, J. Du, K. Pu and X. Peng, Chemiluminescence for bioimaging and therapeutics: recent advances and challenges, *Chem. Soc. Rev.*, 2020, **49**(19), 6800–6815.
204 F. Manea, F. B. Houillon, L. Pasquato and P. Scrimin, Nanozymes: gold-nanoparticle-based transphosphorylation catalysts, *Angew. Chem., Int. Ed.*, 2004, **43**, 6165–6169.

205 L. Gao, J. Zhuang, L. Nie, J. Zhang, Y. Zhang, N. Gu and X. Yan, The intrinsic peroxidase-like activity of ferromagnetic nanoparticles, *Nat. Nanotechnol.*, 2007, **2**(9), 577–583.
206 S. N. A. Shah, A. H. Shah, X. Dou, M. Khan, L. Lin and J. M. Lin, Radical-triggered chemiluminescence of phenanthroline derivatives: an insight into radical–aromatic interaction, *ACS Omega*, 2019, **4**(12), 15004–15011.
207 J. H. Choi, D. H. Lee and W. Y. Lee, Enhanced cathodic electrogenerated chemiluminescence of luminol at a MXene–Nafion composite-modified electrode in neutral aqueous solution, *J. Electroanal. Chem.*, 2023, **936**, 117389.
208 Z. Shi, T. Wu, W. Feng, B. Hu, X. Yan and X. Zheng, Enhanced luminol chemiluminescence with oxidase-like properties of prussian blue/MXene nanocomposite without H_2O_2 for the sensitive detection of uric acid, *Microchem. J.*, 2024, **206**, 111455.
209 R. Rajamanikandan, M. Ilanchelian and H. Ju, Highly selective uricase-based quantification of uric acid using hydrogen peroxide sensitive poly-(vinylpyrrolidone) templated copper nanoclusters as a fluorescence probe, *Chem*, 2023, **11**(5), 268.
210 K. S. Mani, R. Rajamanikandan, M. Ilanchelian, N. Muralidharan, M. Jothi and S. P. Rajendran, Smartphone-assisted quinoline-hemicyanine-based fluorescent probe for the selective detection of glutathione and the application in living cells, *Spectrochim. Acta, Part A*, 2020, **243**, 118809.
211 X. Zheng, Z. Shi, C. Han, H. Mu, S. Cheng and X. Yan, Convenient in situ self-assembled formation of dual-functional Ag/MXene nanozymes for efficient chemiluminescence sensing, *Anal. Methods*, 2024, **16**(48), 8324–8332.
212 Y. Fu, X. Teng and C. Lu, Iridium-based electrochemiluminescence systems and their application in bioanalysis, *TrAC, Trends Anal. Chem.*, 2023, **167**, 117273.
213 M. M. Richter, Electrochemiluminescence (ecl), *Chem. Rev.*, 2004, **104**(6), 3003–3036.
214 L. Li, Y. Chen and J. J. Zhu, Recent advances in electrochemiluminescence analysis, *Anal. Chem.*, 2017, **89**(1), 358–371.
215 Z. Liu, W. Qi and G. Xu, Recent advances in electrochemiluminescence, *Chem. Soc. Rev.*, 2015, **44**(10), 3117–3142.
216 A. J. Bard, *Electrogenerated Chemiluminescence*, Marcel Dekker, New York, 2004.
217 N. Arab, M. Hosseini and G. Xu, Emerging trends and recent advances in MXene/MXene-based nanocomposites toward electrochemiluminescence sensing and biosensing, *Biosens. Bioelectron.*, 2024, 116623.
218 L. Gao and C. He, Advances in MXene-based luminescence sensing strategies, *Anal. Methods*, 2024, **16**, 1718–1735.
219 Y. Fang, X. Yang, T. Chen, G. Xu, M. Liu, J. Liu and Y. Xu, Two-dimensional titanium carbide (MXene)-based solid-state electrochemiluminescent sensor for label-free single-nucleotide mismatch discrimination in human urine, *Sens. Actuators, B*, 2018, **263**, 400–407.
220 S. P. Hong, N. A. Keasberry and M. U. Ahmed, Development of a gliadin immunosensor incorporating gold nanourchin, molybdenum disulfide, titanium dioxide, and Nafion for enhanced electrochemiluminescence, *Microchem. J.*, 2023, **193**, 109059.
221 J. Adhikari, M. Rizwan and M. U. Ahmed, Development of a label-free electrochemiluminescence biosensor for the sensitive detection of porcine gelatin using carbon nanostructured materials, *Sens. Diagn.*, 2022, **1**(5), 968–976.
222 I. Tomac, M. Šeruga and J. Labuda, Evaluation of antioxidant activity of chlorogenic acids and coffee extracts by an electrochemical DNA-based biosensor, *Food Chem.*, 2020, **325**, 126787.
223 T. Zhan, Y. Su, W. Lai, Z. Chen and C. Zhang, A dry chemistry-based ultrasensitive electrochemiluminescence immunosensor for sample-to-answer detection of Cardiac Troponin I, *Biosens. Bioelectron.*, 2022, **214**, 114494.
224 F. Kareem, Y. F. C. Chau and M. U. Ahmed, Nb_2CT_x-supported bimetallic NPs@ ZIF-8 nanohybrid as ECL signal amplifier and peroxidase mimics for chromogranin a immunosensing in human serum and saliva, *Int. J. Biol. Macromol.*, 2025, **287**, 138476.
225 M. Pietrzak and P. Ivanova, Bimetallic and multimetallic nanoparticles as nanozymes, *Sens. Actuators, B*, 2021, **336**, 129736.
226 Y. Lu, X. Li, S. Shi, X. Liu, L. Jia, L. Shang and H. Wang, Tungsten-based polyoxometalate nanoclusters with remarkable reactive oxygen species-scavenging activity efficiently quenched luminol-based electrochemiluminescence for sensitive detection of Her-2, *Microchim. Acta*, 2024, **191**(1), 21.
227 F. Arshad, N. F. Mohd-Naim, R. Chandrawati, D. Cozzolino and M. U. Ahmed, Nanozyme-based sensors for detection of food biomarkers: a review, *RSC Adv.*, 2022, **12**(40), 26160–26175.
228 H. Riazi, G. Taghizadeh and M. Soroush, MXene-based nanocomposite sensors, *ACS Omega*, 2021, **6**(17), 11103–11112.
229 N. H. Solangi, S. A. Mazari, N. M. Mubarak, R. R. Karri, N. Rajamohan and D. V. N. Vo, Recent trends in MXene-based material for biomedical applications, *Environ. Res.*, 2023, **222**, 115337.
230 B. Wang, S. M. Khoshfetrat and H. Mohamadimanesh, Peroxidase-like manganese oxide nanoflowers-delaminated Ti_3C_2 MXene for ultrasensitive dual-mode and real-time detection of H2O2 released from cancer cells, *Microchem. J.*, 2024, **207**, 111796.
231 J. Wang, R. Hong, Z. Yang, X. Meng, R. Wu, Z. Liu and C. Li, Ultrasensitive Electrochemiluminescence Biosensor with ZIF-67@ MXene as an Efficient Co-Reaction Accelerator and Plasmonic Nanozyme as a Smart Signal Amplification Probe, *Small*, 2024, **20**(50), 2404330.
232 J. Liang, X. Guan, G. Bao, Y. Yao and X. Zhong, Molecular subtyping of small cell lung cancer, In *Seminars in Cancer Biology*, Academic Press, 2022, vol. 86, pp. 450–462.

233 M. Chen, Y. Wang, H. Su, L. Mao, X. Jiang, T. Zhang and X. Dai, Three-dimensional electrochemical DNA biosensor based on 3D graphene-Ag nanoparticles for sensitive detection of CYFRA21-1 in non-small cell lung cancer, *Sens. Actuators, B*, 2018, **255**, 2910–2918.

234 X. Ren, M. Shao, Z. Xie, X. Li, H. Ma, D. Fan and Q. Wei, A Co-Reactive Immunosensor Based on $Ti_3C_2T_x$ MXene@ TiO_2–MoS_2 Hybrids Promoting luminol@ Au@ Ni–Co NCs Electrochemiluminescence for CYFRA 21–1 Detection, *ACS Sens.*, 2024, **9**(4), 1992–1999.

235 F. Momeni, S. M. Khoshfetrat, H. Bagheri and K. Zarei, Ti_3C_2 MXene-based nanozyme as a coreaction accelerator for enhancing electrochemiluminescence of glucose biosensing, *Biosens. Bioelectron.*, 2024, **250**, 116078.

236 J. Chen, J. Zheng, K. Zhao, A. Deng and J. Li, Electrochemiluminescence resonance energy transfer system between non-toxic SnS_2 quantum dots and ultrathin Ag@ Au nanosheets for chloramphenicol detection, *Chem. Eng. J.*, 2020, **392**, 123670.

237 D. Jiang, M. Wei, X. Du, M. Qin, X. Shan and Z. Chen, One-pot synthesis of ZnO quantum dots/N-doped Ti_3C_2 MXene: Tunable nitrogen-doping properties and efficient electrochemiluminescence sensing, *Chem. Eng. J.*, 2022, **430**, 132771.

238 R. Joseph, S. K. Rani and N. Vasimalai, A novel molecular imprinted polymer grafted on N, S co-doped carbon quantum dots-based fluorescence sensor for chloramphenicol in food and clinical samples, *Microchem. J.*, 2024, **207**, 111675.

239 Z. Zhang, D. Jiang, H. Ding, X. Shan, W. Wang, H. Shiigi and Z. Chen, Cobaltous sulfide/S-doped Ti_3C_2 MXene nanocomposites with co-rection acceleration effect for high-performance luminol electrochemiluminescence sensing by coupling micro-nano bubbles-mediated amplification strategy, *Chem. Eng. J.*, 2023, **475**, 146182.

240 X. Liu, Y. Li, L. He, Y. Feng, H. Tan, X. Chen and W. Yang, Simultaneous detection of multiple neuroendocrine tumor markers in patient serum with an ultrasensitive and antifouling electrochemical immunosensor, *Biosens. Bioelectron.*, 2021, **194**, 113603.

241 D. R. Iyer, J. Venkatraman, E. Tanguy, N. Vitale and N. R. Mahapatra, Chromogranin A and its derived peptides: potential regulators of cholesterol homeostasis, *Cell. Mol. Life Sci.*, 2023, **80**(9), 271.

242 A. M. Arjun, N. Shabana, M. Ankitha and P. A. Rasheed, Electrochemical deposition of Prussian blue on Nb_2CT_x MXene modified carbon cloth for the non-enzymatic electrochemical detection of hydrogen peroxide, *Microchem. J.*, 2023, **185**, 108301.

243 Z. Otgonbayar and W. C. Oh, Comprehensive and multi-functional MXene based sensors: An updated review, *FlatChem*, 2023, 100524.

244 R. Singh, R. Gupta, D. Bansal, R. Bhateria and M. Sharma, A review on recent trends and future developments in electrochemical sensing, *ACS Omega*, 2024, **9**(7), 7336–7356.

245 A. M. Mohamed, F. H. Fouad, G. R. Fayek, K. M. El Sayed, M. N. Ahmed, R. Z. Mahmoud and R. M. El Nashar, Recent advances in electrochemical sensors based on nanomaterials for detection of red dyes in food products: A review, *Food Chem.*, 2024, **435**, 137656.

246 E. Bakker and M. Telting-Diaz, Electrochemical sensors, *Anal. Chem.*, 2002, **74**(12), 2781–2800.

247 N. Jadon, R. Jain, S. Sharma and K. Singh, Recent trends in electrochemical sensors for multianalyte detection–A review, *Talanta*, 2016, **161**, 894–916.

248 M. Hasanzadeh, N. Shadjou and M. de la Guardia, Early stage screening of breast cancer using electrochemical biomarker detection, *TrAC, Trends Anal. Chem.*, 2017, **91**, 67–76.

249 B. Mohan, S. Kumar, H. Xi, S. Ma, Z. Tao, T. Xing and P. Ren, Fabricated Metal-Organic Frameworks (MOFs) as luminescent and electrochemical biosensors for cancer biomarkers detection, *Biosens. Bioelectron.*, 2022, **197**, 113738.

250 A. Thamilselvan and M. I. Kim, Recent advances on nanozyme-based electrochemical biosensors for cancer biomarker detection, *TrAC, Trends Anal. Chem.*, 2024, 117815.

251 B. S. Munge, T. Stracensky, K. Gamez, D. DiBiase and J. F. Rusling, Multiplex immunosensor arrays for electrochemical detection of cancer biomarker proteins, *Electroanalysis*, 2016, **28**(11), 2644–2658.

252 H. L. Chia, C. C. Mayorga-Martinez, N. Antonatos, Z. Sofer, J. J. Gonzalez-Julian, R. D. Webster and M. Pumera, MXene titanium carbide-based biosensor: strong dependence of exfoliation method on performance, *Anal. Chem.*, 2020, **92**(3), 2452–2459.

253 C. V. Raju, C. H. Cho, G. M. Rani, V. Manju, R. Umapathi, Y. S. Huh and J. P. Park, Emerging insights into the use of carbon-based nanomaterials for the electrochemical detection of heavy metal ions, *Coord. Chem. Rev.*, 2023, **476**, 214920.

254 R. Rajamanikandan and M. Ilanchelian, β-cyclodextrin functionalised silver nanoparticles as a dual colorimetric probe for ultrasensitive detection of Hg^{2+} and S^{2-} ions in environmental water samples, *Mater. Today Commun.*, 2018, **15**, 61–69.

255 T. Liu, R. Zhou, K. Wu and G. Zhu, Colorimetric method transforms into highly sensitive homogeneous voltammetric sensing strategy for mercury ion based on mercury-stimulated $Ti_3C_2T_x$ MXene nanoribbons@ gold nanozyme activity, *Anal. Chim. Acta*, 2023, **1250**, 340975.

256 A. Mukhopadhyay, S. Duttagupta and A. Mukherjee, Emerging organic contaminants in global community drinking water sources and supply: A review of occurrence, processes and remediation, *J. Environ. Chem. Eng.*, 2023, **10**(3), 107560.

257 K. Sasikumar, R. Rajamanikandan and H. Ju, A high-performance $NiMoO_4$/g-C_3N_4 direct Z-scheme heterojunction photocatalyst for the degradation of organic pollutants, *Surf. Interfaces*, 2023, **42**, 103389.

258 M. S. Samuel, K. Jeyaram, S. Datta, N. Chandrasekar, R. Balaji and E. Selvarajan, Detection, contamination, toxicity, and prevention methods of ochratoxins: An update review, *J. Agric. Food Chem.*, 2021, **69**(46), 13974–13989.

259 X. Zhang, F. Wang, H. Zhi, J. Zhao, P. Wan and L. Feng, Electrochemical "signal on/off" paper-based aptasensor for ochratoxin A detection based on MXene-Au and Pt@ NiCo-LDH-catalyzed signal amplification, *Sens. Actuators, B*, 2022, **368**, 132161.

260 B. Zhu, D. An, Z. Bi, W. Liu, W. Shan, Y. Li and M. Qiu, Two-dimensional nitrogen-doped Ti_3C_2 promoted catalysis performance of silver nanozyme for ultrasensitive detection of hydrogen peroxide, *ChemElectroChem*, 2022, **9**(10), e202200050.

261 S. Fu, Y. Zhu, Y. Zhang, M. Zhang, Y. Zhang, L. Qiao and D. Wang, Recent advances in carbon nanomaterials-based electrochemical sensors for phenolic compounds detection, *Microchem. J.*, 2021, **171**, 106776.

262 R. Yu, J. Xue, Y. Wang, J. Qiu, X. Huang, A. Chen and J. Xue, Novel $Ti_3C_2T_x$ MXene nanozyme with manageable catalytic activity and application to electrochemical biosensor, *J. Nanobiotechnol.*, 2022, **20**(1), 119.

263 L. Wu, X. Lu, Z. S. Wu, Y. Dong, X. Wang, S. Zheng and J. Chen, 2D transition metal carbide MXene as a robust biosensing platform for enzyme immobilization and ultrasensitive detection of phenol, *Biosens. Bioelectron.*, 2018, **107**, 69–75.

264 H. Karimi-Maleh, F. Karimi, M. Alizadeh and A. L. Sanati, Electrochemical sensors, a bright future in the fabrication of portable kits in analytical systems, *Chem. Rec.*, 2020, **20**(7), 682–692.

265 X. Zhu, L. Lin, R. Wu, Y. Zhu, Y. Sheng, P. Nie and Y. Wen, Portable wireless intelligent sensing of ultra-trace phytoregulator α-naphthalene acetic acid using self-assembled phosphorene/Ti_3C_2-MXene nanohybrid with high ambient stability on laser-induced porous graphene as nanozyme flexible electrode, *Biosens. Bioelectron.*, 2021, **179**, 113062.

266 M. Bhattu, M. Verma and D. Kathuria, Recent advancements in the detection of organophosphate pesticides: a review, *Anal. Methods*, 2021, **13**(38), 4390–4428.

267 T. O. Ajiboye, P. O. Oladoye, C. A. Olanrewaju and G. O. Akinsola, Organophosphorus pesticides: Impacts, detection and removal strategies, *Environ. Nanotechnol., Monit. Manage.*, 2022, **17**, 100655.

268 L. Wang, N. Wu, L. Wang, Y. Song and G. Ma, Accurate detection of organophosphorus pesticides based on covalent organic framework nanofiber with a turn-on strategy, *Sens. Actuators, B*, 2022, **372**, 132608.

269 L. Yu, J. Chang, X. Zhuang, H. Li, T. Hou and F. Li, Two-dimensional cobalt-doped Ti_3C_2 MXene nanozyme-mediated homogeneous electrochemical strategy for pesticides assay based on in situ generation of electroactive substances, *Anal. Chem.*, 2022, **94**(8), 3669–3676.

270 F. Zhao, Y. Yao, C. Jiang, Y. Shao, D. Barceló, Y. Ying and J. Ping, Self-reduction bimetallic nanoparticles on ultrathin MXene nanosheets as functional platform for pesticide sensing, *J. Hazard. Mater.*, 2020, **384**, 121358.

271 S. Kumar and R. Singh, Recent optical sensing technologies for the detection of various biomolecules, *Opt. Laser Technol.*, 2021, **134**, 106620.

272 J. Zhang, Y. Li, S. Duan and F. He, Highly electrically conductive two-dimensional Ti_3C_2 Mxenes-based 16S rDNA electrochemical sensor for detecting Mycobacterium tuberculosis, *Anal. Chim. Acta*, 2020, **1123**, 9–17.

273 Y. Chen, Y. Gu, X. Yi, H. Huang, Y. Li, B. Yang and L. Bai, Conductive nano-gold self-assembled MXene@ hemin with high catalytic activity achieved by strong metal-support interactions: A powerful nanozyme for development of electrochemical aptasensor in tuberculosis diagnosis, *Chem. Eng. J.*, 2023, **466**, 143112.

274 X. Zheng, Z. Hu, S. Gao, Z. Li, J. Chen, G. Zhang and W. Liu, One-pot assay using a target-driven split aptamer recognition and assembly strategy for convenient and rapid detection of gliotoxin, *Food Chem.*, 2024, **454**, 139738.

275 H. Wang, H. Li, Y. Huang, M. Xiong, F. Wang and C. Li, A label-free electrochemical biosensor for highly sensitive detection of gliotoxin based on DNA nanostructure/MXene nanocomplexes, *Biosens. Bioelectron.*, 2019, **142**, 111531.

276 J. Chen, P. Tong, L. Huang, Z. Yu and D. Tang, Ti_3C_2 MXene nanosheet-based capacitance immunoassay with tyramine-enzyme repeats to detect prostate-specific antigen on interdigitated micro-comb electrode, *Electrochim. Acta*, 2019, **319**, 375–381.

277 G. Jiang, H. Liu, J. Liu, L. E. Liu, Y. Li, L. Xue and R. Yang, Engineering of multifunctional carbon nanodots-decorated plasmonic Au@ Ag nanoenzymes for photoelectrochemical biosensing of microRNA-155, *Sens. Actuators, B*, 2022, **360**, 131653.

278 H. Wang, J. Sun, L. Lu, X. Yang, J. Xia, F. Zhang and Z. Wang, Competitive electrochemical aptasensor based on a cDNA-ferrocene/MXene probe for detection of breast cancer marker Mucin1, *Anal. Chim. Acta*, 2020, **1094**, 18–25.

279 R. Manikandan, M. J. Kim, H. G. Jang, A. Mugunthan, C. S. Kim, J. H. Yoon and S. C. Chang, Fabrication of bio-mimic nanozyme based on Mxene@ AuNPs and molecular imprinted poly (thionine) films for creatinine detection, *Biosens. Bioelectron.*, 2025, **271**, 117075.

280 J. Perumal, Y. Wang, A. B. E. Attia, U. S. Dinish and M. Olivo, Towards a point-of-care SERS sensor for biomedical and agri-food analysis applications: A review of recent advancements, *Nanoscale*, 2021, **13**(2), 553–580.

281 D. Graham, M. Moskovits and Z. Q. Tian, SERS–facts, figures and the future, *Chem. Soc. Rev.*, 2017, **46**(13), 3864–3865.

282 C. Liu, D. Xu, X. Dong and Q. Huang, A review: Research progress of SERS-based sensors for agricultural applications, *Trends Food Sci. Technol.*, 2022, **128**, 90–101.

283 B. Sharma, R. R. Frontiera, A. I. Henry, E. Ringe and R. P. Van Duyne, SERS: Materials, applications, and the future, *Mater. Today*, 2012, **15**(1–2), 16–25.

284 M. Fleischmann, P. J. Hendra and A. J. McQuillan, Raman spectra of pyridine adsorbed at a silver electrode, *Chem. Phys. Lett.*, 1974, **26**(2), 163–166.
285 A. Campion and P. Kambhampati, Surface-enhanced Raman scattering, *Chem. Soc. Rev.*, 1998, **27**(4), 241–250.
286 M. Shameer, K. V. Anand, J. B. Parambath, S. Columbus and H. Alawadhi, Direct detection of melamine in milk via surface-enhanced Raman scattering using gold-silver anisotropic nanostructures, *Spectrochim. Acta, Part A*, 2025, **327**, 125412.
287 A. M. Pisoschi and A. Pop, The role of antioxidants in the chemistry of oxidative stress: A review, *Eur. J. Med. Chem.*, 2015, **97**, 55–74.
288 H. Xi, H. Gu, Y. Han, T. You, P. Wu, Q. Liu and P. Yin, Peroxidase-like single Fe atoms anchored on $Ti_3C_2T_x$ MXene as surface enhanced Raman scattering substrate for the simultaneous discrimination of multiple antioxidants, *Nano Res.*, 2023, **16**(7), 10053–10060.
289 V. G. Gayathri, R. Bartholomew, J. T. Chacko, J. Bayry and P. A. Rasheed, Non-Ti MXenes: new biocompatible and biodegradable candidates for biomedical applications, *J. Mater. Chem. B*, 2025, **13**, 1212–1228.
290 E. Pargoletti and Y. Gogotsi, MXene-Based Nanozymes: Current Challenges and Future Prospects, *ChemCatChem*, 2025, e00730.

